Effect of divalent oxides on the structure of glasses for HLW immobilisation

THE UNIVERSITY OF
WARWICK

M. Moinul Islam

A thesis submitted in partial fulfilment of the requirements of the degree of Doctor of Philosophy in Physics

Department of Physics   **May, 2005**

Table of Contents

Chapter 3 Theory and Structure of Glass   13

Chapter 4 Experimental Techniques   40

List of Figures

List of Tables

List of Abbreviations

BNFL	British Nuclear Fuels, Limited
BO	Bridging Oxygen
CTE	Coefficient of Thermal Expansion
DTA	Differential Thermal Analysis
FWHM	Full Width Half Maximum
MAS	Magic Angle Spinning
Mn	Manganese
MW	Magnox Waste (Base Glass)
NMR	Nuclear Magnetic Resonance
NBO	Non-bridging Oxygens
SYNROC	Synthetic Rock
UV	Ultra-Violet
XRD	X-ray Diffraction

Acknowledgements

Declaration

The work for this thesis was carried out in the Department of Physics at the University of Warwick, unless otherwise stated. The work was completed during the period from November 2001 to October 2004 and, except where specially acknowledged in the text, is the result of my own independent research and has not been previously submitted at the University of Warwick, or any other institution, in respect of a higher degree. Parts of this thesis have been published or submitted for publication with the following reference:

1. **A. Duddridge, M. Islam**, D. Holland and C. R. Scales, 'Chemical durability studies of waste-simulant doped borosilicate glasses' Scientific Basis for Nuclear Waste Management XXVII, 2003, ed. L. Werme. Accepted for publication.

9th, May 2005

M. Moinul Islam

Date

Abstract

The mixed alkali borosilicate glass system used for high-level waste immobilisation, has been studied with different divalent additive oxides such as CaO, SrO, BaO, MnO, ZnO and PbO added to the BNFL base glass (MW). A number of techniques have been employed in order to study the effect of these oxide additives. ^{11}B MAS NMR was performed to measure the fraction of tetrahedrally coordinated boron atoms N_4 and ^{29}Si MAS NMR to measure the Q^n speciation. Durability tests were carried out and compared with electrical conduction behaviour. Densities, glass transition temperatures and thermal expansion coefficients are also reported.

The change in N_4 with concentration has been determined for different additive oxides. The addition of BaO, CaO and SrO to the base (MW) BNFL vitrification glass caused N_4 to increase with alkaline earth content, and maximum values were attained at compositions depending on the M^{2+} ion type. In contrast, the addition of divalent oxides such as ZnO and PbO to MW reduced the N_4 values, with the rate of decrease being greater for ZnO than PbO. The ^{29}Si NMR studies have shown the presence of significant concentrations of non-bridging oxygens which can influence the aqueous corrosion behaviour of the glass.

The durability tests revealed that the alkaline earth oxides BaO, SrO and CaO decrease the durability. In contrast, oxides such as ZnO and PbO improve the corrosion resistance. The presence of a surface Mn_7SiO_{12} crystallisation phase was identified on corroded MnO containing glasses.

The reduction in electrical conductivity with oxide addition shows a similar trend to the corrosion behaviour for chemically resistant glasses. In contrast, the opposite trend is found for less durable glasses.

UV visible transmission of MnO doped glass shows a decrease in transmittance at ~ 380 nm. The absorption band centred at ~ 490nm, moves towards longer wavelength, caused by generation of NBOs on the $[SiO_4]$ tetrahedral unit.

Chapter1

Introduction

1.1. Background

The composition of spent nuclear fuel depends on the type of reactor and the operating conditions, but differences in the radioactive fission products that are obtained are normally small. Reprocessing of spent fuel rods normally involves removal of the cladding material followed by dissolution in nitric acid. This stage is then followed by chemical solvent extraction of the uranium together with the plutonium formed during the fuel burn-up process. The remaining solution contains the dissolved fission products together with impurities from the cladding materials, inactive process chemicals, transuranic elements formed by neutron capture and traces of unseparated Pu. This constitutes a high level liquid waste product (HLW). This high level liquid waste product is normally concentrated by evaporation and stored as aqueous nitric acid solution in stainless steel tanks. Alternatively the solution may be neutralized by addition of an alkali. These solutions therefore contain a host of products including fission products e.g. Rb, Sr, Y, Zr, Nb, Mo, Tc, Ru, Rh, Pd, Cs, Ba, La, Ce, Pr, Nd.

The treatment and disposal of HLW have become major operating expenses for nuclear power plants. Volume reduction of radioactive waste is one of the most important issues for waste management with regard to rapidly increasing cost of the waste storage and disposal. Vitrification is very attractive among the technologies for the volume reduction of HLW. Every major country, in the west, which is producing high-level waste, has selected borosilicate glass as the preferred waste form, because of its excellent combination of reliable processing and acceptable product performance.

High-level waste, usually held in tank storage, is pumped into the vitrification plant's highly active liquor tank. It is then fed into a rotating tube inside a heated furnace. Here the liquid is evaporated and the waste dried into powder. The dried powder is fed into a melting pot together with glass making material at an approximate ratio of 25% waste to 75% glass. Over the course of about eight hours, the powder and glass fuse together. The molten mixture is then poured into a 4ft high stainless steel canister that is waiting under the melter. The resulting radioactive solid may then be disposed of after vitrification as a borosilicate glass.

1

The characteristics of the waste glass are determined by the amount and type of oxides added to it. Additives in the glass can change the glass properties adversely; it is therefore important to investigate the role of additives in order to obtain a final waste glass with the desired property. Divalent additives, which are the subject of this thesis, can change the properties of waste form glass in different ways. Therefore a selection of divalent oxides have been chosen to represent modifier and intermediate behaviour.

For example, as a result of beta decay caesium will transmute to barium, which differs substantially in size and charge and can have significant impact on the glass behaviour [1]. Manganese is usually present in HLW glasses at concentrations very different from those in commercial glasses. Mn can become a significant constituent in some radioactive wastes, because of the use of Mn-compounds in waste pre-treatment processes [2].

Although borosilicate glass has proved to be an excellent choice for HLW immobilisation, fundamental research is needed to identify the structural roles of various oxides in waste glasses. The current project, following on work by Roderick [3] and Duddridge [4], examines the effects of various waste constituents on the structure and properties of the BNFL waste glass. A number of different divalent additives have been doped into BNFL HLW borosilicate base glass system in order to examine thermal, physical and structural properties of the glass systems as a function of the level of doping.

1.2. Aims of the work

Boron can exist in many coordination states in glass which have a profound effect on properties. However, it is virtually impossible to predict what form boron will take in a given glass because of the complexity of the composition. A major aim is to identify changes in the environment of boron in waste glasses as a function of glass composition. The changes in the relative fraction of 4-coordinated boron atoms obtained from ^{11}B and the ^{29}Si species deduced from ^{29}Si NMR are compared with a structural model. Chemical durability and ionic conduction of the glass system are also studied in order to relate ionic mobility to the structure.

This fundamental research has provided the following important information on the MW doped glass system:

- relative fraction of 4-cordinated boron atoms in the various oxide doped glasses
- glass durability
- ionic mobility at elevated temperature
- phase separation of the manganese containing glasses
- structural role of the +2 ions in the studied glass systems
- change in the thermal, physical and optical properties with different additives.

1.3. References

[1]   E. R. Vance, R. Roy, J. G. Pepin and D. K. Agrawal, J. Mat. Sci. **17** (1982) 947-952.

[2]   D. A. Mckeown, W. K. Kot, H. Gan and I. L. Pegg. J. Non-Cryst. Solids **328** (2003) 71-89.

[3]   J. M. Roderick, PhD Thesis, Department of Physics, University of Warwick, UK, Feb (2001).

[4]   A. Duddridge, PhD Thesis, Department of Physics, University of Warwick, UK, May (2004).

Chapter 2
Radioactive Waste Disposal

2.1. Introduction

The average life of a nuclear fuel rod in a nuclear power stations is about 4 years. After this period, waste products have built up in the fuel rod making it less efficient. A chemical operation is carried out to separate the 3% of waste products in a typical fuel rod, called the nuclear fuel cycle. The processing of spent fuel rods generates large quantities of waste containing radionuclides, some of which have long half lives. The wastes are stored in the form of solutions and clearly this is very unsatisfactory in view of the difficulties of ensuring that no leaks into the environment ever occur during the necessarily very long storage period. The nuclear power industry has developed a process to convert the radioactive wastes into a chemically stable glass, which is a more manageable waste form.

The majority of used nuclear fuel is not waste. Only 3% of the fuel is the fission products such as ^{90}Sr, ^{99}Tc, ^{106}Ru, ^{129}I, ^{137}Cs and higher actinides e.g., ^{239}Pu, ^{241}Pu, ^{241}Am, ^{242}Cm which form the waste after reprocessing. The remaining 96%, which is uranium, and 1% which is plutonium can be recycled and used again to make more nuclear fuel. Even though the amount of nuclear waste that is produced is very small, because it is radioactive, extreme care must be taken when dealing with it.

High level waste in practice is considered long lived. One of the characteristics which distinguishes HLW from less active waste is its level of thermal power. This waste contains a wide range of both short and long lived radionuclides and a significant quantity of heat from radioactive decay normally continues to be generated for several centuries. The major long-lived radionuclides present in HLW are shown in Table 2.01. A single large power generating reactor may contain in excess of 10^8 TBq [1] of fission products and there are several hundreds of power reactors in the world. With the increasing emphasis on protection of the environment, the management of these wastes is becoming an important factor in both the economics and the public acceptability of nuclear power. Therefore a high degree of isolation from the biosphere, usually via geological disposal, is needed to ensure disposal safety.

Radionuclide	Half-life (y)
^{79}Se	7×10^4
^{90}Sr	28.0
^{93}Zr	1.5×10^6
^{99}Tc	2.1×10^5
^{107}Pd	6.5×10^6
^{126}Sn	10^5
^{129}I	1.57×10^7
^{135}Cs	2×10^6
^{137}Cs	30
^{151}Sm	93
^{237}Np	2.14×10^6
^{238}Pu	87.7
^{239}Pu	2.41×10^4
^{240}Pu	6569
^{241}Pu	14.4
^{242}Pu	3.7×10^5
^{241}Am	432.2
^{243}Am	7380
^{244}Cm	18.1
^{245}Cm	8500

Table 2.01. Main long - lived radionuclides in nuclear waste [2].

2.2. Waste types

2.2.1. Introduction

A widely used qualitative classification system separates radioactive wastes into four classes. Each one is dealt with according to how radioactive it is- very low, low, intermediate (medium) and high.

2.2.2. Very Low-level Waste (VLLW)

This comprises material containing less than 400Bq/m^3 of beta/gamma activity or single items containing less than 40kBq beta/gamma activity. It contains so little radioactive material that it cannot be considered 'radioactive' and might be exempted from nuclear regulatory control. Although still radioactive from a physical point of view, the waste may be safely disposed of, without specially considering its

radioactive property. The activity levels are at or below clearance levels, which are based on an annual dose to members of the public of less than 0.01mSv [3].

2.2.3. Low-level Waste (LLW)

Solid low-level waste includes paper, rags, tools, clothing and laboratory equipment, which have been used in areas where radioactive materials are used. Hospitals and research establishments also produce low-level wastes. Low-level waste is less radioactive than some rocks in Cornwall, where there are high levels of natural radioactivity. Reprocessing one tonne of used nuclear fuel produces about 4 cubic metres of low-level waste, which contains 0.001% of the radioactivity in the used fuel. About 30,000 m^3 [4] of low level solid waste is produced each year in UK.

In the UK, all low level waste is safely disposed of in containers inside a concrete vault at Drigg, near Sellafield. Approximately 1 million m^3 LLW [5] is currently stored at Drigg. A typical vault is an above-ground or below-ground reinforced concrete structure containing an array of storage cavities, each of which could hold one or more waste packages. In the UK, NIREX has indicated that it would plan to store low-level waste in an underground repository as well as intermediate level waste.

2.2.4. Intermediate-level Waste (ILW)

Intermediate level waste is far less radioactive than high-level waste. It is made up of such things as fuel element cladding, contaminated equipment and sludge that comes from the treatment processes. Reprocessing one tonne of used nuclear fuel produces about 1 cubic metre of intermediate-level waste, which contains nearly 1% of the radioactivity in the used fuel. Intermediate level waste can be safely stored in cement inside steel drums. Currently, in the UK this is then put into a concrete store above ground, it is planned that it will be eventually disposed of in a repository. In its cemented form in a drum, the waste is in a solid form, and it is very difficult for radioactivity to escape into the environment. Less than 5,000 m^3 of ILW is produced every year in the UK and ~ 70,000m^3 [5] is currently being stored.

Intermediate and high level wastes contain over 99.9% of the radioactivity in the used fuel. Intermediate waste is also formed at the power station from ion exchange resin. Intermediate waste will also need to be treated as it is removed during decommissioning of nuclear facilities. At present there is no permanent facility for disposing of high and intermediate-level nuclear waste over the long term.

2.2.5. High-level Waste (HLW)

High-level waste is radioactive enough to generate significant quantities of heat from radioactive decay, and normally continues to generate heat for several centuries. This waste is what is left when the uranium and plutonium have been removed from the spent fuel. Reprocessing one tonne of used nuclear fuel produces about 0.1 cubic meters of high-level waste, which contains nearly 99% of the radioactivity in the used nuclear fuel.

The high level waste is concentrated by evaporation and stored inside double-walled stainless steel tanks inside thick concrete walls. Huge cooling coils inside the tanks remove the heat that the waste produces. There are several sets of these coils in case any one fails. In the longer term, to store the high level waste safely, it can be vitrified, which will turn the waste into very dense solid-glass blocks. First, the liquid is calcined to powder and mixed with glass-making materials and then poured into stainless steel containers. Since the 1950s, the nuclear industry in the UK has just stored 1800 m^3 of HLW [5]. Vitrified waste can be stored at least 50 years for the short-lived radionucides to decay and heat generation to reduce. Waste management strategies after this period have yet to be decided.

2.3. Basic Steps in Radioactive Waste Management

The waste is characterised in order to determine its physical, chemical and radiological properties, and to facilitate record keeping and acceptance of radioactive waste from one step to another.

a) Characterisation

It is applied, in order to segregate radioactive materials for exemption or for reuse or according to disposal methods or to assure compliance of waste packages with requirements for storage and disposal.

b) Transport to a disposal or storage facility

Transportation of radioactive waste involved the movement of radioactive material by any mode on land, water or in the air. Transportation of radioactive waste may be necessary between the radioactive waste management steps.

c) Storage

Storage of radioactive waste involves isolation, treatment, conditioning and disposal. Storage of radioactive waste containing mainly short lived radionuclides for

decay and subsequent release within authorised limits or storage of high level radioactive waste for thermal considerations prior to disposal.

d) Interim storage

This occurs at the site of origin i.e. the placement of waste in a nuclear facility where isolation, environmental protection and monitoring are provided with the intent that the waste will be retrieved for exemption or processing and disposal at a later time.

e) Pre-treatment

Pre-treatment of radioactive waste is the initial step in waste management that occurs after waste generation. It consists of, collection, segregation, chemical adjustment and decontamination and may include a period of interim storage.

f) Treatment

Treatment of radioactive wastes involves those operations intended to improve safety or economy by changing the characteristics of radioactive waste. The basic objectives are: volume reduction, removal of radionuclides from the waste, change of composition. Incineration of combustible waste or compaction of dry solid waste is the volume reduction. Evaporation, filtration or ion exchange of liquid waste is the change of composition.

g) Conditioning

Conditioning of radioactive waste involves those operations that transform radioactive waste into a form suitable for handling, transportation, storage and disposal. The operation may include immobilisation of radioactive waste, placing the waste into containers and providing additional packaging. Common immobilisation methods include solidification of low and intermediate level liquid radioactive waste, in cement or bitumen and vitrification of high-level radioactive waste in a glass matrix. Immobilisation waste, in turn, may be packaged in containers ranging from 200 litre [3] steel drums to highly engineered thick walled containers, depending on the nature of radionuclides and their concentrations. Treatment and conditioning may take place in close conjunction with one another.

h) Disposal

Disposal is the final step in the radioactive waste management system. It consists mainly of the placement of radioactive waste in a disposal facility with a reasonable assurance for safety, without intention of retrieval and without reliance on

long-term surveillance and maintenance. Disposal may also include the approved direct discharge of effluents (e.g. liquid and gaseous waste) into the environment.

Concentration and containment mainly achieve this safety, which involves the isolation of suitably conditioned radioactive waste in a disposal facility. Isolation is attained by placing barriers around the radioactive waste in order to restrict the release of radionuclide into the environment. The barriers can be either natural or engineered. An isolation system can consist of one or more barriers. Systems of multiple barriers give greater assurance of isolation and ensure that release of radionuclides to the environment will occur at an acceptably low rate. The barrier system is designed according to the disposal option chosen and the radioactive waste form involved.

2.4. Materials used in HLW waste disposal

2.4.1. Requirements

The solidification of high-level liquid wastes from nuclear fuel reprocessing plants is the most acceptable way to manage high level waste. Glass is attractive for large scale solidification of nuclear wastes and borosilicate glass in particular has proved to be an excellent choice for HLW immobilisation.
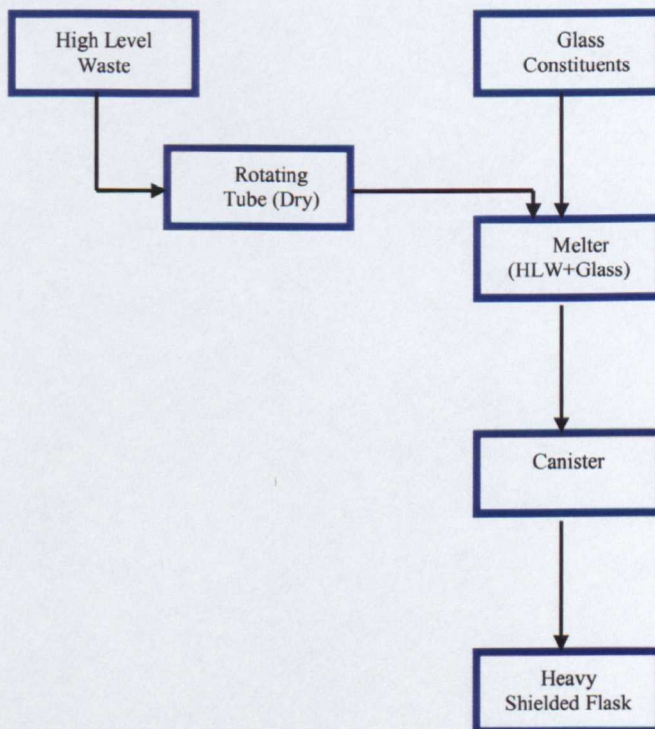
Fig. 2.01. Representation of high-level waste immobilisation.

The molecular structure of glass is amorphous i.e., there is no geometric repetition at a scale beyond a few atoms. Structural units of borosilicate glass are formed from combination of oxygen, boron and silicon, they form inorganic polymers that are stable at very high temperatures. The most important requirement for a storage medium is that it must have good chemical stability to prevent the leaking out of radioactive elements like ^{137}Cs, ^{90}Sr, etc. if contact with water occurred. Good physical stability and high strength are also desirable. HLW waste contained in the material generates heat and therefore it is necessary to have good temperature stability combined with as high as possible thermal conductivity to allow adequate heat removal from the blocks.

2.4.2. Summary of various hosts considered

Several types of waste form have been developed and tested by various methods. The large number of possibilities reflects the need to have more than one solution to a problem that is very complex due to the compositional diversity of nuclear waste and due to the geological variations in potential repository sites. Different types of possible waste forms are listed in Table 2.02, which gives a simplified classification based on their structural nature.

Amorphous form	Glass-ceramic form	Crystalline form
Alkali-borosilicate form	Sphene-glass	SYNROC
Phosphate glass	Zirconolite-glass	Phosphate
Aluminosilicate oxide glass	Hollandite-glass	Titanate
Aluminosilicate oxy-nitride glass	Apatite-glass	Silicate

Table 2.02. Materials used to isolate nuclear waste [2].

Among amorphous materials, alkali borosilicate and phosphate glasses are considered as generic waste forms able to immobilise fission products, activation products and actinides. Glass-ceramic forms have recently appeared as good candidates for nuclear waste hosting [6]. The radionuclide is preferentially trapped in the crystalline phase surrounded by a glassy envelope. Synthetic rock and Na-Zr phosphate are also generic waste forms. SYNROC is the only multiphase ceramic selected for nuclear waste confinement. Although many different types of glass and

10

ceramic materials have been investigated as possible candidates for the immobilisation of HLW, at the present time borosilicate glass is the generally accepted first generation waste form. Many commercial vitrification plants are now in operation throughout the world using borosilicate glass for HLW immobilisation. Table 2.03 describes compositions of calcined Magnox fission products.

Components	Amount (wt%)	Components	Amount (wt%)
MoO_3	14.4	SrO	2.9
ZrO_2	13.9	Sm_2O_3	2.6
Nd_2O_3	13.1	Rh_2O_3	2.2
Cs_2O	9.4	Y_2O_3	1.7
CeO_2	8.5	TeO_2	1.6
RuO_2	7.8	Rb_2O	2.2
BaO	4.6	Pm_2O_3	0.5
La_2O_3	4.2	CaO	0.01
Pr_6O_{11}	4.0	MgO	5.74
Te_2O_3	3.8	SiO_2	46.1
PdO	3.3	Al_2O_3	6.58
Fe_2O_3	3.0	Na_2O	8.29

Table 2.03. BNFL HLW Waste glass components [6].

The present study is based on the mixed alkali borosilicate glass currently used for immobilisation of HLW in BNFL. A wide range of materials properties such as density, glass transition temperature, thermal expansion, chemical durability and ionic conductivity have been studied.

2.5. References

[1] A. Martin and S. A. Harbison, An introduction to Radiation protection, 2nd edition, Chapman and Hall, London, March (1979) 155.

[2] P. Trocellier, Ann. Chim. Sci. Mat. **26** (2) (2001) 113-130.

[3]   International Atomic Energy Agency, Establishing a National System for Radioactive Waste Management, Safety Series no 11-S-1 IAEA, Vienna, (1995).

[4]   Environment and Nuclear Power, AEA Technology, Harwell, Didcot, Oxfordshire (1994).

[5]   Radioactive wastes in the UK, DETR/ NIREX, July (1998).

[6]   I. W. Donald and B. L. Metcalfe, J. Mat. Sci. **32** (1997) 5851.

Chapter 3
Theory and Structure of Glass

3.1. Definition of Glass

Glasses do not have a well-defined melting point. A glass is generally obtained by under-cooling a liquid below its melting point. The relationship between the glass, crystal and liquid phases can be explained by means of a volume-temperature diagram as in Figure 3.01. On cooling of a liquid, the volume will decrease steadily if the rate of cooling is sufficiently slow and, if nuclei are present, crystallisation will commence at or slightly below the melting temperature, T_m. The density increases and volume decreases from A to B, at constant temperature and subsequently, it contracts with decreasing temperature along BD. The resulting crystal is the thermodynamically stable phase.

If the rate of cooling is sufficiently rapid, crystallisation does not take place at T_m and the volume of the under-cooled liquid decreases along AC. At a certain temperature T_g, the volume-temperature graph undergoes a significant change in slope and continues almost parallel to the contraction curve BD of the crystal form. T_g is called the glass transition temperature and varies with the rate of cooling.
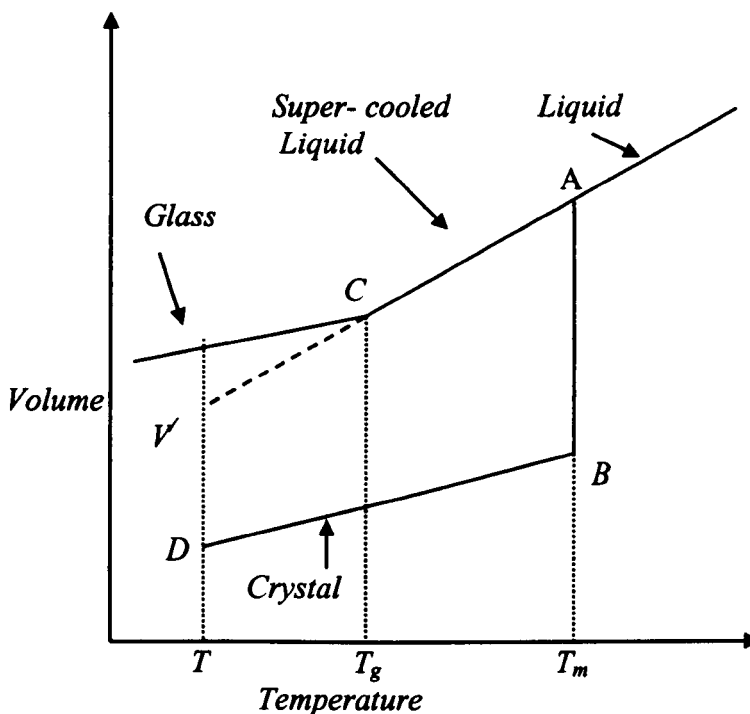
Fig. 3.01. Represents transition from liquid to a glass.

13

If the temperature of the glass is held constant at T, which is below T_g, the volume will decrease slowly. At infinite time it would reach the level $V^/$ on the dashed curve. The structure of the glass approaches an 'equilibrium configuration' which is characteristic of the under-cooled melt at temperature T.

3.1.1. Glass former, Intermediate and Modifier Oxides

The characteristics of the waste glass are determined by the amount and type of the intermediate and modifiers added. Sometimes, the same compounds may be classified into different categories when used for different purposes. Alumina for example, serves as a network former in aluminate glasses, but is considered as a modifier in most silicate glasses [1]. Arsenic oxide may be either a glass former or a fining agent, depending upon the purpose for which it has been added to the batch. Waste glass formulation then consists of adding supplemental intermediates and modifiers, in addition to the basic glass formers. The waste constituents act as glass intermediates or modifiers.

The primary glass formers in commercial oxide glasses are silica (SiO_2) and boric oxide (B_2O_3), which readily form single component glasses. These glass formers are essential constituents of all waste glasses. A large number of other compounds may act as glassformers under certain circumstances including GeO_2, As_2O_3, Sb_2O_3, TeO_2, and V_2O_5.

The intermediates can enter the network as formers or modifiers depending on the overall composition and processing conditions, e.g., Al_2O_3, Bi_2O_3, PbO, and ZnO, but generally increase the chemical durability.

The modifiers, which include the alkali oxides Na_2O, Li_2O and alkaline earth oxides BaO, CaO and SrO, tend to weaken the structural network and lower the melt viscosity. The oxides BaO, SrO decrease the chemical durability.

3.2. Structure of Glass

According to Zachariasen's theory the ordinary rules of crystal structure can be applied to silicate glasses, just the same as silicate crystals. The basic building unit of silicate crystals is the SiO_4 tetrahedron. Exactly the same situation exists in a silicate glass. These tetrahedra are joined together at their corners only, not along their edges or faces; they can be edge shared in crystals. In a crystalline material the same geometric pattern is repeated over large distances throughout the material. Angles

between bonds of the same type are constant and distances between pairs of atoms, such as the silicon and oxygen atoms, are constant. However, in the glass material, the bond angles and bond distances vary.

One of the features of glassy structures considered by Zachariasen is that, since they are built from similar polyhedra joined only at their corners, the structures are relatively open and contain relatively large voids. From the structure of a Na_2O-SiO_2 glass, the sodium ions are situated in the voids in the network formed by the SiO_4 tetrahedra. The difference between the structure of a hypothetical crystalline compound (a) and the Zachariasen model for the glassy form of the same compound (b), is shown in Figure 3.02.

(a)

(b)
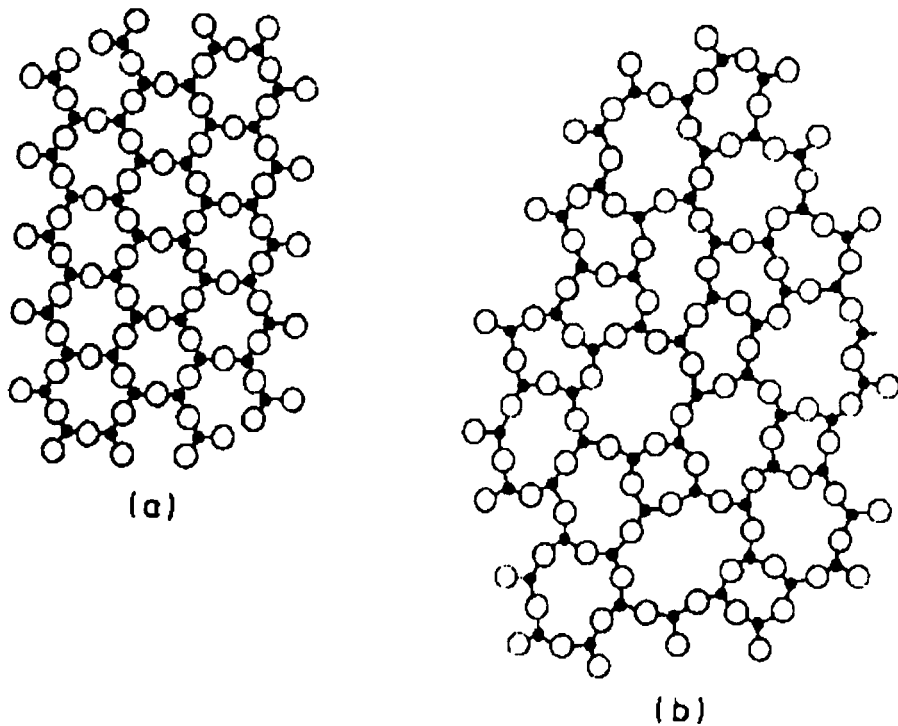
Fig. 3.02. Two-dimensional representation of (a) Crystalline (b) Glass structure [2].

The oxygen ions, introduced together with the sodium ions in the form of Na_2O, are incorporated by the rupture of some of the Si-O-Si linkages which are present in the SiO_2 glass. The non–bridging oxygen ions produced carry a negative charge to neutralize the positive charge of the sodium ions and therefore these sodium ions are likely to be found adjacent to the singly-bonded oxygen ions so that electro-

neutrality is maintained locally in the structure. The Na-O bonds are largely ionic and are much weaker than Si-O bonds, which have a strongly covalent character [2].

Zachariasen and Warren discussed [3] the anomalies in the behaviour of glasses containing B_2O_3 as a network former. This oxide may be present with co-ordination 3 or 4, in the form of triangular $[BO_3]$ or tetrahedral $[BO_4]$ formations. Introduction of Na_2O brings about conversion of $[BO_3]$ to $[BO_4]$ and strengthening of the network as a result of creation of extra B-O-B bonds. The coordination change results in anomalous changes in properties. Nuclear magnetic resonance experiments have confirmed a change in the co-ordination of boron due to the introduction of alkalis, however, the structural changes are not in full agreement with the anomalies in the physical properties.

3.3. Silicate Structure Types

The basic structural units of the silicate framework are SiO_4 tetrahedra which link together in a variety of ways by sharing oxygen atoms at their sites. In crystalline solids, SiO_4 tetrahedra may exist as isolated monomeric anions or may be connected by sharing oxygens. Initially, one or two oxygen atoms are shared forming dimeric and trimeric structures. Single rings and chains may be put together to build up double rings or multiple chains respectively. By linking an infinite number of chains, two–dimensional single layers are formed. Connection of two or more tetrahedral layers results in the formation of double layers and finally infinite three-dimensional frameworks.

The number of oxygen atoms not shared by a second silicon atom, called non-bridging oxygens, determines the negative charge of the complex anionic silicate network, which is balanced by the positive charge of cations located within the interstices of the structure.

For the representation of the building units or silicate anions the commonly used notation is Q^n, where Q represents a silicon atom bonded to four oxygen atoms forming a tetrahedron. The superscript n indicates the number of bridging oxygen attached to a silica tetrahedron. The five Q^n environments are displayed in Figure 3.03.

In alkali silicate glasses, A_2O-SiO_2, according to binary distribution theory, Q^4 units convert to Q^3 units in the region $0 \leq A_2O \leq 33.3$ mol%, Q^3 units convert to Q^2

units in the range between $33.3 \leq A_2O \leq 50$ mol%. On further addition of alkali, $50 \leq A_2O \leq 60$ mol%, Q^2 units convert to Q^1 units and between $60 \leq A_2O \leq 66.7$ mol% Q^1 units convert to Q^0. For $A_2O \geq 66.7$ mol %, all the silicate units are hypothesised to have all non-bridging oxygens.
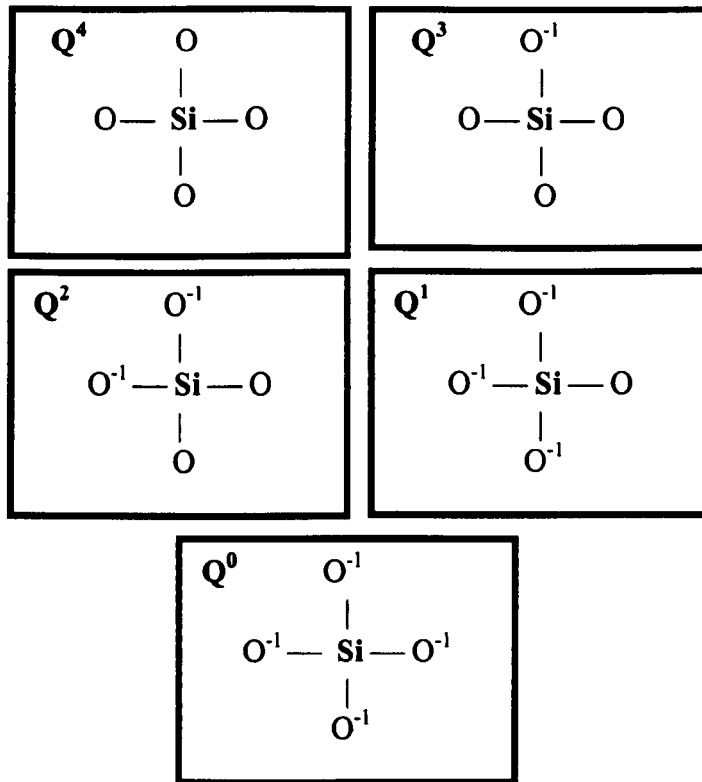
Fig. 3.03. The structural units hypothesized to exist in silicate glasses, denoted Q^n, where n is number of bridging oxygen.

3.4. Borate Structure Types

Bray and O'Keefe in the 1960s [4] and Yun, Dell and Feller in 1980s [5, 6] gained structural detail of borate glasses by the use of ^{11}B NMR to identify [BO$_3$] and [BO$_4$] units in various borate systems. An understanding of simple glass structure is essential in order to examine a more complex glass system like mixed alkali borosilicate glass. It is assumed that the B-O polyhedra can exist as either tetrahedral or trigonal units depending on the type of alkali and concentration.

Considering f_i as the fraction of the i th boron unit as follows:

f_1 - fraction of three-coordinated boron (trigonal) with all bridging oxygens

f_2 - fraction of four-coordinated boron (tetrahedral) with all bridging oxygens and one alkali ion associated (A$^+$) with it

f_3 - fraction of three-coordinated boron with one non-bridging oxygen and one associated A$^+$ ion

f_4 - fraction of three coordinated boron with two non-bridging and two A$^+$ ions

f_5 - fraction of three coordinated boron with three non-bridging oxygens and three associated A$^+$ ions
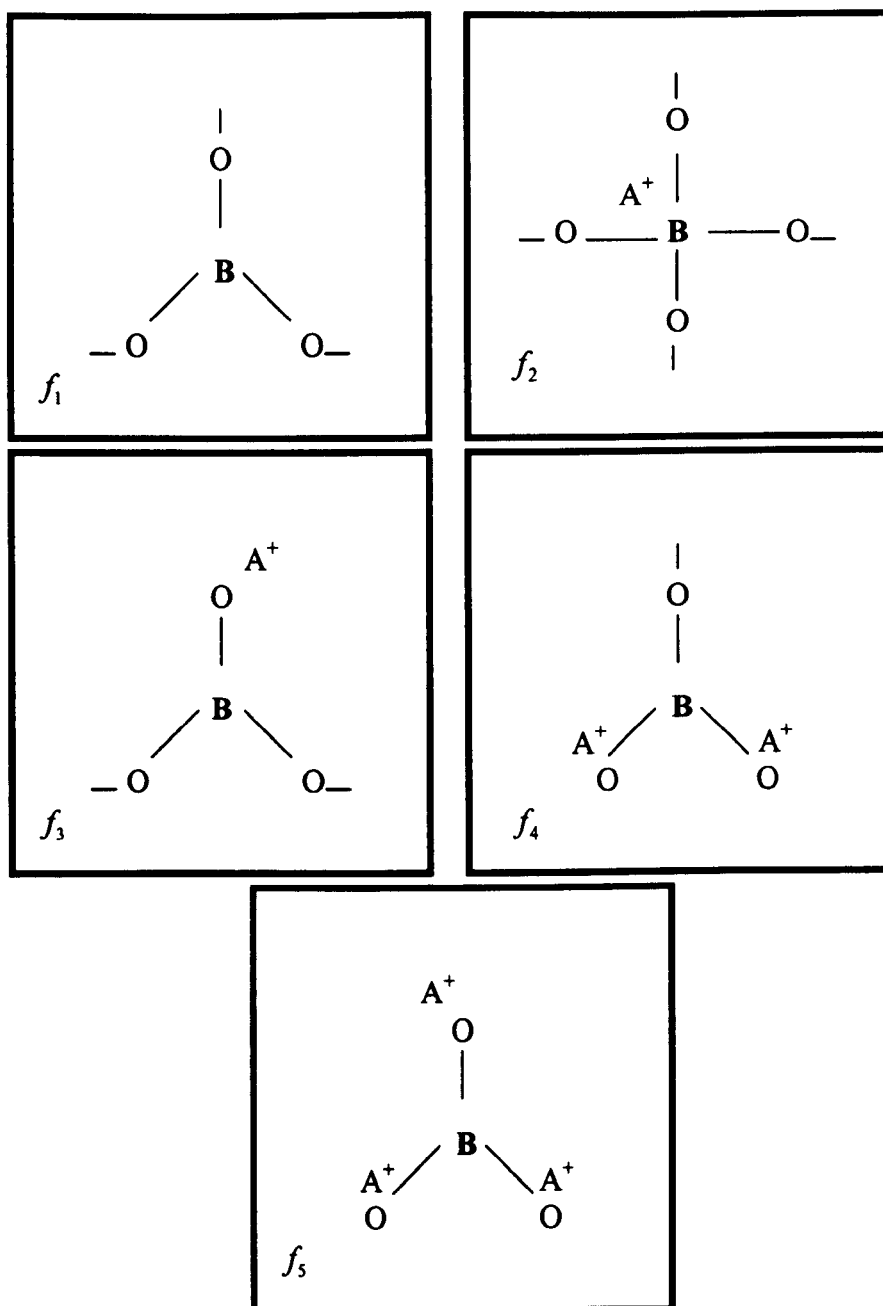
Fig. 3.04. Borate structural units deduced from NMR spectroscopy.

18

The three coordinated boron unit f_1 with all bridging oxygens is called symmetric [BO$_3$], and f_3 unit is referred to as asymmetric [BO$_3$].

The fraction of tetrahedral boron unit $N_4 = \dfrac{f_2}{\Sigma f}$ increases with $R = \dfrac{mol\% Na_2O}{mol\% B_2O_3}$. Figure 3.05 shows the variation of N_4 with the addition of alkali to Li$_2$O-B$_2$O$_3$ glass. At $R = 0.5$ the N$_4$ values reaches the maximum value, thereafter N$_4$ decreases at higher values of R. With the destruction of f_2 units, asymmetric f_3 and f_4 units with non-bridging oxygens are formed.

R= mol% metal oxide/ mol% B$_2$O$_3$
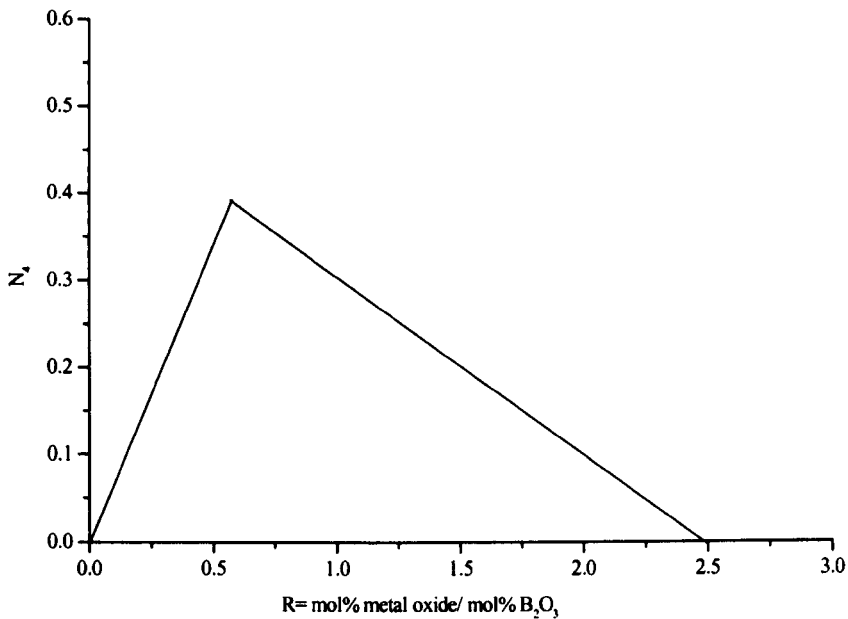
Fig. 3.05. The general behaviour of the fraction of four coordinated boron atoms in binary borate glass [7].

Work by Jellison et al. [8] and Feller et al. [9] showed that N$_4$ reaches a maximum with progression from [BO$_3$] to [BO$_4$]$^-$ to [BO$_3$]$^-$ units. The original ^{11}B NMR study of alkali borate glass by Bray and O' Keefe [4], showed an alkali independence of N$_4$ as shown in Figure 3.06. Zhong and Bray [10] determined that the fraction N$_4$, in a glass is not only dependent on the amount of alkali metal but also on the specific metal being used. They showed divergence of N$_4$ values commencing around $R = 0.25$ with the maximum divergence occurring around $R = 0.65$, where

$$R = \frac{mol\% \ alkali \ oxide}{mol\% \ boron \ oxide}$$. The obtained data indicated greater values for N_4 in glasses

with smaller alkali ions.
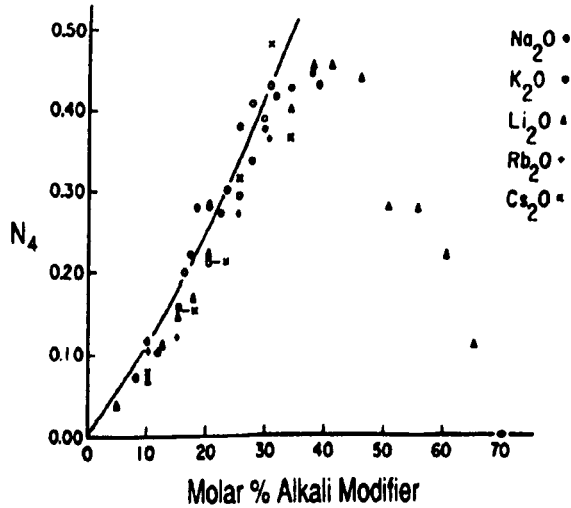
Fig. 3.06. The fraction N_4 of four-coordinated boron atoms in alkali borate glasses as a function of the mol% alkali oxide.

3.5. Phase Separation

Phase separation is the formation of two or more stable glassy phases from a less stable single-phase glass. It occurs when a single-phase liquid either cannot be quenched rapidly enough to avoid separation into two amorphous phases, or is heat treated at a temperature sufficient to allow the separation to proceed. It can enhance the properties of glass, or change them adversely.

The following types of phase separation are usually observed in glass; crystallisation, surface crystallisation, volume crystallisation, liquid-liquid phase separation and spinodal decomposition. The sodium borosilicate glass system, in particular, exhibits a region of spinodal phase separation at low alkali contents. The phase separation in HLW glass system may influence the glass stability, since the durability of phase-separated glass is always poorer than that of homogeneous glasses.
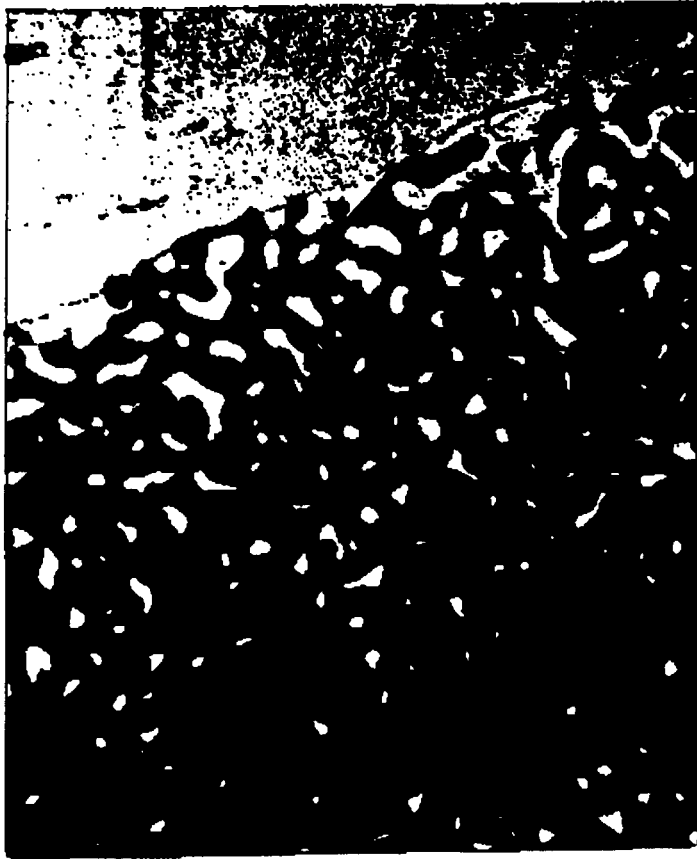
Fig. 3.07. Phase separation in a sodium borosilicate glass [11].

3.6. Corrosion

Glass is a thermodynamically metastable highly viscous liquid phase. When glass is placed in aqueous environments, various reactions such as ion exchange, hydrolysis and transformation to more stable phases occur simultaneously, and the effects of these reactions are generally referred to as 'corrosion'. Corrosion is a chemical or electrochemical attack on the surface of a glass material, thereby destroying the surface. Continual corrosion may penetrate or consume the material.

Borosilicate glass has been selected for the immobilisation of high-level nuclear waste from the geosphere and biosphere, because it is expected that borosilicate glass is durable and corrosion rates are very slow.

Waste glass corrosion and associated radionuclide release for the long term are the most important phenomena to be evaluated for safety assessment of the disposal system.
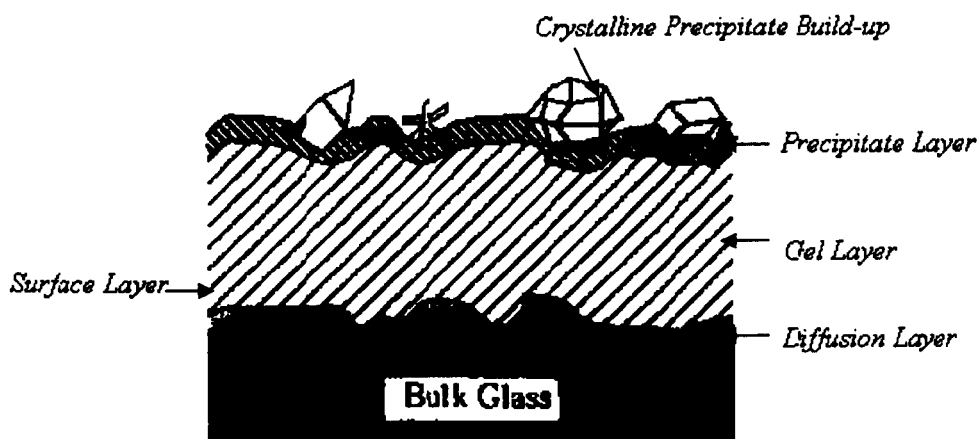
Fig. 3.08. Schematic representation of the glass surface exposed to water [12].

Corrosion studies on simulated waste filled glass performance have been studied in this regard. The waste glass performance for the long–term storage of many thousands of years cannot be measured directly, and it must be evaluated from short-term tests. Solubilities of actinides and fission products under disposal conditions are uncertain. The effects of various reactions and interactions occurring in the engineered barrier system, such as corrosion of overpack and canister and chemical interactions of the released glass constituents with them have not been fully investigated yet.

Radiation from alpha and beta decays of radionuclides in the waste glass can influence the glass performance by radiation damage to the solid glass, and by radiolysis of water and gases contacting the glass. This type of damage has been shown to increase the release rates of glass constituents up to four-fold during subsequent corrosion tests [13,14], although an annealing process may negate the radiation damage under actual disposal conditions. In addition to the solid glass itself, radiation may damage the secondary phases formed in the surface layers. And this is expected to greatly affect the release of less-soluble elements, because the equilibrium solubilities of solid phases in the solution vary depending on the crystallinity of solid phases. Ionizing radiation excites electrons, which lead to ionization of water molecules and dissolved gases to form reactive radicals and new molecules. The OH and O_2^- can influence the glass corrosion.

Studies on the waste glass corrosion have been focused on the reaction of glass with water. L. L. Hench et al. [15] and W. L. Ebert [16] have concluded that reaction of borosilicate waste glass is dominated by two primary reactions, ion

exchange reaction to release alkali metals and network hydrolysis to release boron and silicon. These reactions may dominate at different stages.

Ion exchange reaction involves a hydronium ion from a water molecule exchanging with the alkali metal, A^+ in the glass matrix, as shown in the following reaction:

$$\equiv Si - O - A + H^+ \leftrightarrow \equiv Si - O - H + A^+ , \tag{3.1}$$

$$\equiv Si - O - A + H_3O^+ \leftrightarrow \equiv Si - O - H + A^+ + H_2O \tag{3.2}$$
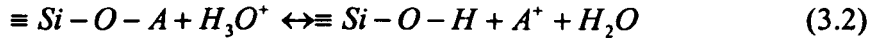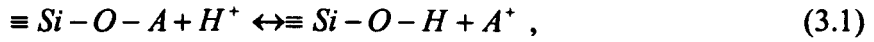
The ion exchange reaction increases the leachate pH value.

The major hydrolysis reactions for nuclear waste glasses can be expressed as follows:

$$\equiv Si - O - Si \equiv + OH^- \leftrightarrow \equiv Si - O^- + \equiv Si - O - H , \tag{3.3}$$

$$\equiv Si - O - Si \equiv + H_2O \leftrightarrow 2 \equiv Si - O - H . \tag{3.4}$$
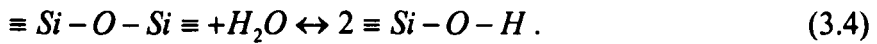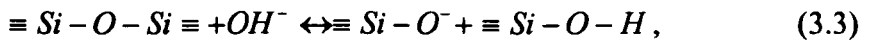
Network hydrolysis breaks down the glass network and leads to glass dissolution.

The waste glass contains some redox active elements. The equilibrium solubilities, precipitation and sorption reactions are greatly affected by redox conditions. Therefore, redox conditions can greatly affect the glass corrosion and associated radionuclide release in the repository environments. It is predicted that redox conditions in repository environments are reducing, because redox conditions in deep geological formations are weakly reducing, and corrosion of the steel overpack is expected to make them strongly reducing. In recent years, studies of the effects of redox conditions of solutions on glass corrosion have shown that they cannot have a large influence on the reactions of glass with water because major glass constituents such as Si, B and Na are not redox active. However, the release of redox active radionuclides, such as actinides and transition metals, is expected to be greatly affected by redox conditions [12]. On the other hand, redox conditions can greatly affect interactions of additional engineered barriers with the released glass constituents, which may influence the glass corrosion and associated radionuclide release [12].

3.7. Ionic conductivity and chemical durability

Mixed alkali glasses typically have higher chemical durability than single alkali glasses [17-20] but this generalization must be qualified by our knowledge that

chemical durability is a complex property, being highly dependent upon the test methods and conditions. In water and mildly acidic liquids, where the mechanism of chemical attack involves the exchange of alkali ions in a glass by protons from the surrounding media, the chemical durability of mixed alkali glasses parallels the change in alkali ion mobility reasonably well. In glasses where the alkali ion mobility controls the exchange rate for protons, the lower alkali ion mobility in mixed alkali glasses would be expected to lower the rate of chemical attack.

An adequate and generally applicable fundamental explanation for the mixed alkali effect in glass is still lacking. Properties related to alkali ion movement such as electrical conductivity, alkali exchange and thermal effects show the largest deviation from additivity, but the compositional dependence of these properties is entirely consistent with the change in alkali mobility in mixed alkali glasses. These properties depend upon the alkali ion of either higher or lower mobility and the magnitude of departure from linearity, as well as the composition at which the maximum or minimum is observed, correlate well with the relative mobility of the alkali ions.

It is known that when a second alkali oxide is added to an alkali silicate glass, the conductivities decrease sharply. This mixed-alkali effect is also found for mixed binary alkali silicate glasses [21], but the reason for the mobility reductions in terms of the mechanism of diffusion is uncertain [11]. Borate glasses also show the mixed alkali effect [22].

Although no data were found for ionic mobility in MW glasses, the knowledge acquired from this investigation may be used for future reference.

3.8. Radiation effects on glass

The major sources of radiation damage in high level nuclear waste forms are beta-decay of fission products. For example, ^{137}Cs has a half life $T_{1/2} = 30.00y \pm 73.05d$ and decays by β^- emission to ^{137}Ba. Approximately 85% of the β decays are through ^{137m}Ba and thus are accompanied by the emission of 662keV photons. ^{90}Sr is one of the most abundant fission products. It has a half-life $T_{1/2} = 29.12y \pm 87.66d$. ^{90}Sr is a pure β^- emitter and is often found in equilibrium with its daughter ^{90}Y. Beta decay of fission products is responsible for most of the heat generation and thermal events early in the history of the waste form.

Alpha decay becomes dominant and remains important after approximately 1000 years. The actinides in the high level waste glass decay by alpha particle emission e.g. ^{238}U ($T_{1/2}$ = 4.468 × 10^9y), ^{237}Np ($T_{1/2}$ = 144 ×10^6y), ^{239}Pu ($T_{1/2}$ = 24.11ky ± 40.00y), ^{241}Am ($T_{1/2}$ = 432.71y ± 182.62d).

Atomic displacements caused by the alpha decay event are responsible for the atomic scale rearrangement of the structure and hence, lead to the greatest change in the physical and chemical properties of the borosilicate glass. Some of the property changes as a result of radiation damage to waste glass have been described as follows.

3.8.1. Volumetric Changes

The density of HLW glasses can decrease, increase or remain unchanged as a result of radiation damage [23]. Volume change can cause internal stresses in the waste glass, particularly in partially devitrified glass where differential volume expansion can occur, and can also lead to possible strains in the metal canister. The glass density increases or decreases, depending on composition. The changes tend to follow an exponential behavior as a function of dose, and can be described by following equation

$$\frac{\Delta \rho}{\rho} = A[1 - \exp(-BD)] \qquad (3.5)$$

where ρ is the density of the glass, D is the dose due to α decay per cubic meter, A is the density change at saturation and B determines the rate of density change. These are all material – dependent parameters.

In an earlier work, the effects of radiation damage on borosilicate and phosphate glasses doped with ^{238}PuO$_2$ were studied [24, 25]. The changes in density as a function of cumulative dose in these glasses are shown in Figure 3.09. Borosilicate glass doped with ^{238}PuO$_2$ increased in length by 0.02% after 2 × 10^{24} alpha decay per m^3 at a storage temperature of 50°C and when stored at 170°C, the length increased by 0.4 % after an alpha exposure of 0.27 × 10^{24} per m^3 and then decreased slowly with dose [26].
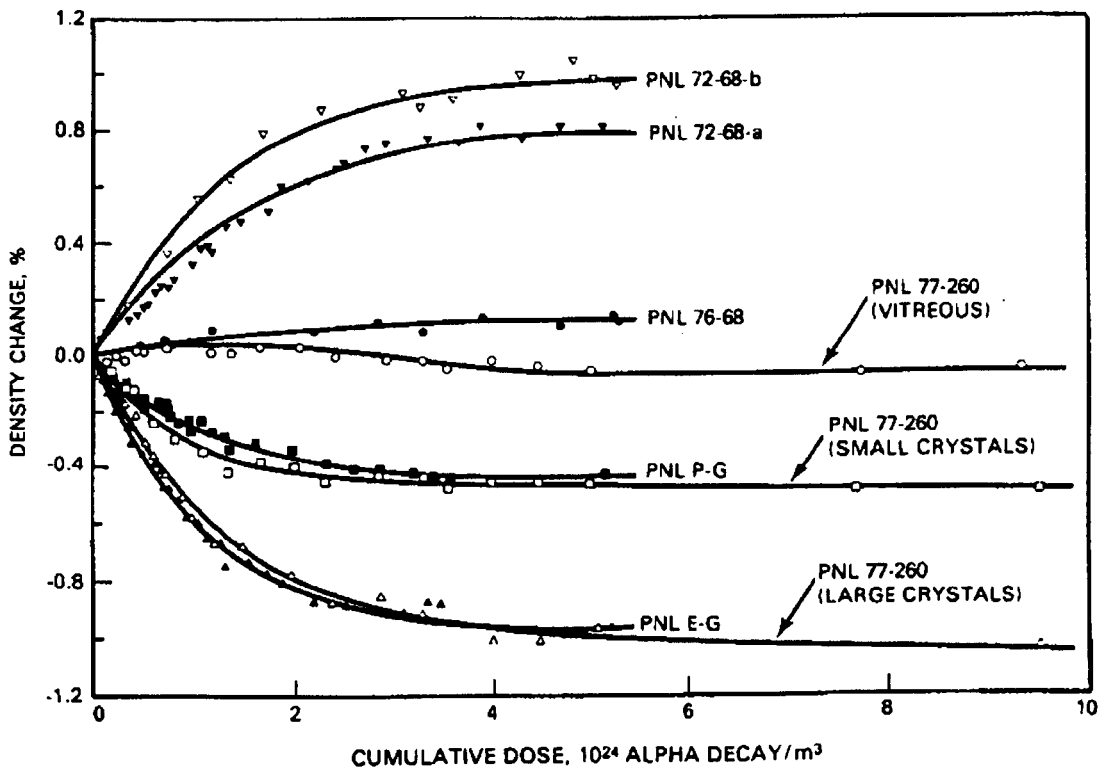
Fig. 3.09. Changes in density as a function of cumulative dose in borosilicate glass [23].

Gamma irradiation studies with ^{60}Co over a dose range from 10^8 to 10^{11} rad on some commercial borosilicate glasses showed radiation induced densification which increased with dose and apparently with boron content. The volume compaction observed was ~1.0 % [27].

3.8.2. Leach rate changes

The leach rate of a waste form is important in geologic disposal because the primary pathway of radionuclide migration to the biosphere begins with ground water leaching of the waste form. Radiation damage may affect the leach rate by producing physical and chemical changes in the waste form or by producing chemical changes in the surrounding environment, e.g. groundwater. Most data on the change in leach rate in actinide doped HLW glasses have been measured using the Soxhlet technique and calculated based on weight loss. The Soxhlet technique yielded fairly reproducible results; calculations based on weight loss can provide a better indication of actual leach rates [23]. Rauscher and Tischer [28] reported increased solubility of some commercial borosilicate glasses after neutron irradiation. The solubilities increased by a factor of 3 after flux of 1.4×10^{25} n/m^2.
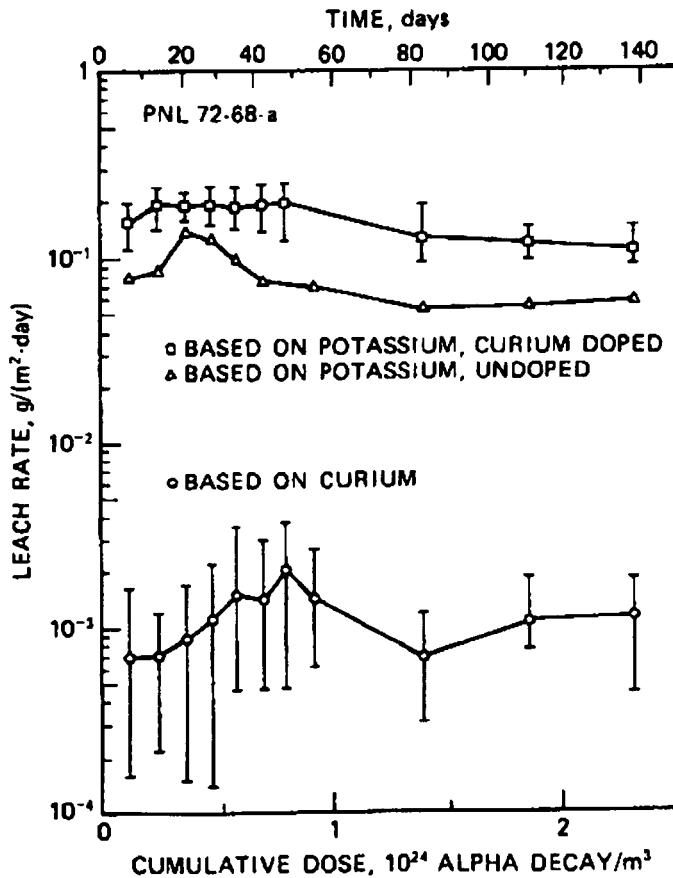
Fig. 3.10. Changes in leach rate as a function of cumulative dose in borosilicate glass [23].

3.8.3. Stored Energy Changes

The latent energy stored in a glass matrix as a result of irradiation, arises through atomic displacement. The stored energy is released as heat when the irradiated material is thermally annealed. If the quantity of stored energy is large and the release rate is high, an uncontrolled release could produce sudden excessively high waste-form temperatures. Such high temperatures could affect the physical and chemical properties of the waste forms and the integrity of the waste-form canister. The stored energy in simulated high-level waste glasses is released over a broad temperature range from about 100°C to 600°C [23, 29].

27

3.9. Previous work on borosilicate glasses

3.9.1. Introduction

The important requisites for the waste forms are thermo-physical, chemical and structural integrity. Low melting and glass transition temperatures enable a wide range of waste components to be dissolved in the glass but reduce resistance to change due to radiogenic heat. This means that waste loading must be low. From the literature the existing data suggest the glass transition temperature of borosilicate waste glasses is between ~ 450°C and 600°C, depending on the glass composition [30]. Thermal characterisation of glasses as a function of composition is an important requirement.

A number of techniques such as, DTA, AC impedance, dilatometry, dynamic leach testing can be applied in order to understand the thermo-physical and chemical behaviour of these glasses. At the same time, useful structural information can be determined by using NMR methods.

3.9.2. ^{11}B NMR and ^{29}Si NMR

The structural model of Dell, Bray and Xiao [31] is an extension of earlier work by Yun and Bray [32, 33]. They postulated that the single alkali borosilicate system can be subdivided into four regions in terms of alkali oxide/boron oxide ratios, R. These regions are:

Region 1: $R < 0.5$

In this region the system behaves like a binary borate system. Any added alkali goes to convert three-coordinated boron to four-coordinated boron. The interaction between the borate and silicate network is expected to be negligible. The [BO$_3$] and [BO$_4$] units present at $R = 0.5$ are hypothesised to exist in diborate groups, having the formula $A_2O.2B_2O_3$.

Region 2: $0.5 \leq R \leq R_{max} = \frac{1}{2} + \frac{1}{16}K$

K is defined as the ratio between mol % SiO$_2$ and mol % B$_2$O$_3$. In this region, alkali oxide combines with [BO$_3$] and [BO$_4$] units, in the form of diborate ($A_2O.2B_2O_3$) and reedmergnerite units $\frac{1}{2}(A_2O.B_2O_3.8SiO_2)$ a boron tetrahedron

bonded with four silica tetrahedra. The conversion of diborate groups to reedmergnerite units can be written by assuming if m moles of A_2O are added to the R = 0.5 composition, then for one mole of B_2O_3:

$$\tfrac{1}{2}(A_2O.2B_2O_3) + K(SiO_2) + m(A_2O) \longrightarrow (\tfrac{1}{2}-m)(A_2O.2B_2O_3)$$

$$+ 2m(A_2O.2B_2O_3.8SiO_2) + (K - 16m)SiO_2 \qquad (3.6)$$
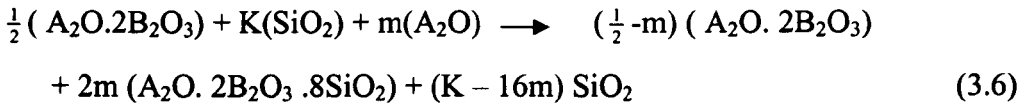
This process ends when K = 16m or when R = R_{max} = $\tfrac{1}{2} + \tfrac{1}{16}$ K
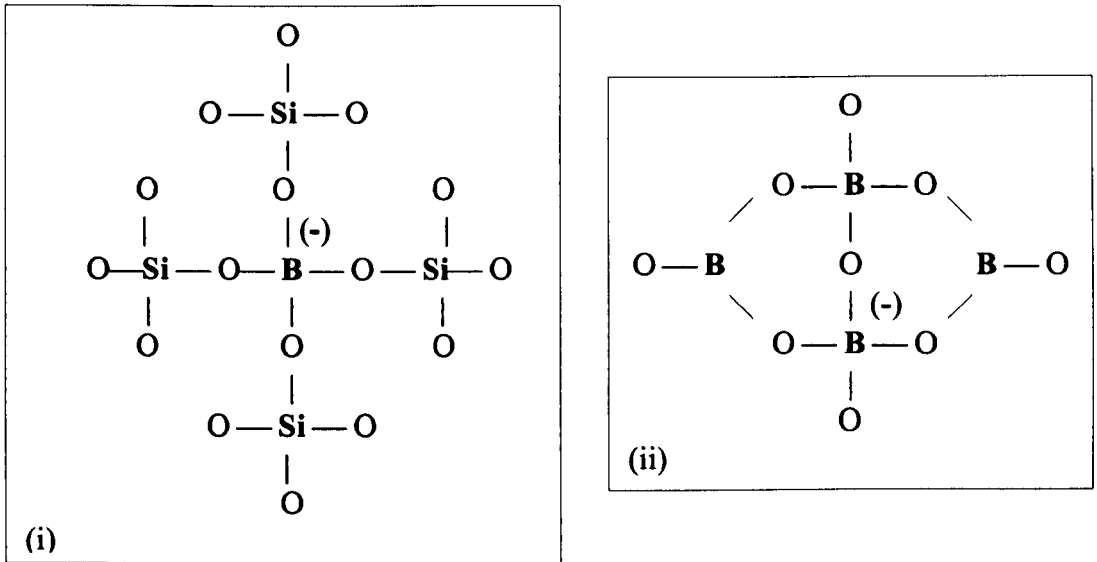
Fig. 3.11. (i) Reedmergnerite ($\tfrac{1}{2}$ ($A_2O.B_2O_3.8SiO_2$)) and (ii) *Diborate ($A_2O.2B_2O_3$) units hypothesised from boron NMR.*

Region 3: $R_{max} \le R \le R_{d1} = \tfrac{1}{2} + \tfrac{1}{4}K$

In this region, the alkali oxide combines with reedmergnerite groups forming non-bridging oxygens (NBOs) on the silica tetrahedra. This means that the amount of boron tetrahedral unit [BO_4] will not change in this region.

At the end of this process each pair of reedmergnerite groups has absorbed 1.5 additional molecules of A_2O

$$R_{d1}(A_2O).B_2O_3.K(SiO_2) = (\tfrac{1}{2} - \tfrac{1}{16}K)(A_2O.2B_2O_3)$$

$$+ \tfrac{1}{8}K(2.5\ A_2O.B_2O_3.8SiO_2) \qquad (3.7)$$
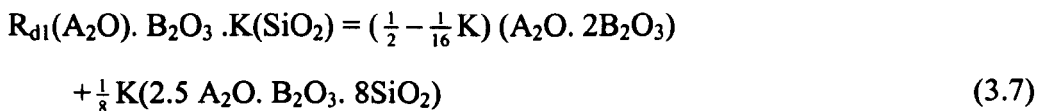
Region 4: $R_{d1} \leq R \leq R_{d3} = 2 + K$

The alkali oxide combines with the diborate groups and reedmergnerite groups to form pyroborate units and silica tetrahedra with two NBOs per silicon atom. In this region the alkali oxide divides itself proportionately between the diborate and reedmergnerite groups according to the total number of B and Si atoms in each. If m_1 moles of A_2O combine with the diborate groups and m_2 moles of A_2O combine with the reedmergnerite groups, the process can be written as:

$$(\tfrac{1}{2} - \tfrac{1}{16} K)(A_2O. \ 2B_2O_3) + m_1(A_2O) \longrightarrow$$

$$(\tfrac{1}{2} - \tfrac{1}{16} K - \tfrac{1}{3} m_1)(A_2O. \ 2B_2O_3) + \tfrac{2}{3} m_1(2A_2O. \ B_2O_3) \qquad (3.8)$$

and

$$\tfrac{1}{8} K(2.5 \ A_2O. \ B_2O_3. \ 8SiO_2) + m_2(A_2O) \longrightarrow$$

$$(\tfrac{1}{8} K - \tfrac{2}{15} m_2)(2.5 \ A_2O. \ B_2O_3. \ 8SiO_2)$$

$$+ \tfrac{2}{15} m_2[(2 \ A_2O. \ B_2O_3) + 8(SiO_2 + A_2O)] \qquad (3.9)$$
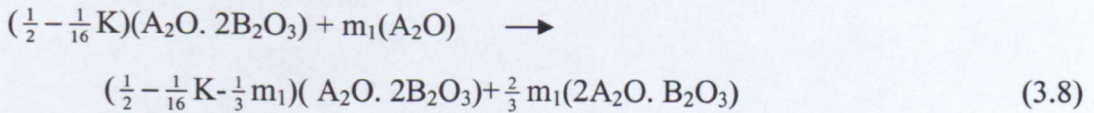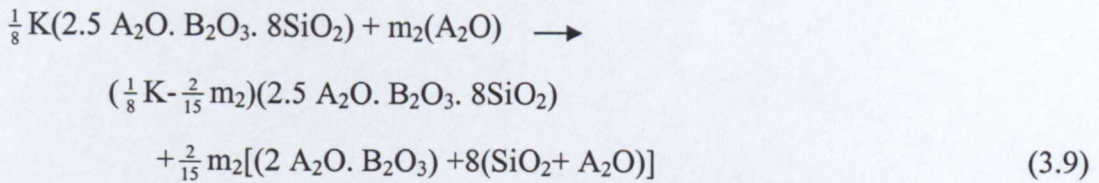
where $(m_1 + m_2) = R - R_{d1}$ and $m_1/m_2 = (2 - K/4)/(K + K/4)$

These processes end when the diborate and reedmergnerite units are fully converted to pyroborate unit. This happens at $R_{d3} = (m_1 + m_2) + R_{d1} = 2 + K$ at this point $N_4 = 0$ and $N_3 = 1$. Theoretical analysis of this model shown in Figure 3.12.
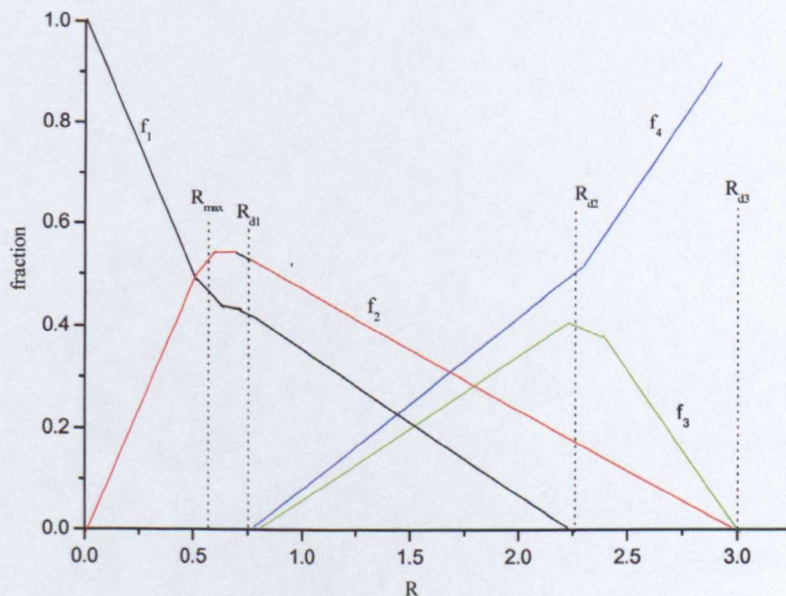
Fig. 3.12. Change in fraction of borate units present in the alkali borosilicate system [31].

From Figure 3.12 it can be seen that at low alkali content, trigonal borate units f_1 i.e [BO$_3$] are steadily converted to tetrahedral f_2 i.e [BO$_4$] units. This process continues till R_{d1}.

At this point, the trigonal boron units with one or two NBOs f_3 and f_4, begin to form with decrease in the f_1 and f_2 fraction. At high values of R, the f_4 unit is expected to become dominant, until the network is sufficiently disrupted that glass formation becomes impossible, due to the large number of NBOs.

Fraction of unit	Region	Fraction of borate unit present
f_1		R
f_2		1-R
f_3	$0.5 \leq R \leq R_{max}$	0
f_4		0
f_1		R_{max}
f_2		$1 - R_{max}$
f_3	$R_{max} \leq R \leq R_{d1}$	0
f_4		0
f_1		$(1-K/8).[\tfrac{3}{4} - R/(2+K)]$
f_2		$(8+K).(\tfrac{1}{12} - R/(24+12K))$
f_3	$R_{d1} \leq R \leq R_{d2}$	$\tfrac{1}{3}(R-R_{d1}).(2-K/4)/(2+K)$
f_4		$\tfrac{1}{2}(R-R_{d1}).(2-K/4)/(2+K)$ $+\tfrac{2}{3}(KR/(8+4K)-K/16)$
f_1		0
f_2		$(8+K).(\tfrac{1}{12}) - R/(24+12K))$
f_3	$R_{d2} \leq R \leq R_{d3}$	$(\tfrac{2}{3} -K/6).(1- R/(2+K))$
f_4		$\tfrac{1}{2}(1-K/8) + (R-R_{d2}).(2-K/4)/(2+K)$ $+ \tfrac{2}{15}(5KR/(8+4K) - 5K/16)$

Table 3.01. Equations used to calculate the fractions of each borate unit present in the four regions [31].

Information regarding the arrangements of silicon atoms in the borosilicate glass has been obtained from ^{29}Si MAS NMR. The chemical environment around the silicon atom changes as the alkali concentration increases. ^{29}Si MAS NMR has been used to analyse the short-range order in alkali borosilicate glasses by Martin et al. [34] and Mackenzie [35]. Based on earlier studies on alkali silicate glasses, they found that as the amount of alkali oxide increased the chemical shift of the silicon peak moves to

31

more positive values. This indicates that depolymerisation of the silicate network is taking place as the number of Si-O-Si decreases. The rate of depolymerisation is related to the value of K, the ratio of silica to boron oxide. It can be explained by the fact that higher silica concentration in the glass requires more alkali to be added for the modifications to be observed [35].
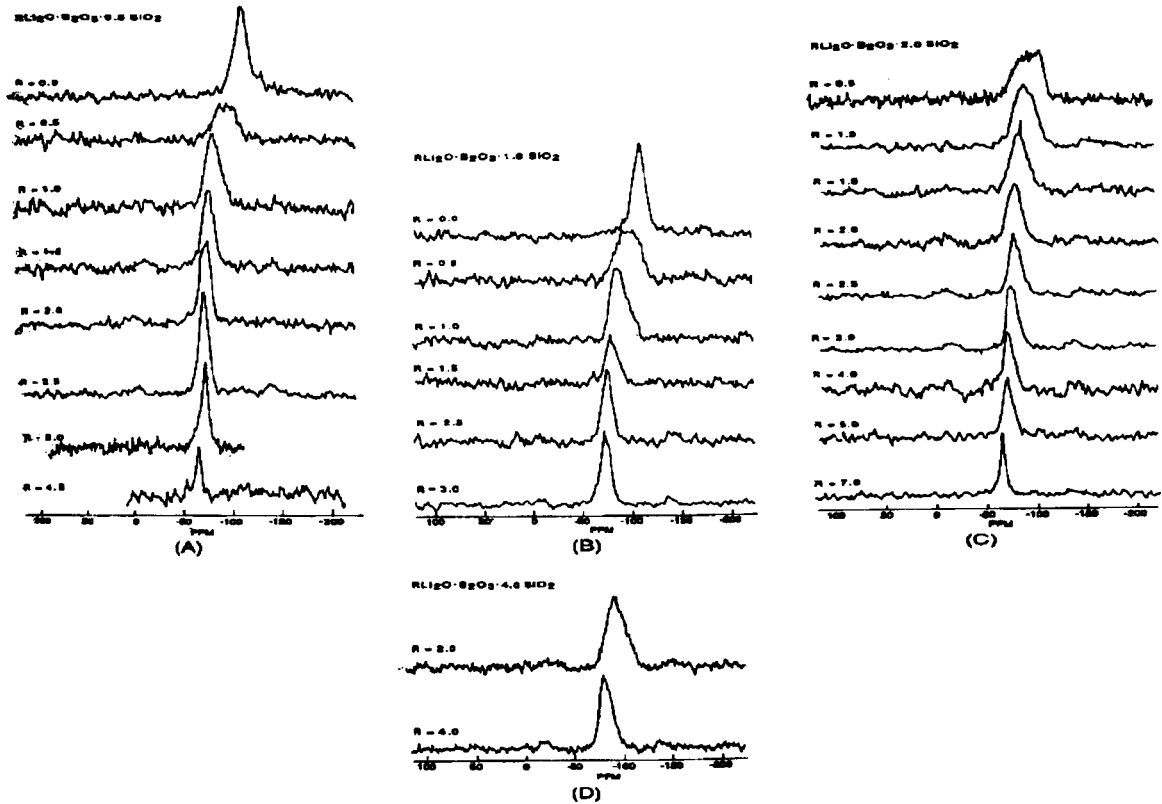
Fig. 3.13. ^{29}Si MAS-NMR spectra for lithium borosilicates as a function of R (molar ratio of lithia to boron oxide) for K (molar ratio of silica to boron oxide families : (A) K = 0.5, (B) K= 1.0 (C), K = 2.0, (D) K= 4.0 [34].

3.9.3. Wu et al. [36] Zhong et al. [37] and Martin et al. [38, 39] Models

The models of Wu et al. [36] and Zhong et al. [37] are based on ^{11}B NMR studies of the sharing of lithia in lithium borosilicate glasses. Both models propose a proportional sharing of the alkali between the borate and silicate networks after a certain value of R, R_{max}, is reached. The hypothesis is that for $R < R_{max}$, all alkali introduced into the glass is incorporated into the borate network. In order to

generalize this model for all alkali borosilicate glasses it is useful to divide R into two components: R_{Si} is the alkali associated with the silicate network and R_B is the alkali associated with the borate system, $R = R_{Si} + R_B$. The number of oxygens added per silicon is equal to the amount of alkali entering the silicate network, divided by the amount of silica in the glass. The equations for R_{Si} and the number of added oxygen per silicon $\frac{O_a}{Si}$ are as follows:

$$R_{Si} = 0, \quad \frac{O_a}{Si} = 0, \ R \leq R_{max} \tag{3.10}$$

$$R_{Si} = \frac{(R - R_{max})K}{(1 + K)}, \frac{O_a}{Si} = \frac{R - R_{max}}{1 + K}, R_{max} \leq R \leq R_{max} + 2(1 + K) \tag{3.11}$$

where the upper limit of R is determined by the formation of the Q_0 unit.

The models by Wu et al. [36] and Zhong et al. [37] differ in the values that they propose for R_{max}. Wu et al. suggest that R_{max} is 0.4 for all families of K while Zhong et al. [37] suggest that R_{max} varies as a function of K, with the values shown in Table 3.02.

On the other hand, the model of Martin et al. [38, 39] is based on ^{29}Si NMR of lithium and potassium borosilicates, and can be expressed in terms of the previous two models by setting $R_{max} = 0$.
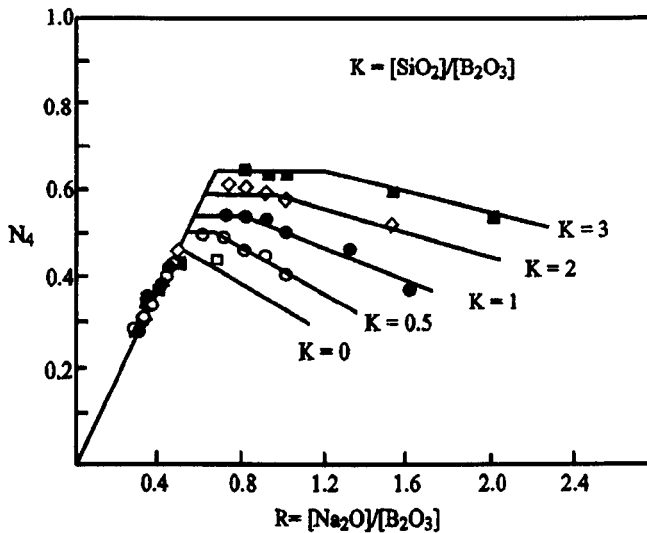
Fig. 3.14. The fraction of tetrahedrally coordinated boron (N₄) as a function of the R and K ratios in sodium borosilicate glasses [37].

K	R_{max}
0.5	0.270
1.0	0.279
2.0	0.312
4.0	0.408

Table 3.02. R_{max} values as a function of K as determined by Zhong et al.[37] from their ^{11}B NMR studies of lithium borosilicate glasses.

3.9.4. Multi component borosilicate glass

The effect of divalent additives on the structure of alkali borosilicate glass is important in order to predict the durability of the waste form. The change in structure in waste glass can be determined by the nature of the oxide being added, i.e whether it is a glass former, intermediate or modifier. Glass formers and intermediates behave in similar ways, that is they can enter the structure and consume the oxygen from the alkali oxide in preference to the boron network, converting the [BO$_4$] into [BO$_3$] units, thus reducing the value of N$_4$. Glass formers tend to cause the conversion of the [BO$_4$] units into the symmetric trigonal borate unit (f$_1$).

If the divalent oxide enters in the structure as a modifier, the trend of N$_4$ as a function of additives is similar to that observed in alkaline earth borate glass, shown in Figure 3.15. It was found that N$_4$ increased with alkaline earth content, and attained maximum values at a composition depending on the M^{2+} ion type [40].

El-Damrawi et al. [41] found that some of the alkali oxide must associate itself with the silicate part of the glass, and therefore form NBOs even below R$_o$. If it is assumed that the A$_2$O associate with MO first and the borate network second before the remainder is consumed by the silicate network [41], then, if the mol% of A$_2$O, [A$_2$O] present is greater than mol% of MO, [MO], the amount of A$_2$O that is left to be incorporated into the borate and silicate networks $= [A_2O(a)]$, can be calculated using equation (3.12). Using the value of N$_4$ obtained from ^{11}B MAS-NMR, the amount of modifier A$_2$O i.e. (Na$_2$O+Li$_2$O) associated with the borate network $= [A_2O(b)]$, is derived from equation (3.13). Finally, the amount of A$_2$O remaining to be used by the silicate network $= [A_2O(Si)]$, can be easily calculated from equation (3.14), all values are in mol%.

34

$$[A_2O(a)] = [A_2O] - [MO] \qquad (3.12)$$

$$[A_2O(b)] = N_4[B_2O_3] \qquad (3.13)$$

$$[A_2O(Si)] = [A_2O(a)] - [A_2O(b)] \qquad (3.14)$$

If the additive oxide is a modifier, then equation (3.12) becomes

$$[A_2O(a)] = [A_2O + MO] \qquad (3.15)$$

The NBO/ Si can be determined from the following relation:

$$NBO/Si = [A_2O(Si)/(SiO_2/2)] \qquad (3.16)$$
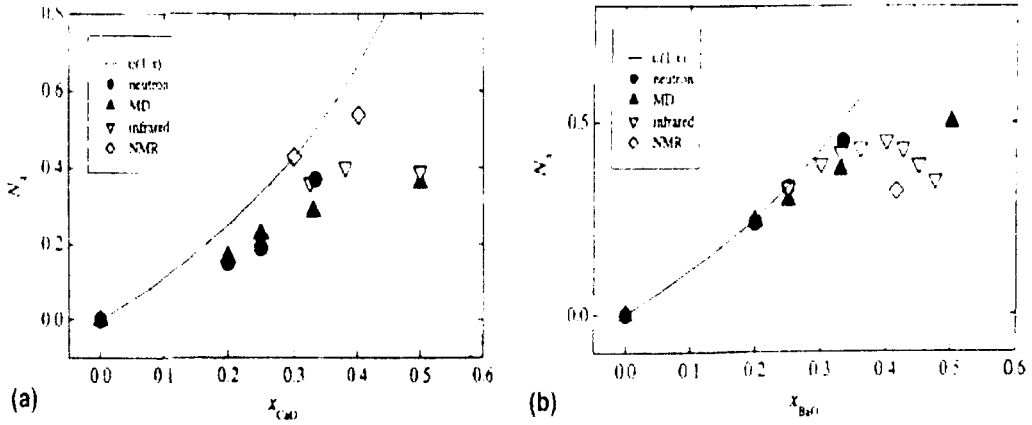
Fig. 3.15. Fraction of four-coordinated boron atoms N_4 as a function of mole fraction (a) CaO and (b) BaO content in $MO.nB_2O_3$ (M = Ca and Ba, n=2,3 and 4) [from 42].

3.9.5. Structure and chemical durability of zinc-containing glasses [43]

The ability of zinc oxide to improve the mechanical properties and chemical durability of silicate glasses has been known for a long time. For example the glass system $Na_2O-Li_2O-ZnO-SiO_2-B_2O_3$ was investigated in order to define the structural role of Zn(II) ions using X-ray diffraction. It was concluded that the transition metal atom is surrounded by approximately four oxygen neighbours at distances expected for fourfold coordination [43]. Recently [44,45] zinc borosilicate glasses, whose leaching rate is constantly reduced by increasing ZnO content, have been studied by Rutherford back scattering. The existence of a surface layer poor in zinc and rich in

silicon has been observed. The improved durability of zinc glasses is not due to a surface layer effect, but to bulk structural properties [44,45].

3.9.6. XRD study of manganese-containing borosilicate glasses [46]

Borosilicate glasses containing different concentrations of manganese dioxide up to 30 mol% were prepared, their physical characteristics studied and the crystalline product formed identified [46]. The presence of a crystalline Mn_7SiO_{12} phase in the glasses with > 20 mol% of MnO_2 was detected. No other crystalline phase in the ternary system Si-Mn-O was detected in the otherwise homogeneous glass.
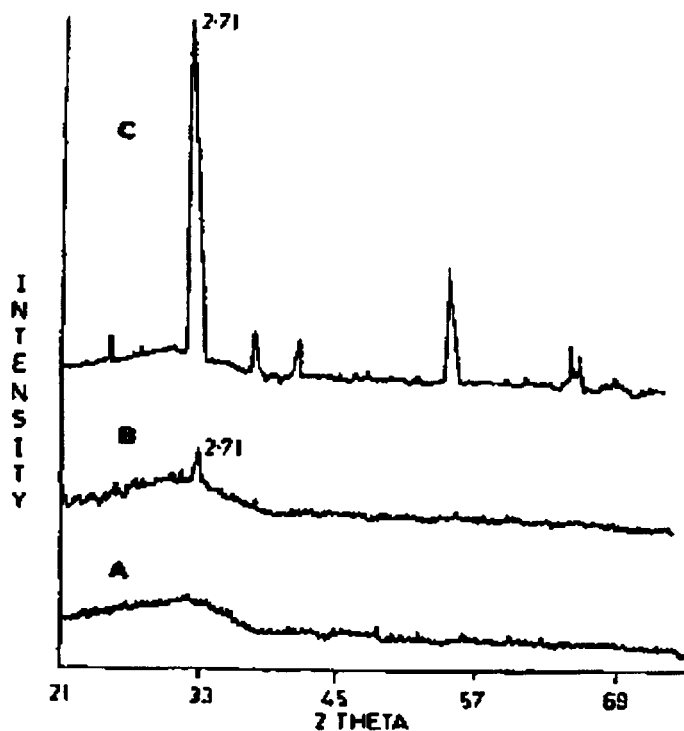
Fig. 3.16. XRD patterns of selected glass composition in the SiO_2–Na_2O-B_2O_3 glass system containing (a) 20, (b) 25, and (c) 30 mol% MnO_2 [from 46].

3. 10. References

[1]   J. E. Shelby, Introduction to Glass Science and Technology, Royal Society of Chemistry, Cambridge (1997) 27.

[2]   H. Rawson, Properties and Applications of Glass, Elsevier, New York (1980) 29.

[3]   W. J. Zachariasen, J. Am. Ceram. Soc. **54** (1932) 3841.

[4]   P. J. Bray and J. G. O'Keefe, Phys. Chem. Glasses **4** (2) (1963) 37.

[5]   Y. H.Yun and P. J. Bray, J. Non-Cryst. Solids **44** (1981) 227.

[6]   S. A. Feller, W. J. Dell and P. J. Bray, J. Non-Cryst. Solids **51** (1982) 21.

[7]   Y. H.Yun and P. J. Bray, J. Non-Cryst. Solids **44** (1981) 227.

[8]   G. E. Jellison, S. A. Feller and P. J. Bray, Phys. Chem. Glasses **19** (3) (1978) 52-53.

[9]   W. J. Clarida, J. R. Berryman, M. Affatigato, S. A. Feller, Phys. Chem. Glasses **44** (3)(2003) 215-217.

[10]   J. Zhong and P. J Bray, J. Non-Cryst. Solids **111** (1989) 67.

[11]   R. H. Doremus, Glass Science, 2nd edition, John Wiley and Sons (1994).

[12]   Y. Inagaki, H. Furuya, K. Idemitsu & T. Arima, Progress in Nuclear Energy **32** (3/4) (1998) 501-508.

[13]   W. J. Weber, Nucl. Inst. Methods in Phys. Res. **B62** (1988) 471.

[14]   W. J. Weber, J. W. Walad and G. L. McVay, J. Am.Ceram. Soc. **68** (1985) C253.

[15]   L. L. Hench, D. E. Clark, A. B. Harker. J. Mat. Science **21** (1986) 1457-78.

[16]   W. L Ebert Phys.Chem. Glasses **34** (2)(1993) 58-65.

[17]   C. J. Peddle, J. Soc. Glass Technol. **5** (1921) 195.

[18]   L. S. Yastrebova and N. I. Antonova, Inorg. Mater. Consult. Bur. Transl. **3** (1967) 327.

[19]   S. Sen and F. V. Tooley, J. Am. Ceram. Soc. **8** (1935) 175.

[20]   D. Hubbard, M. H. Black, S. F. Holley and G. F. Rodgers, J. Res. Nat. Bur. Stand **46** (1951) 168.

[21]   B. Lengyel and Z. Boksay, Z. Phys. Chem. **203** (1954) 93; **204** (1955) 157.

[22]   H. Jain, H. L. Downing and N. L. Peterson, J. Non-Crystalline Solids **64** (1984) 335.

[23]   W. J. Weber and F. P. Roberts, Nuclear Technology **60** (1983)178-198.

[24]   G. Malow, J. A. C. Marples and C. Sombert, Radioactive Waste Management and Disposal (1980) 341.

[25]   R. Simon and S. Orlowski, Radioactive Waste Management and Disposal, Harwood Academic Publishers, Switzerland (1980).

[26]   A. R. Hall, J. T. Dalton, B. Hudson and A.C. Marples, IAEA-SEM-207 (2) (1976) 3.

[27]   J. E. Shelby, J. Appl. Physics **51** (1980) 2561.

[28]   H. E. Rauscher and R. E. Tischer, The effect of $^{10}B(n,d)^{7}Li$ Reactions on the solubility of Borosilicate Glasses' L-241, Corning Glass Works, Corning, New York (1964).

[29]   F. P. Roberts, G. H. Jenks and C. D. Bopp, 'Radiation Effects in Solidified High-Level Wastes, Part1, Stored Energy'' BNWL (1944) (Richland, W A: Pacific Northwest Laboratory (1976).

[30]   W. Lutze and R. C. Ewing, Scientific Basis for Nuclear Waste Management XII, MRS, **127** (1989) 153 -162.

[31]   W. J. Dell, P. J. Bray and S. Z. Xiao, J. Non-Cryst. Solids **58** (1983) 1-16.

[32]   Y. H. Yun and P. J. Bray, J. Non-Cryst. Solids **44** (1981) 227.

[33]   Y. H. Yun and P. J. Bray, J. Non-Cryst. Solids **27** (1978) 363-80.

[34]   S. W. Martin, D. Bain, K. Buddhwani and S. Feller J. Am. Ceram. Soc. **75** (5) (1992) 1117-22.

[35]   J. W. Mackenzie, A. Bhatnagar, D. Bain, S. Bhowmik, C. Parameswar, K. Budhwani, S. A. Feller, M. L. Royle and S. W. Martin, J. Non-Cryst. Solids **177** (1994) 269.

[36]   X. W. Wu, F. Tian, X. Q. Zhang, L. Z. Pan and S. L. Wu in: collected Papers, 14th Int. Congr. On Glass **1** (1986) 32.

[37]   J. Zhong, X. Wu, M. L. Liu and P. J. Bray, J. Non-Cryst. Solids **107** (1988) 81-87.

[38]   S. W. Martin, D. Bain, K. Budhwani and S. Feller, J. Am. Ceram. Soc. **75** (1992) 1117.

[39]   S. W. Martin, A. Bhatnagar, C. Parameswar and S. Feller, J. Am. Ceram Soc. (1993).

[40] H. Yamashita, K. Inoue, T. Nakajin, H. Inoue and T. Maekawa, J. Non-Cryst. Solids **331** (2003) 128-136.

[41] G. El-Damrawi, W. Müller-Warmuth, H. Doweidar and I. A. Gohar, Phys. Chem. Glasses **34** (1993) 52-57.

[42] N. Ohtori, K. Takase, and I. Akiyama, J. Non-Cryst. Solids **293-295** (2001) 136-145.

[43] G. Ennas, A. Musinu and G. Piccalua, J. Non-Cryst. Solids **125** (1990) 181-185.

[44] G. Della Mea, A. Gassparotto, M. Bettinelli and A. Montenero, J. Non-Cryst. Solids **84** (1986) 443.

[45] A. Montenero, E. Ferraguti, G. Ingletto and M. Bettineli, J. Non-Cryst.Solids **84** (1986) 452.

[46] J. G. Shah, V. A. Patki, Waste Management **15** (5/6)(1995) 417- 421.

Chapter 4
Experimental Techniques

4.1. Glass Preparation

All the samples were prepared from high purity sodium tetraborate ($Na_2B_4O_7$), lithium carbonate (Li_2CO_3), sodium carbonate (Na_2CO_3) and reagent grade silica (SiO_2) by fusion with different additives. Glass systems xBaO(1-x) MW, xPbO(1-x) MW and xZnO(1-x) MW, have been prepared with the additives in the range $2.4 \leq x \leq 15$ mol% and the systems xMnO(1-x) MW, xCaO(1-x) MW and xSrO(1-x) MW have been prepared in the range $2.4 \leq x \leq 11.98$ mol%. Where MW is the base glass defined in Table 4.01.

Details of glass composition are given in Table 4.01.The spin lattice relaxation time for the Si nucleus is generally very long (from a few minutes to an hour) but can be shortened by spin diffusion from paramagnetic centres [1]. Therefore 0.1 mol% Fe_2O_3 was added to all glasses, except for the system containing MnO, for NMR experiments.

Sample Name	Mol %				
	SiO_2	B_2O_3	Na_2O	Li_2O	$^*M''O$
MW	60.61	18.57	10.54	10.28	0
$^*M''2$	59.1	18.1	10.29	10.04	2.4
$M''3$	58.31	17.9	10.15	9.92	3.62
$M''4$	57.6	17.65	10.03	9.79	4.83
$M''7$	56.16	17.20	9.74	9.55	7.25
$M''9$	54.68	16.75	9.52	9.29	9.66
$M''11$	53.28	16.32	9.27	9.05	11.98
$M''15$	51.45	15.76	8.95	8.74	15

$^*M'' = $ Ba, Sr, Ca, Mn, Zn and Pb

Table 4.01. The compositions of HLW glasses used for the present study.

All compositions were thoroughly mixed and placed into a 90% Pt 10% Rh crucible and heated in an electric furnace to 1350°C. After reaching this temperature, the melt was held for about 20 minutes at this temperature and then poured into de-ionised water to produce a frit, which was then allowed to dry. A small amount of the dried frit was taken for DTA, to determine glass transition temperature, and checked for amorphicity by X-ray diffraction. The dried glass frit was then replaced in the crucible and remelted at the same temperature. After reaching the melting temperature the melt was held for about 10 minutes, at this temperature, and then poured into the required mould to form a suitable glass block. The resulting glass block was annealed for 4 hours at a temperature 50°C below the glass transition temperature (determined by DTA measurement).

4.2. Glass Characterisation Techniques
4.2.1. X-ray diffraction

Samples were examined to determine if they contained any crystals using the X-ray diffraction method. If no crystals were detected, the sample was deemed to be glass, if crystals were detected, it was described as either partially or fully crystallised depending upon the extent of crystallisation.

Bragg has shown that any diffracted ray can be regarded as if it were reflected from a three-dimensional lattice, which has an infinite number of sets of equally spaced planes. The diffracted beams are found only when reflections from parallel planes of atoms interfere constructively, which occurs when:

$$n\lambda = 2d\sin\theta \qquad (4.1)$$

where n is an integer, λ is the wavelength of X-radiation, d is the distance between adjacent planes and θ is the angle of the incident and outgoing radiation (Figure 4.01).

A typical spectrum for glass material is shown in Figure 4.02. If there are crystalline phases within the glass sample, sharp peaks will also be observed. An example of a fully crystalline sample is shown in Figure 4.03.

X-ray diffraction spectra were obtained from glass powder samples in an aluminium holder using a Philips X-ray generator (at 40 kV, 30 mA) with a CuK$_\alpha$ source and horizontal goniometer. Crystalline samples were examined using a high resolution Bruker D5005 X-ray diffractometer (at 40 kV, 30 mA) with CuK$_\alpha$

radiation. The diffracted X-ray intensity was scanned through a 2θ range of 10° to 70° using a step size of 0.02° and a count time of 8 seconds.
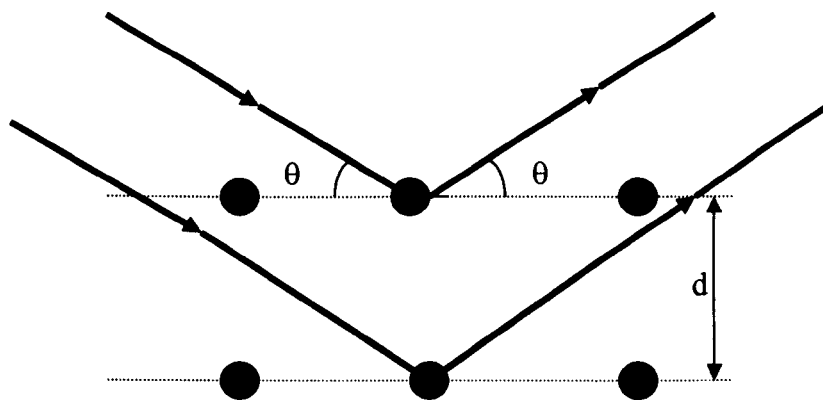
Fig. 4.01. Schematic representation of parallel scattering planes in a crystal lattice. The dashed lines are the planes of atoms.
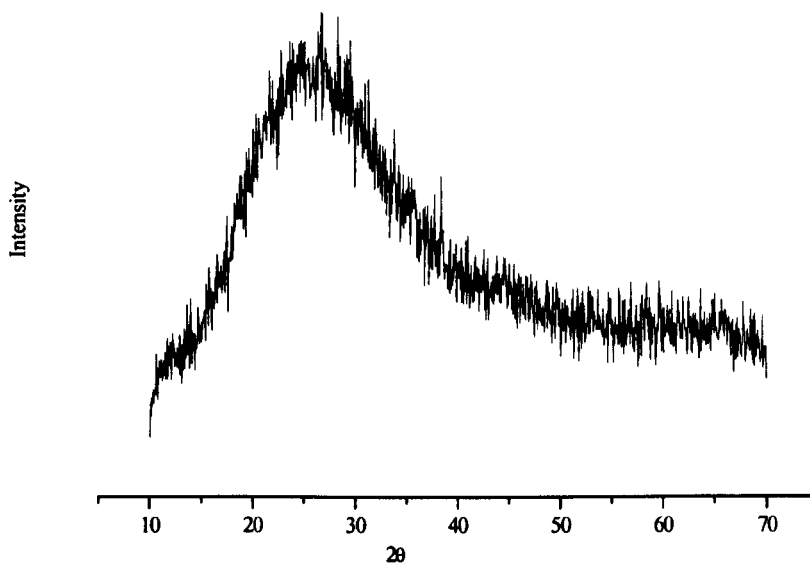
Fig. 4.02. Typical X-ray spectrum obtained from a glass sample MW-ZnO.
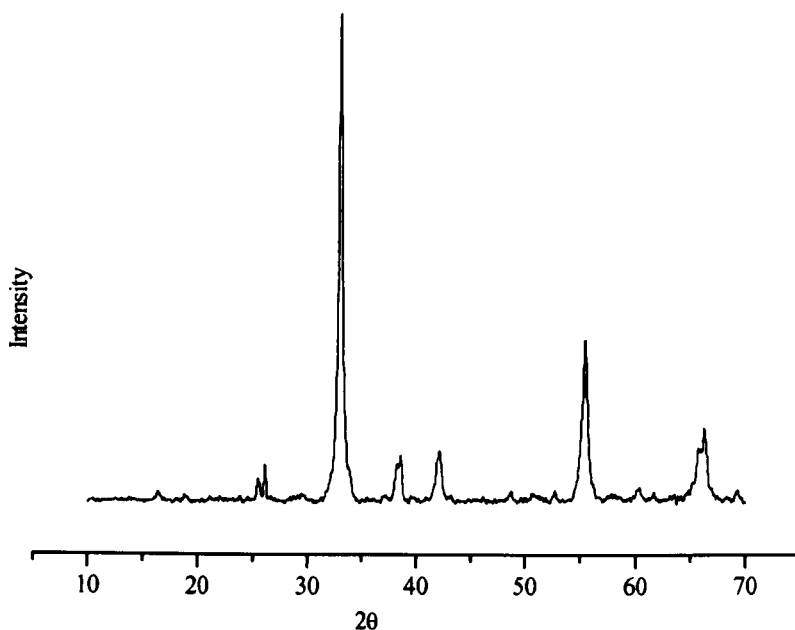
Fig. 4.03. High resolution XRD trace, peaks attributed to crystallisation phase present in the MW-MnO glass system.

4.2.2. Differential Thermal Analysis (DTA)

Differential thermal analysis is a simple and widely used thermal analysis technique. The difference in temperature ΔT, between sample and reference material is recorded while both are subjected to the same heating program.

The sample and reference material are heated in the furnace, within symmetrical cavities in an alumina head. This has low thermal conductivity to ensure an adequate differential temperature signal during a thermal event. If an endothermic thermal event occurs in the sample, the temperature of the sample T_1 will lag behind the temperature of the reference, T_2, which follows the heating program. The output from thermocouples $\Delta T = T_1 - T_2$, is recorded against T_2 (or the furnace temperature; $(T_f \approx T_2)$. If an exothermic process occurs in the sample, the response will be in the opposite direction. 90% platinum 10 % rhodium sample crucibles were used for the present study.

43
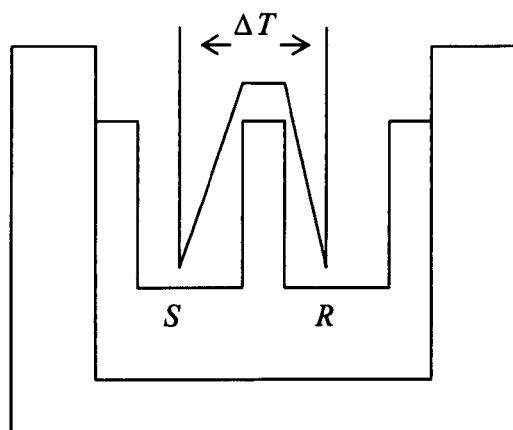
Fig. 4.04. Schematic diagram of DTA apparatus showing positions of sample (S) and reference(R).

The thermal behaviour of the glass was studied on powder samples using a Stanton Redcroft 673-4 DTA-1200. An alumina or quartz reference was used and approximately 0.1g of each sample was placed in the crucible and heated at 10°C/min over the temperature range 10-950°C. The glass transition temperature (T_g) was determined from the pseudo second order inflection in the ΔT versus T plot.

A simple DTA arrangement is shown in Figure 4.04 and a typical DTA plot for MW BNFL base glass system is shown in Figure 4.05.
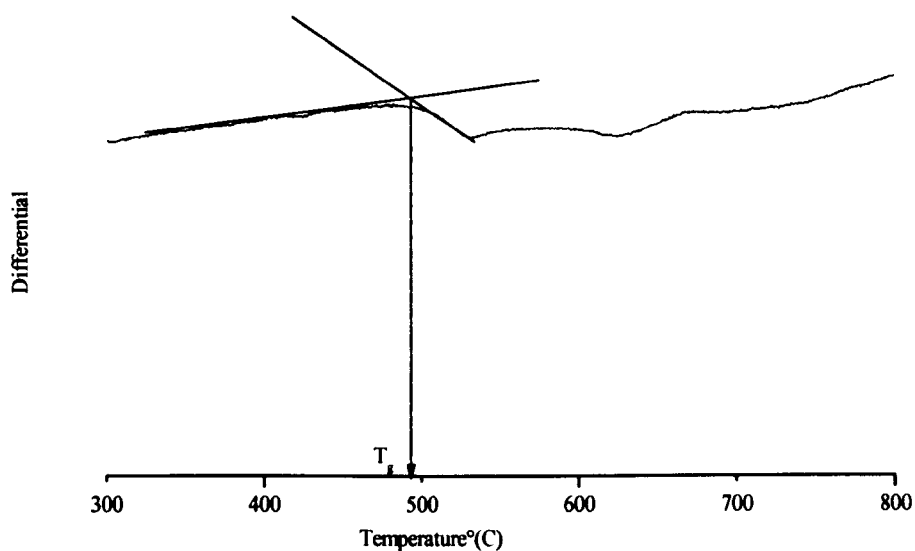
Fig. 4.05. A Typical DTA graph showing the glass transition temperature (T_g).

4.3. Density Measurement

Density measurements are much more sensitive to variations in glass composition than any other physical property of glass and they can be used to investigate the structure of the glassy network to a certain extent [2]. Since the density of glasses is controlled by the free volume of the vitreous network and masses of the ions present [3], the addition of species that enter interstices of the vitreous network generally tends to increase density by reducing the free volume. The addition of other ions into a glass alters the density in proportion to the mass of the added ions, relative to that of the ions already present in the glass [3].

Glass density ρ, was determined for bulk samples by the Archimedes method. The density (ρ) and molar volume (V_M) of the glass were calculated using equations (4.2) and (4.3) respectively.

$$\rho = \frac{W_a \rho_L}{W_a - W_w} \tag{4.2}$$

where W_a is the weight of the sample in air and W_w the suspended weight of the sample in de–ionized water, ρ_L is the density of the displacement fluid, de–ionised water.

$$V_M = \frac{M}{\rho} \tag{4.3}$$

where M is the molar weight of the glass composition.

4.4. Dilatometry

The coefficient of thermal expansion has a significant effect during the manufacture of vitrified products. The thermal expansion of vitreous bonding systems is dependent on the oxide content of the glass, the additive property of various oxides contributing to the overall coefficient of thermal expansion of any glass. Thermal expansion properties of the glass samples were determined using a vertical quartz push-rod dilatometer, designed at the University of Warwick. The sample was placed between two quartz rods and the movement of the upper rod monitored. The heating rate was 2°C min^{-1} and measurements were taken between 20°C and 1050°C. The linear thermal expansion coefficient α of the glass sample was determined on a rod specimen and calculated between 100°C and 300°C according to the equation (4.4)

$$\alpha_{\Delta T} = \frac{1}{l_o} \frac{\Delta l}{\Delta T} \qquad (4.4)$$

where $\alpha_{\Delta T}$ is the linear thermal expansion coefficient in the range 100–300°C, l_o the initial length and Δl is the change of length with change of temperature ΔT.
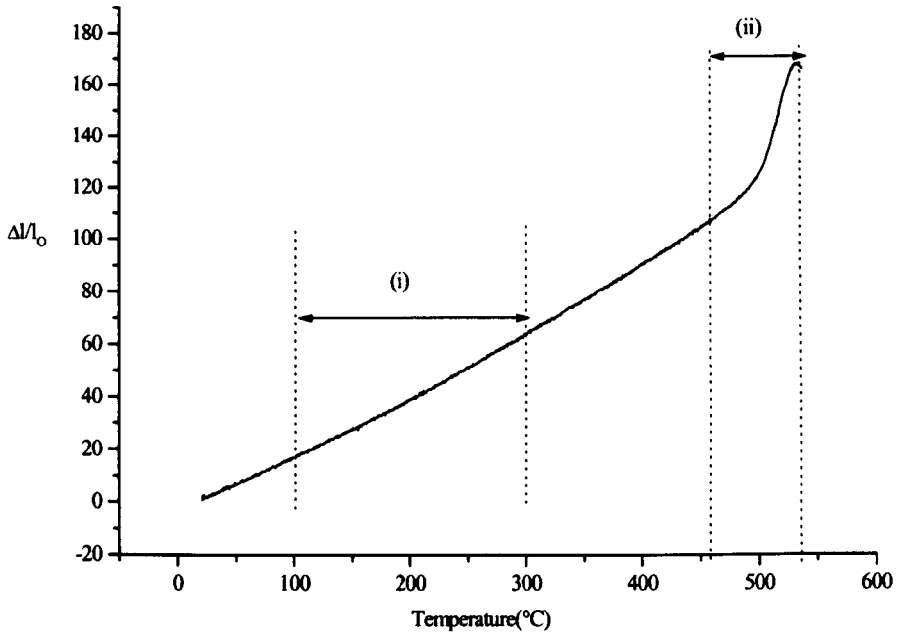
Fig. 4.06. Thermal expansion curves for annealed glass, showing the (i) CTE region and (ii) glass transition temperature.

4.5. NMR Spectroscopy

4.5.1. Theory

Borosilicate glasses do not only belong to the most widely used families of non-crystalline solids they are also part of those glassy systems, which, independently have been investigated most frequently. However, despite various studies, an understanding of the structure at the atomic environment level still has not fully been achieved. Nuclear magnetic resonance can be of considerable value in investigating the local atomic environment. NMR is a phenomenon, which occurs when the nuclei of certain atoms are immersed in a static magnetic field and are exposed to a second oscillating magnetic field resulting in absorption of energy. Nuclear magnetic resonance studies have been successful in determining structure and chemical bonding

in borate glasses. A schematic diagram of an NMR instrument is shown in Figure 4.07.
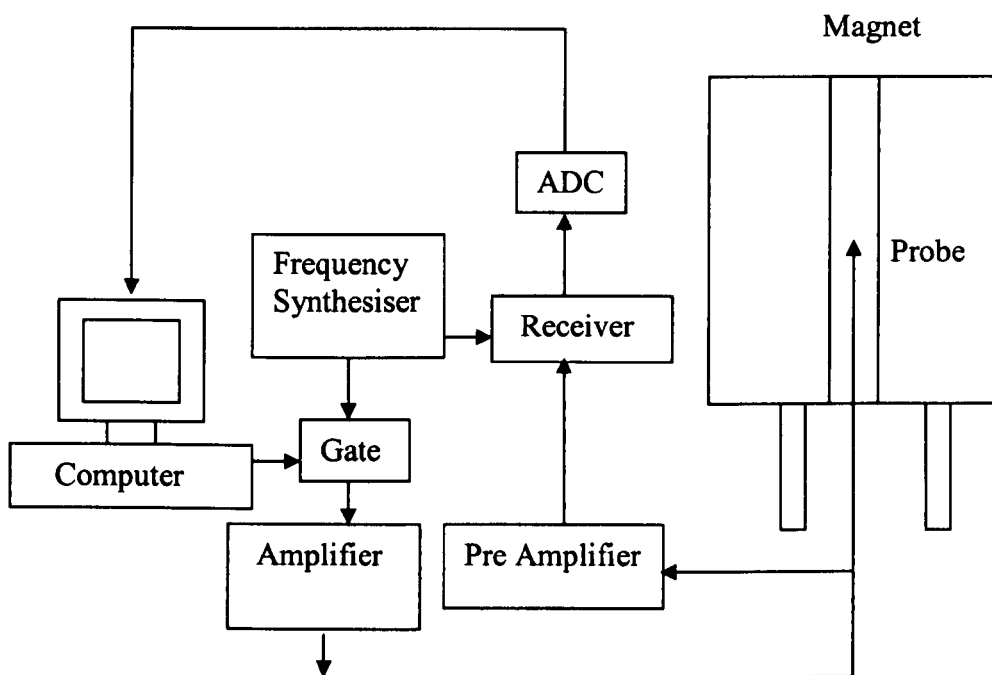
Fig. 4.07. Schematic Diagram of an NMR instrument.

Many atomic nuclei have a quantum mechanical property called spin which can be characterised by the physical spinning of the nucleus. The angular momentum J, of such a nucleus is given by

$$J = \hbar [I(I + 1)]^{\frac{1}{2}} \qquad (4.5)$$

Where $\hbar = \dfrac{h}{2\pi}$ and I is the spin quantum number. Nuclides with even mass number and even charge have zero spin and are of no interest to NMR spectroscopy. The magnetic moment μ of a nucleus is a fundamental property and is given by

$$\vec{\mu} = \gamma \vec{J} \qquad (4.6)$$

where γ is the gyromagnetic ratio of the nucleus. If the nuclei are subjected to a magnetic field H applied in the z-direction, the Hamiltonian of the interaction between the field and a dipole moment becomes

$$\vec{H} = -\vec{\mu} H = -\gamma \hbar H_z \vec{I}_z \qquad (4.7)$$

The eigenvalues of this Hamiltonian

$$E = -\gamma \hbar m H_z \qquad (4.8)$$

47

correspond to $m = 2I + 1$ equally spaced energy levels, described by the quantum number m. In the absence of a magnetic field these energy levels are degenerate, but when a magnetic field is present, interaction between them and the field lifts this degeneracy. Transition between adjacent levels may occur when radio-frequency irradiation is applied whose frequency ω_0 satisfies the Bohr frequency condition

$$\hbar\omega_0 = \Delta E = \gamma\hbar H_z \qquad (4.9)$$

ω_0 is referred to as the Larmor frequency.
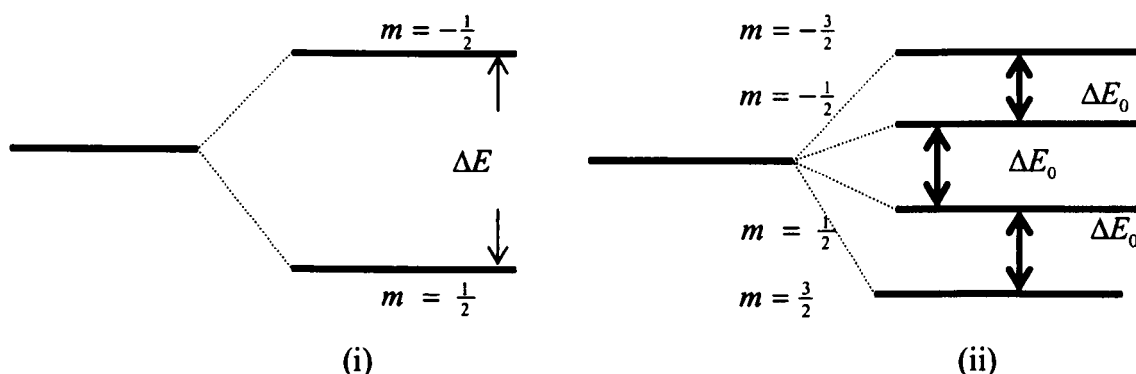
Fig. 4.08. Nuclear spin energy level diagram for a (i) spin $I = \frac{1}{2}$ nuclide (ii) energy levels for a spin $I = \frac{3}{2}$ nucleus in the presence of a magnetic field.

The NMR phenomenon is chemically and structurally useful, because the electrons in the vicinity of the atom shield the nucleus producing a shift at the ppm level from the applied magnetic field H_z. Nuclei in different structural environments will have slightly different local magnetic fields and consequently absorb and emit photons of slightly different frequencies. The Hamiltonian for this effect is

$$\overline{H_\sigma} = \gamma\hbar\sigma_{ij}\overline{I}\overline{H} \qquad (4.10)$$

where σ_{ij} is the chemical shift tensor. The first order contribution in a resonance shift is

$$\omega = \omega_0(1 - \sigma_{zz}) \qquad (4.11)$$

where σ_{zz} is the component of the shift tensor along the direction of the applied field

$$H_z = \frac{\omega_0}{\gamma} \qquad (4.12)$$

Because the absolute values of H_z are difficult to measure, values of NMR frequencies are normally reported as chemical shifts, δ, relative to an experimentally useful standard.

Both continuous wave spectroscopy and pulse methods are utilized when NMR is applied to glass. Structural information about glasses is obtained from shifts and splitting of the obtained spectra.

In pulsed NMR spectroscopy the entire frequency range of interest is irradiated at once. For a pulse length of t_p with angular frequency γH_1 the sample magnetizations are rotated away from the z axis by the angle

$$\theta_p = \gamma H_1 t_p \qquad (4.13)$$

The magnetization $\overrightarrow{M}$ in the xy plane will induce a signal called the free induction in a receiver coil. Immediately following the pulse the individual spins are aligned but the spin–spin interactions cause dephasing of the spins with a reduction in the magnitude of $\overrightarrow{M}$. The decaying signal is termed the free induction decay (FID). The Fourier transform of the real part of the FID gives the NMR absorption spectrum.
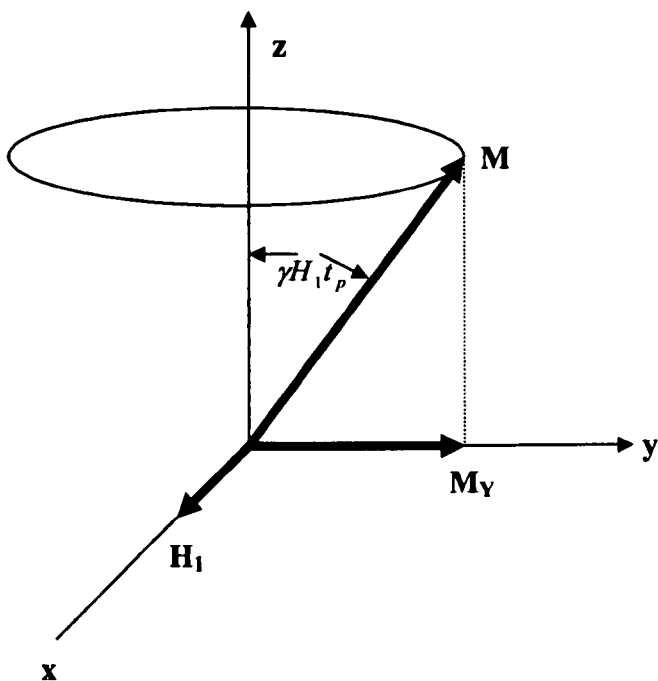
Fig. 4.09. shows the displacement and precession of the magnetic moment due to the radiofrequency (RF) pulse.

Dipolar, chemical shift and first order quadrupolar interactions can contribute to the broadening. These terms have an angular dependence of $1 - 3\cos^2\theta$, where θ is the angle between the internuclear and the external field. For $\theta = 54.74^o$ these terms are zero, thus narrowing the overall NMR response. In MAS NMR the sample is placed in a rotor, which spins the sample at this angle relative to the direction of the static-field.

Although the first-order term in the Hamiltonian decribes the quadrupole perturbation to Zeeman interaction contain $(1 - 3\cos^2\theta)$ terms, the second order terms do not. So the second-order quadrupole can complicate lineshapes such as for [11]B. This has more complex angular variation so that under MAS only partial narrowing can occur and gives the distinctive lineshapes.

4.5.2. NMR Spectroscopy of Amorphous Solids

Glasses and other amorphous solids have no long range order and no regularity in the arrangement of their atomic, ionic or molecular constituents, at least not on a large scale. Thus their structure cannot be effectively examined by X-ray diffraction (XRD) techniques. NMR spectroscopy has been successfully applied to highly disordered solids. The electron density around each nucleus in a molecule varies according to the types of nuclei and bonds in the molecule. The opposing field and therefore the effective field at each nucleus will vary - this is called the chemical shift.

4.5.2.1. ^{29}Si NMR

The natural abundance of [29]Si is 4.7 % and it has a spin of $\frac{1}{2}$. The low natural abundance of [29]Si greatly reduces the homonuclear dipole interaction.

For silicate glasses [29]Si provides most information but, due to lack of resolution in the chemical shift broadened spectrum, less information about the glass composition can be found. However there are systematic changes in chemical shift and peak width that provide information about the glass structure. The [29]Si chemical shifts are sensitive to variation of the Si-O bond length and Si-O-Si bridging angles as well as to change of second and third neighbour environments. The chemical shift becomes less negative [1] as the numbers of attached bridging oxygen (BO) atoms decrease. The [29]Si atoms surrounded by different numbers of BO atoms are identified as separated peaks in ^{29}Si NMR spectra.

From each of the annealed, glass block samples a small amount was powdered for the NMR experiment. Measurements of ^{29}Si MAS- NMR were made for all the series of the glasses except for MW-MnO, as Mn concentrations greater than 1-2% cause extensive peak broadening. All the samples were measured with a Bruker MSL 360 from 1000 acquisitions at room temperature using a spinning speed of 3-5 kHz. A pulse delay of 5s was used with a pulse length of 2 μs at a frequency of 71.54 MHz and line broadening of 20 Hz was applied to each spectrum. The chemical shift of the ^{29}Si was referenced to tetramethylsilane. The spectra obtained from the ^{29}Si MAS NMR were fitted satisfactorily with at least two Gaussian peaks.

4.5.2.2. ^{11}B NMR

The natural abundance of ^{11}B is 80.42 % and it has a spin of $\frac{3}{2}$. ^{11}B NMR methods are proving to be very useful for the analysis of glass structure. Much of the NMR work on borate glasses has involved the use of ^{11}B spectra to calculate the fraction of four co-ordinated boron in various borate systems, to compare glasses and to obtain information concerning structural groupings.

For quadrupolar nuclei $(I \geq 1)$ such as ^{11}B $(I = \frac{3}{2})$, two parameters are commonly used to characterize the interaction between the nuclear charge distribution and surrounding electron distribution. The quadrupole coupling constant Q_{cc} measures the lack of spherical symmetry of the nuclear charge distribution (i.e. the nuclear electrical quadrupole moment) and its interaction with the electric field gradient at the nuclear site, and the asymmetry parameter η indicates the deviation of the electric field gradient from cylindrical symmetry. Since the closed electron shells surrounding a nucleus are spherical and give rise to no electric field gradient at the nucleus, the electric field gradient arises principally from the electrons in the outer shell (i.e. bonding electrons) of the atom containing the nucleus. The quadrupolar interaction is, then, a very sensitive probe of the bond symmetry and electron distributions. Due to the quite different bond configurations and the electron distributions for the 4- and 3-coordinated borons there is a large difference in the sizes of the quadrupole coupling constants for the two configurations.

The NMR response of borons in the two different coordinations can easily be assigned using a minimum of three peaks exhibiting quadrupolar line shapes Figure 4.10. ^{11}B MAS can clearly separate [BO$_3$] and [BO$_4$] peaks and sometimes, with the

51

help from parameters derived from wide line studies, can partially resolve [BO$_{3A}$] and [BO$_{3S}$] sites. The broader peak with larger Q$_{cc}$ is due to the trigonal [BO$_3$], while the sharp peak is from tetrahedral [BO$_4$] boron. The trigonal boron consists of symmetric boron (sites with three bridging oxygen, BO) and asymmetric boron (sites with one or two NBO). The ^{11}B NMR techniques were employed to determine the relative fraction of different boron atoms in the glass system by measuring the area due to the response from 4-coordinated boron and the area due to the response from 3-coordinated borons, which is a summation of the response from symmetric and asymmetric 3-coordinated borons.

^{11}B NMR spectra were obtained with a 14.1T, Varian/Chemagnetics Infinity 600 NMR spectrometer, acquiring typically 1000 acquisitions at room temperature using a spinning speed of 15kHz. A pulse delay of 1.5s was used with a pulse length of 0.6μs at a frequency of 192.54 MHz. The chemical shift of the [11]B was referenced to Pyrex (0 ppm) or boron phosphate (-3.3 ppm) as secondary references, enabling their shift relative to the primary reference (CH$_3$)$_2$O: BF$_3$ to be calculated. The [11]B chemical shifts for the BO$_4$ units ranges between 0 and −3.3 ppm and for BO$_3$ has chemical shifts between 11 and 19 ppm.
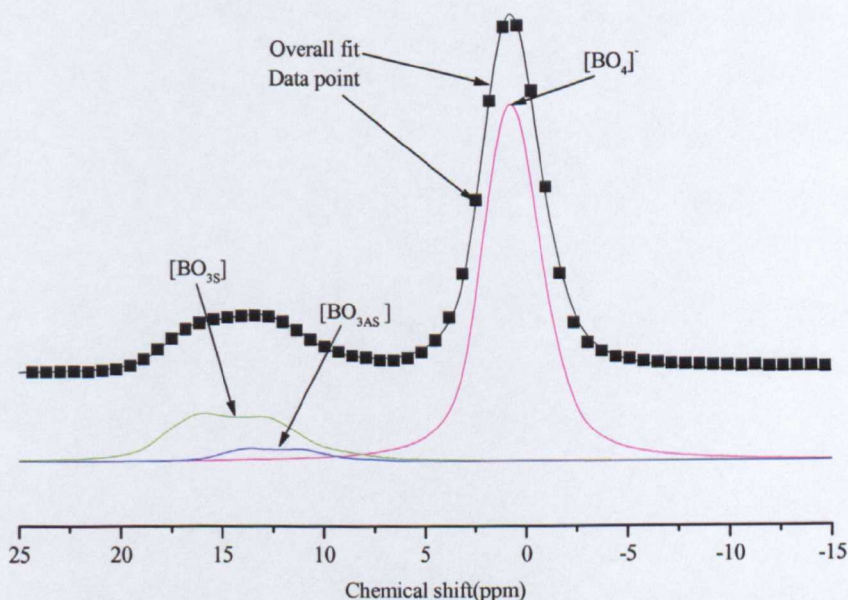
Fig. 4.10. Simulation of the ^{11}B MAS-NMR spectrum of MW-SrO glass showing the fitted peaks, tetrahedral boron, [BO$_4$,] symmetric trigonal boron [BO$_{3S}$], and asymmetric trigonal boron, [BO$_{3AS}$].

To confirm the structural change in the glass system, fractions of 4-co-ordinated boron units were calculated using a line shape computer simulation for each of the samples [4]. An example of the simulation of an ^{11}B MAS-NMR spectrum obtained from MW-SrO glass is depicted in Figure 4.10. The fitted peaks are from tetrahedral boron, [BO$_4$], symmetric trigonal boron [BO$_{3s}$], and asymmetric trigonal boron, [BO$_{3A}$].

4.6. UV–Visible spectroscopy

UV/Visible spectroscopy is an useful analytical technique for the study of the short-range structure of glasses, that is, the immediate surroundings of the absorbing atom because of the influences of the symmetry produced by the ligand arrangement.

In the ultra violet spectral region, transmission is limited by the electronic transitions. It is known that colourless glasses cannot transmit radiation at wavelengths beyond their inherent ultra violet edge [5]. This frequency is believed to be due to the transition of a valence electron of a network anion to an excited state. Very intense colour can arise due to $d - d$ and $\pi - \pi^*$ transitions [6].

Manganese can be present in the glasses as Mn^{2+}, Mn^{3+}, Mn^{4+}. Divalent manganese ions have the d^5 configuration and the energy levels of this configuration in an octahedral ligand field are such that any transitions between them would involve a change in the electron spin and would therefore give very weak absorption bands. Trivalent manganese ions have the d^4 configuration which gives a single absorption band in an octahedral ligand field corresponding to the $^5\Gamma_3(D){\rightarrow}^5\Gamma_5(D)$ transition [7].

Glass disks 0.5mm thick were cut and polished for UV characterisation of the MW-MnO glass system. A Jenway 6505 UV/Vis spectrophotometer was used to record the ultra-violet spectra over the 190-900nm range.

4.7. Ionic (DC) Conductivity

The glasses that are used for high level waste immobilisation are good electrical insulators at room temperature. HLW that results from the reprocessing of spent nuclear fuel contains highly radioactive fission products such as ^{144}Ce, ^{144}Pr, ^{137}Cs, ^{90}Sr actinides like ^{238}U, ^{237}Np, ^{239}Pu, ^{241}Am and small amount of ^{241}Pu. These produce a significant heat output which can increase mobility of alkali ions in the

waste glass and may affect the chemical durability. Chemical composition can thus have a significant effect on electrical properties; therefore it should be taken into account during the composition selection stage. John Mauro [8] state that 'A high-alkali glass has a much larger diffusion gradient than a low-alkali glass' (it is assumed that he in fact refers to concentration gradient), so more ionic diffusion occurs.

4.7.1. AC theory of ionic conductivity

The ionic conductivity of glass materials can be determined using a direct current or alternating current technique. In order to examine the dc ionic conductivity of the MW doped glass the ac impedance technique has been used.

The sinusoidal voltage $V = V_m \exp(j\omega t)$ applied to an electrical circuit causes a current to flow within the circuit which can be represented by

$$I = I_m \exp\left(j\omega t + j\phi\right) \qquad (4.14)$$

where ω and ϕ are the angular frequency and phase difference between V and I respectively.

The relationship between the applied voltage and resultant current can be written,

$$Z = \frac{V_m}{I_m} = Z_m \exp(-j\phi) = Z' - jZ'' \qquad (4.15)$$

where Z is the impedance and Z' and Z'' represent the real and imaginary parts respectively.

The complex admittance Y, is the inverse of Z

$$Y = \frac{1}{Z} = \frac{Z' + jZ''}{Z'^2 + Z''^2} = Y + jY'' \qquad (4.16)$$

4.7.2. Methods of determining ionic conductivity

The impedance plots commonly used in the measurement of dc conductivity are obtained by plotting the real part (Z') against the imaginary part (Z'') of the complex impedance plane. In the complex plane of impedance, a series or a parallel equivalent circuit can represent the R and C elements. Basically, in the complex impedance plane, the above equation describes a semi-circle with real axis intercepts at 0 and R, the resistance R of the glass sample can thus be determined from the intercept of the graph on the real axis of the complex impedance plane.

The dc ionic conductivity can be calculated using the relation (4.17)

$$\sigma = \frac{1}{R} \cdot \frac{t}{A}$$
(4.17)

where t is the thickness and A is the electrode surface area of the glass sample.

4.7.3. Sample preparation and experimental details

Glass disks 1mm thick and 25mm in diameter were cut and polished. A layer of platinum was deposited on both faces of the sample, providing a contact between the electrodes and samples. DC ionic conductivity of the borosilicate glasses with different additives was measured by attaching electrodes to the surface of the glass sample and determining the complex impedance diagram over the range 5Hz to 1MHz using a frequency impedance analyser. The sample is pressed firmly between two ceramic discs, with a piece of gold foil inserted between the sample and each disc. Each gold electrode was attached to lengths of platinum wire connected to a Hewlett Packard 4921 Impedance Analyser. A thermocouple was positioned very close to the edge of the sample to measure its temperature.

It was found that samples did not begin to show any significant conduction until the sample temperature was raised to approximately 200°C. Measurements were made in the range 200–350°C, for a frequency sweep of 5Hz-1MHz.
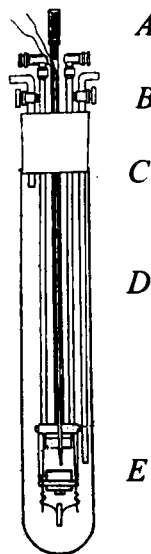
Fig. 4.11. Schematic diagram of the ionic conductivity jig design. A-Spring loaded plunger, B- BNC head, C- rubber bung, D- Pyrex glass, E- Ceramic disc.

The resistance R is determined by finding the intercept of the semicircle from the $(Z' - Z'')$ complex impedance plot [9]. Origin software was used to fit the function to the $(Z' - Z'')$ plot.
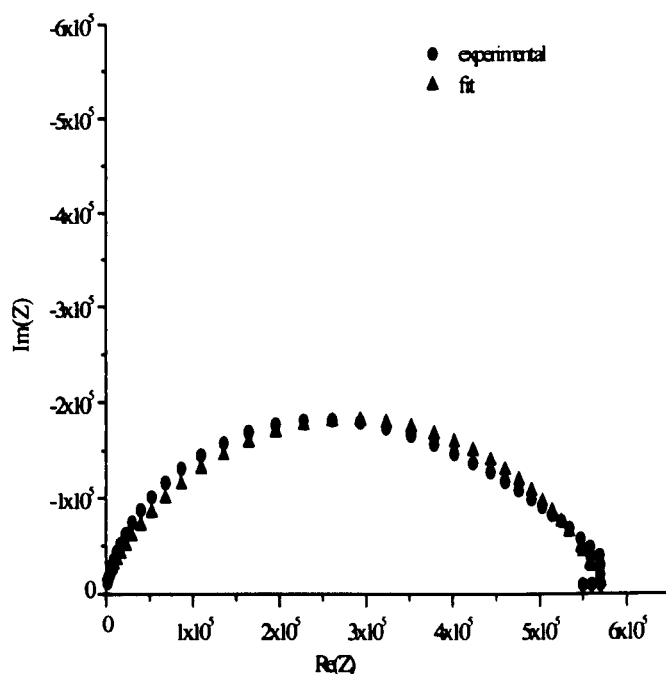
Fig. 4.12. The complex impedance $(Z' - Z'')$ plot, used to obtain dc ionic conductivity parameters.

4.8. Chemical durability

Chemical durability has been used to express the resistance offered by a glass towards attack by aqueous solutions and atmospheric agents. It is one of the most important properties of a radioactive waste form.

A Soxhlet leaching (dynamic) method was carried out to determine the chemical durability for BNFL HLW glass containing PbO, ZnO, BaO, SrO, CaO, MnO.

Leach rate is the rate of dissolution or erosion of material from the surface of a solid. The test results may be used for judging and comparing different types of waste form or may serve as input data for a long-term safety assessment of a repository.

The samples, of 25mm diameter and 1 mm thickness, were washed with acetone and dried in an oven. Sample area, thickness and weight were determined from the average of three measurements. Optical micrographs of each sample were

taken to provide a comparison with the leached sample. Each round flask shown in Figure 4.13 was filled with 300ml of deionised water and a sample placed at the bottom of each Soxhlet. The apparatus was connected and the cooling water system turned-on. Isomantles were used to keep the water at 100°C, as a result the sample experienced a temperature of approximately 75°C. A 'blank' was run alongside each set of samples to examine the contribution to the leachate from the experimental apparatus.
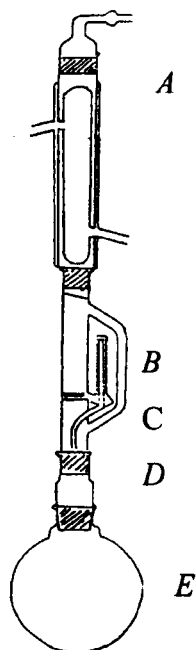
Fig. 4.13. Schematic Diagram of the leach test apparatus, A- Condenser, B-Soxhlet C- glass sample, D- Adaptor, E- Flask. Each sample was tested for 14 days at 75 °C.

Each test was carried out for 14 days. After 14 days, the isomantles were switched off and leachates allowed to cool down to room temperature. Leachate pH measurements were made using standard pH 7 and pH 10 buffer solutions and a digital pH meter HI-931410 pH/mV. Samples were dried and weighed again to determine sample weight loss. All the leachates were acidified with 2.5M nitric acid to a pH of approximately 2.7 and analysed for sodium and lithium [10]. The surface of the corroded sample was also monitored by SEM and high resolution X-ray diffraction to check for the presence of any crystalline material.

4.9. References

[1] Hideki Maekawa, Takashi Maekawa, Katsuyuki Kawamura and Toshio Yokokawa, J. Non-Cryst. Solids **127** (1991) 53-64.

[2] L. Barbieri, C. Leonelli, T. Manfredini, and C. Siligardi, J. Mater. Sci. Lett. **13** (1994) 180.

[3] T. P. Seward and P. S. Danielson, in Application for Glasses, Ceramics and Glasses- Engineered Materials Handbook, ASM International, USA, **4** (1991) 1015-1100.

[4] D. Massiot, F. Fayon, M. Capron, I. Kings, S. Le Calvè, B. Alonso, J-O. Durand, B. Bujoli, Z. Gan and G. Hoatson, Magnetic Resonance in Chemistry, **40** (2002) 70.

[5] J. E. Shelby, Introduction to Glass Science and Technology, Royal Society of Chemistry, Cambridge (1997) 201.

[6] R. C. Denney, R Sinclair, Visible and ultraviolet spectroscopy, Analytical Chemistry by Open Learning, London (1987) 54.

[7] C. R. Bamford, Phys. Chem. Glasses **3** (1962) 189.

[8] John Mauro, Glass properties and their relationships to network forming and modifying agents, New York State College of Ceramics (2000).

[9] M. D. Ingram, Phys. Chem. Glasses **28** (6) (1987).

[10] CERAM Research Ltd, Queens Road, Penkhull, Stoke-on-Trent, ST4 71Q, England.

[11] High Temperature processes- Leach Tests, BNFL Research and Technology Operating Instruction HTP 07, Issue 2 (12/99).

[12] M. E. Brown, Introduction to thermal analysis: techniques and applications, Chapman and Hall Ltd. Cambridge (1988).

Chapter 5

Thermal and Physical Properties

5.1. Introduction

The thermal and physicochemical properties, which are of importance for fabrication and long-term storage of waste glasses, are determined on non-radioactive glasses. For example, any tendency to partial crystallisation could negatively affect the integrity of the glass blocks, introducing cracks or porosity into the original homogeneous glass. Changes in the composition of the glass may also occur which would change the thermal and physical properties and therefore this compositional dependence needs to be determined.

5.2. Thermal Characterisation

5.2.1. Glass Transition temperature– results and discussion

The DTA results for the MW-SrO and MW-PbO system are shown in Figures 5.01 (i) and (ii). These are typical of the various glass series studied. The lack of any significant crystallisation event demonstrates the stability of these systems. The glass transition temperature T_g was obtained using the slope intercept method, with a reproducibility of ± 5 °C. The values of T_g are shown in Table 5.01.

Different trends are observed depending on the type of additives in the MW glass and several factors control these trends. In the case of PbO, ZnO and MnO, T_g decreases with mole percent of additives. In contrast, an increase in T_g was observed in the case of BaO, CaO and SrO containing glasses.
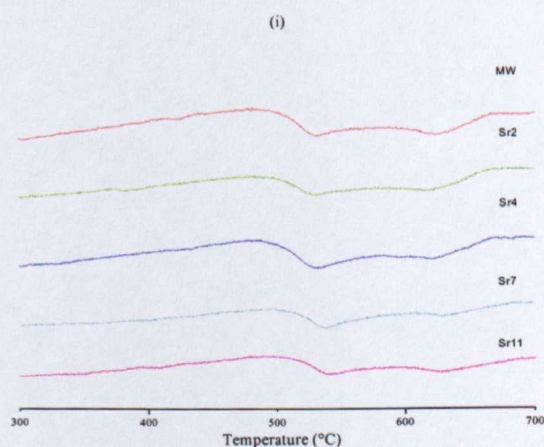
Fig. 5.01. (i) DTA curve obtained from the MW-SrO glass system.
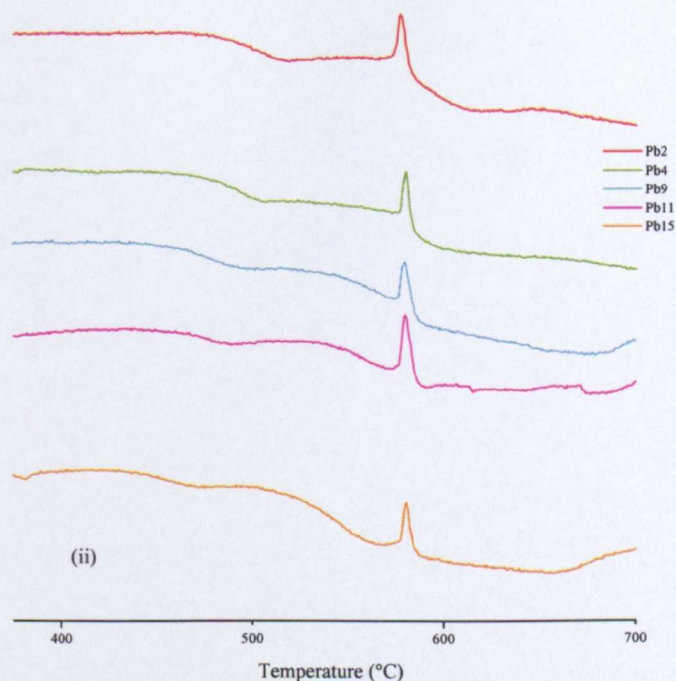
Fig. 5.01. (ii) DTA curves obtained from the MW-PbO glass system. The sharp peak is from the α-β quartz transition in the reference.

Sample name	mol % of additives	Ba (±5°C)	Sr (±5°C)	Ca (±5°C)	Pb (±5°C)	Zn (±5°C)	Mn (±5°C)
MW	0	497	497	497	497	497	497
2	2.4	486	488	485	484	503	488
3	3.62	490	-	-	481	499	484
4	4.83	493	493	497	475	489	478
7	7.25	495	499	499	467	478	476
9	9.66	497	-	-	455	475	473
11	11.98	490	503	514	442	466	472
15	15	496	-	-	434	463	-

Table 5.01. Glass transition temperatures for the MW-BaO, MW-CaO, MW-SrO and MW-PbO, MW-ZnO and MW-MnO glass systems.

60
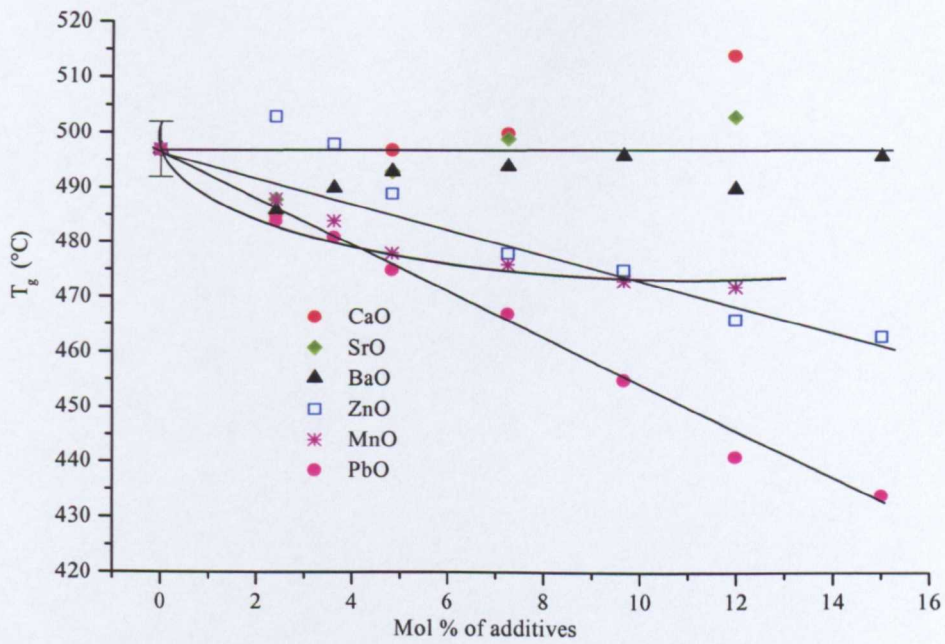
Fig. 5.02. Variation of glass transition temperature with the addition of CaO, BaO, SrO, ZnO, MnO and PbO. The lines are straight line fits for PbO, ZnO and alkaline earths. The curve shows the trend for MnO.
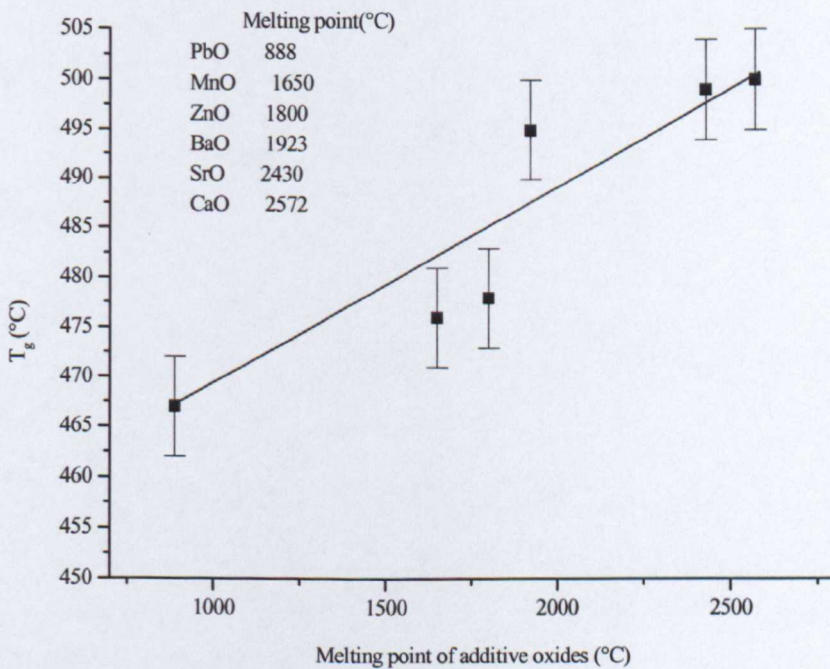
Fig. 5.03. Variation of glass transition temperature with the melting point of the additive oxides for a fixed concentration of 7.25 mol%.
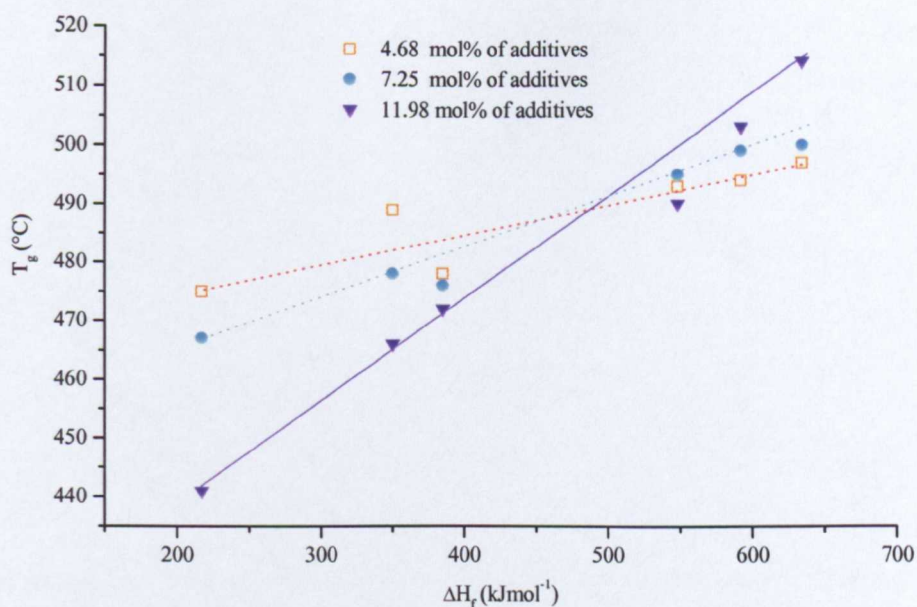
Fig. 5.04. Variation of glass transition temperature with the heats of formation of the additive oxides for three compositions, 4.68 mol%, 7.25 mol% and 11.98 mol%.

Oxides	Melting point (^{O}C)	Heat of formation ΔH_f (kJmol^{-1})
BaO	1923	-548.0
CaO	2572	-634.9
SrO	2430	-592.0
PbO	888	-217.3
MnO	1650	-385.2
ZnO	>1800	-350.5

Table 5.02. Melting points of the oxide additives and their respective heats of formation [1].

The relative proportions of the MW components remain constant so any changes to the physical properties must be caused by the introduction of the additives. Figure 5.03 demonstrates the relation between T_g and the melting point of the additives. When PbO is added to the MW (base) glass the glass transition temperature decreases, reflecting the lower melting temperature of PbO.

The glass transition temperature of an oxide network also depends upon the tightness of packing in the network, the more open the network, the smaller is the increase in internal energy needed to attain the degree of mobility required for the transition and hence the transformation temperature decreases when the network becomes less tightly packed [2]. Therefore, the introduction of ZnO, PbO and MnO which form network polyhedra, results in a decrease of T_g with the increasing mol percent of additives, whilst interstitial alkaline earth cations increase packing and T_g. It can also be seen from Figure 5.02, that the MW-MnO glass shows different behaviour because of the variable valence states of manganese.

It has been shown that T_g is closely related to the fraction of four-coordinated boron [3]. In chapter 6 it will be seen that there is a gradual decrease in N_4 values with the increase of PbO and ZnO. This conversion from $[BO_4]$ to $[BO_3]$ units, causes the glass structure of MW-PbO and MW-ZnO to become less cross-linked.

Another physical parameter, which is found to correlate with T_g, is the heat of formation of the oxide additive. The effect on the glass transition temperature becomes more evident as the concentration of the additive oxide increases (Figure 5.04).

5.2.2. Thermal expansion-results and discussion

The thermal expansion of glass depends, among other factors, on composition. It is also sensitive to the structure of the glass, e.g. degree of polymerisation, type of structural units, the nature and contribution of the different cations, whether they occupy forming or modifying positions in the glass network. Accordingly, thermal expansion data can yield valuable information about the structural changes induced by modification of composition or heat treatment [4].

The values of linear thermal expansion coefficients for the systems containing BaO, CaO and SrO were calculated between 100-300°C and are shown in Figure 5.05 as a function of concentration. After an initial decrease at 2.4 mol%, there is a linear increase in CTE of the MW-CaO and MW-SrO systems up to 11.98 mol%. In the glass system containing BaO the CTE increases up to 9.66 mol% and then decreases. A similar trend in N_4 values for the MW-BaO series glass system can be seen in chapter 6. From 11.98 to 15 mol% of BaO, the large size of the Ba^{2+} may cause the decrease in CTE.

Sample name	mol % of additives	Ba (± 0.5 MK^{-1})	Sr (± 0.5 MK^{-1})	Ca (± 0.5 MK^{-1})	Mn (± 0.5 MK^{-1})	Zn (± 0.5 MK^{-1})	Pb (± 0.5 MK^{-1})
MW	0	8.22	8.22	8.22	8.22	8.22	8.22
2	2.4	9.30	7.60	7.71	8.82	6.2	7.08
3	3.62	-	-	-	-	-	-
4	4.83	9.60	7.81	7.96	9.59	8.04	8.88
7	7.25	-	8.04	8.20	8.54	9.17	10.3
9	9.66	9.81	-	-	-	-	-
11	11.98	9.38	8.62	8.78	7.76	9.41	10.7
15	15	9.04	-	-	-	-	-

Table 5.03. Thermal expansion coefficients for MW-BaO, MW-SrO, MW-CaO and MW-PbO, MW-ZnO, MW-MnO glasses.
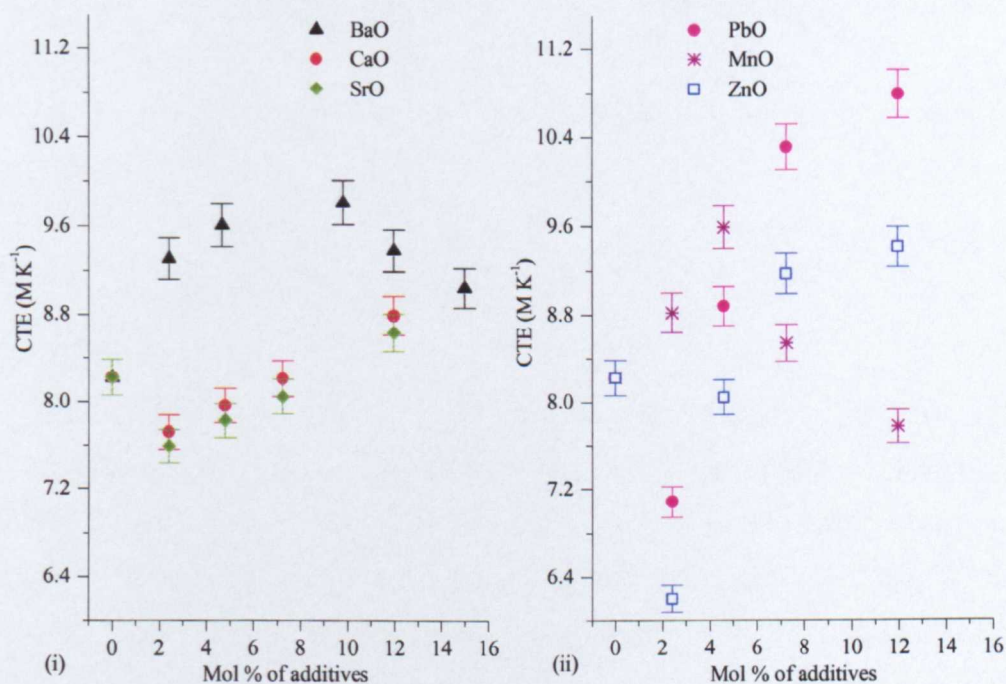
Fig. 5.05. Variation in thermal expansion coefficient with (i) alkaline earth additives and (ii) ZnO, PbO and MnO additives.

According to Jackson et al. [5] and Uhlmann et al. [6] the ionic radii of the cations present in glasses can influence the thermal expansion coefficient. It is known

that the expansion coefficient of modifier silicate glasses increases as the modifier ions fill the interstices between the structural units [7]. Larger network modifying ions give greater thermal expansion coefficients. The coefficient of linear thermal expansion of MW-BaO glass is higher than that of the systems containing MW-CaO and MW-SrO and similarly that of MW-PbO is greater than that of MW-ZnO. The size of the modifying Ba^{2+}, Pb^{2+} cations are dominating in these glass systems.

According to Ray [3] the thermal expansion of an oxide network would be expected to increase as the network becomes more open or exhibits a less rigid structure. In a study of lead silicate glass [8] it was found that increasing rigidity of the glass structure led to a decrease in thermal expansion coefficient and increased values of the glass transition temperature. In the MW-PbO and MW-ZnO glass transition temperature decreases and thermal expansion increases, showing the structure to be less rigid.

Introduction of MnO produces an increase in CTE up to 4.83 mol percent, followed by a rapid decrease. Manganese can be present in the glasses as divalent or trivalent ions, and the change in their relative amounts with concentration may explain the anomaly in CTE.

All of these factors will also be supplemented by changes in N_4 with composition.

5.3. Density– results and discussion
5.3.1. Density

The densities of the glass specimens were measured in water by the Archimedes method, at room temperature. Figure 5.06 (i) shows the change in density of the MW-BaO, MW-CaO and MW-SrO series glasses as the amount of additives is increased. Figure 5.06 (ii) shows the sample density as a function of the addition of PbO, ZnO and MnO. Table 5.04 presents the experimental data from the present study.
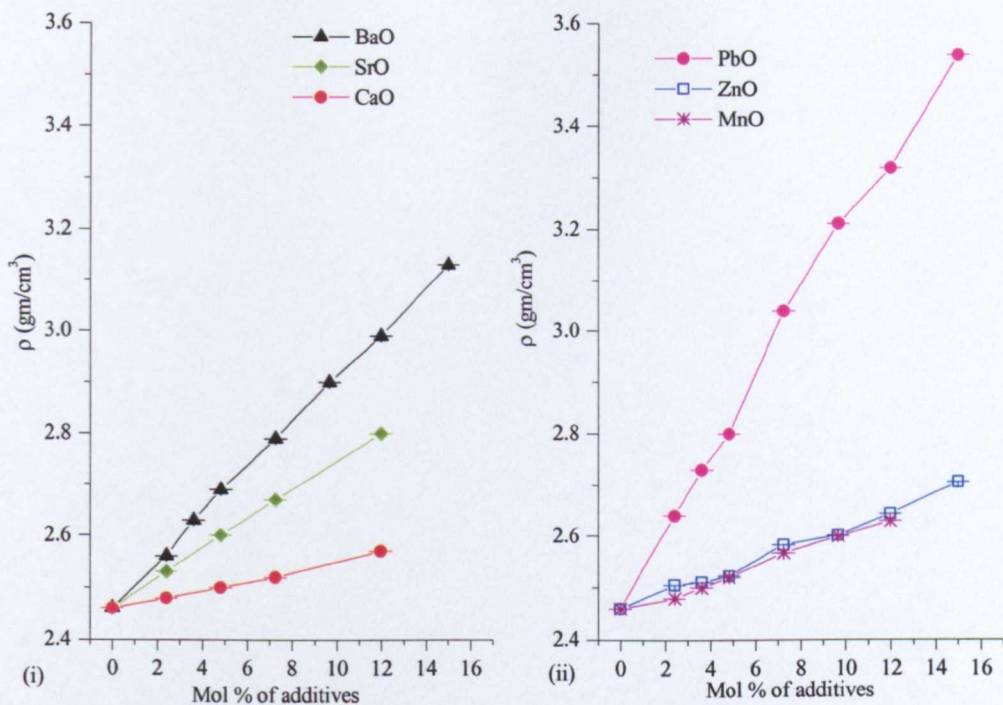
Fig. 5.06. Change in glass density with increasing concentration of the additives (i) BaO, CaO, SrO and (ii) PbO, ZnO, MnO.

Sample name	mol % of additives	Ba ρ (gcm⁻³) ± 0.02	Sr ρ (gcm⁻³) ± 0.02	Ca ρ (gcm⁻³) ± 0.02	Pb ρ (gcm⁻³) ± 0.02	Zn ρ (gcm⁻³) ± 0.02	Mn ρ (gcm⁻³) ± 0.02
MW	0	2.46	2.46	2.46	2.46	2.46	2.46
2	2.4	2.56	2.53	2.48	2.64	2.50	2.48
3	3.62	2.63	-	-	2.73	2.51	2.5
4	4.83	2.69	2.6	2.50	2.80	2.52	2.52
7	7.25	2.79	2.67	2.52	3.04	2.58	2.56
9	9.66	2.9	-	-	3.21	2.60	2.6
11	11.98	2.99	2.8	2.57	3.32	2.64	2.63
15	15	3.13	-	-	3.53	2.70	-

Table 5.04. Densities of MW glasses with various additions.

Cation	Ion radius ($\overset{\circ}{A}$)
Ba	1.35
Sr	1.13
Ca	0.99
Pb	1.2
Zn	0.74
Mn(3)	0.65
Mn(2)	0.82

Table 5.05. Ionic radius of additive ions [2].

The increase in density can be most easily explained by considering the large masses of the added cations, which exceed those of the other glass components. Therefore, in Figure 5.06 (i) the density of the glass increases linearly in the order Ba> Sr> Ca. As suggested by Coon and Shelby [9] the physical effects of any structural rearrangements involving boron, silicon and the modifier oxides will be dominated by increasing concentration of the modifier additives. In both silicate and phosphate glasses increased densities were observed with the addition of CaO, SrO and BaO [10].

Figure 5.06 (ii) shows similarly that density increases with relative molecular mass of PbO > ZnO ~ MnO.

5.3.2. Molar Volume - results and discussion

Figure 5.07 (i) shows the trend of molar volume of the MW-BaO, MW-SrO and MW-CaO glasses as the amount of additives is increased. Figure 5.07 (ii) shows the change in molar volume in MW-PbO, MW-ZnO and MW-MnO glasses. The corresponding values of the molar volume are shown in Table 5.06. The molar volume in these glass systems decreases in a linear fashion with increasing concentration of SrO, CaO, MnO and approximately linear for ZnO. In the case of BaO and PbO the decrease is non-linear.
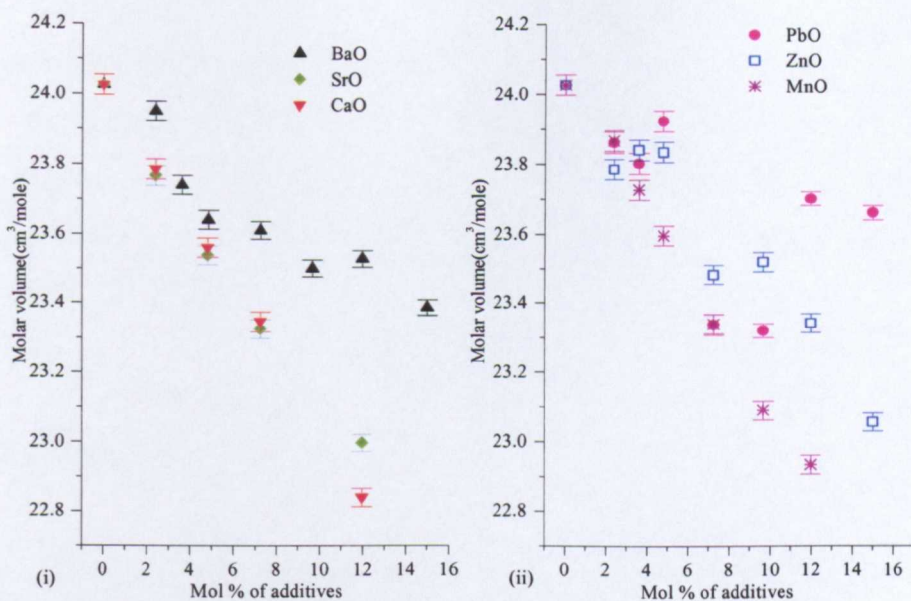
Fig. 5.07. Effect of (i) BaO, CaO or SrO (ii) PbO, ZnO and MnO on molar volume of MW glass system.

Sample name	mol % of additives	Ba (cm³/mole) ± 0.02	Sr (cm³/mole) ± 0.02	Ca (cm³/mole) ± 0.02	Pb (cm³/mole) ± 0.02	Zn (cm³/mole) ± 0.02	Mn (cm³/mole) ± 0.02
MW	0	24.02	24.02	24.02	24.02	24.02	24.02
2	2.4	23.95	23.76	23.79	23.86	23.78	23.86
3	3.62	23.74	-	-	23.8	23.83	23.72
4	4.83	23.64	23.53	23.56	23.92	23.83	23.59
7	7.25	23.61	23.32	23.34	23.33	23.48	23.33
9	9.66	23.50	-	-	23.32	23.51	23.09
11	11.98	23.52	22.99	22.84	23.70	23.34	22.93
15	15	23.38	-	-	23.6	23.056	-

Table 5.06. Molar Volume of MW glass systems with the addition of BaO, SrO, CaO PbO, ZnO and MnO.

The alkaline earth cation can be thought of as filling voids, with the reduction in molar volume arising from the replacement of some network formers and also the relaxation of network oxygen about the M^{2+} sites. However, the large size of Ba^{2+} ultimately causes an expansion of these sites. Molar volumes are also affected by

68

adding BaO which removes silicate and borate polyhedra from glass network. Mn^{2+} and Mn^{3+} similarly fill voids.

It is known that PbO and ZnO can enter the glass network both as network formers and also network modifiers and, due to this, the structure of MW-PbO and MW-ZnO glass is expected to be different from other glasses. Changes in N_4 will also influence molar volume.

5.4. References

[1]   CRC handbook of chemistry and physics, 82nd edition, CRC press, London, 2001.

[2]   N. H. Ray, J. Non-Cryst. Solids **15** (1974) 423-434.

[3]   J. Zhong and P. J. Bray, J. Non-Cryst. Solids **111** (1989) 67-76.

[4]   A. A. Ahmed, A. F. Abbas and S. M. Salman, Phys. Chem. Glasses **36** (1) 1985 17-23.

[5]   M. J. Jackson and B. Mills, J. Mat. Sci. Lett. **169** (1997) 1264-1266.

[6]   D. R. Uhlmann and R. R. Shaw, J. Non-Cryst. Solids **1** (1969) 347.

[7]   J. M. Roderick, PhD Thesis, University of Warwick (2001).

[8]   V. Sudarsan, V. K. Shrikhande, G. P. Kothiyal and S. Kulshreshtha, J. Phys. Condens. Matter **14** (2002) 6553-6565.

[9]   J. Coon and Shelby, Phys. Chem. Glasses **35** (2) (1994) 47-51.

[10]   J. E. Shelby, J. Non-Cryst. Solids **263** and **264** (2000) 271-276.

[11]   H. Doweidar, J. Non-Cryst. Solids **249** (1999) 194-200.

Chapter 6

Structural Characterisation

6.1. Introduction

In order to obtain information on the effect of divalent additives on the general structural behaviour of MW glass, ^{11}B and ^{29}Si MAS-NMR experiments were performed. MW-MnO glasses were also studied by means of UV-Visible spectroscopy.

6.2. ^{11}B MAS-NMR

Some of the ^{11}B MAS NMR spectra obtained from glasses containing BaO, CaO, and SrO are shown in Figure 6.01. The fraction of four co-ordinated boron atoms [BO$_4$]$^-$, N$_4$, was obtained by fitting quadrupole line shapes to each spectrum using an NMR simulation program [1]. Three peaks were fitted, defined as [BO$_4$]$^-$, [BO$_{3S}$] and [BO$_{3AS}$] units. An example of the peak fitting was shown in chapter 4. The broader peak in Figure 6.01 is due to trigonal boron [BO$_3$], while the sharp peak is from tetrahedral boron [BO$_4$]. The trigonal boron consists of symmetric [BO$_{3S}$] boron and asymmetric [BO$_{3AS}$] boron sites.

The values of the chemical shift δ, quadrupolar coupling constant Q$_{cc}$, and asymmetry parameter, η, of each simulation were recorded (Tables 6.01-6.05). From ^{11}B MAS-NMR spectra, it is possible in principle to separate the trigonal boron site into the individual [BO$_{3S}$] and [BO$_{3AS}$] groups, though it is difficult to derive a unique fit to the trigonal [BO$_3$] contribution. However, from the contribution of [BO$_4$], it is possible to observe different N$_4$ trends depending on the nature of the additive oxide. It can be seen from the fitting parameters obtained from simulation that there are discontinuities in [BO$_{3S}$] and [BO$_{3AS}$] values i.e. they follow no sensible trends - a consequence of the difficulty in obtaining a unique fit.

Work by Dell et al. [2] on the boron environment in alkali borosilicate glass produced the relationship between N$_4$ and R shown in Figure 3.12 in chapter 3, for K = 1. The base glass (MW) has R = 1.12, K = 3.26, R$_{max}$ = 0.709 and R$_{d1}$ = 1.32 which is in region 2 of the Dell model (R$_{max}$<R< R$_{d1}$) and is therefore already near the maximum expected value for N$_4$.

70
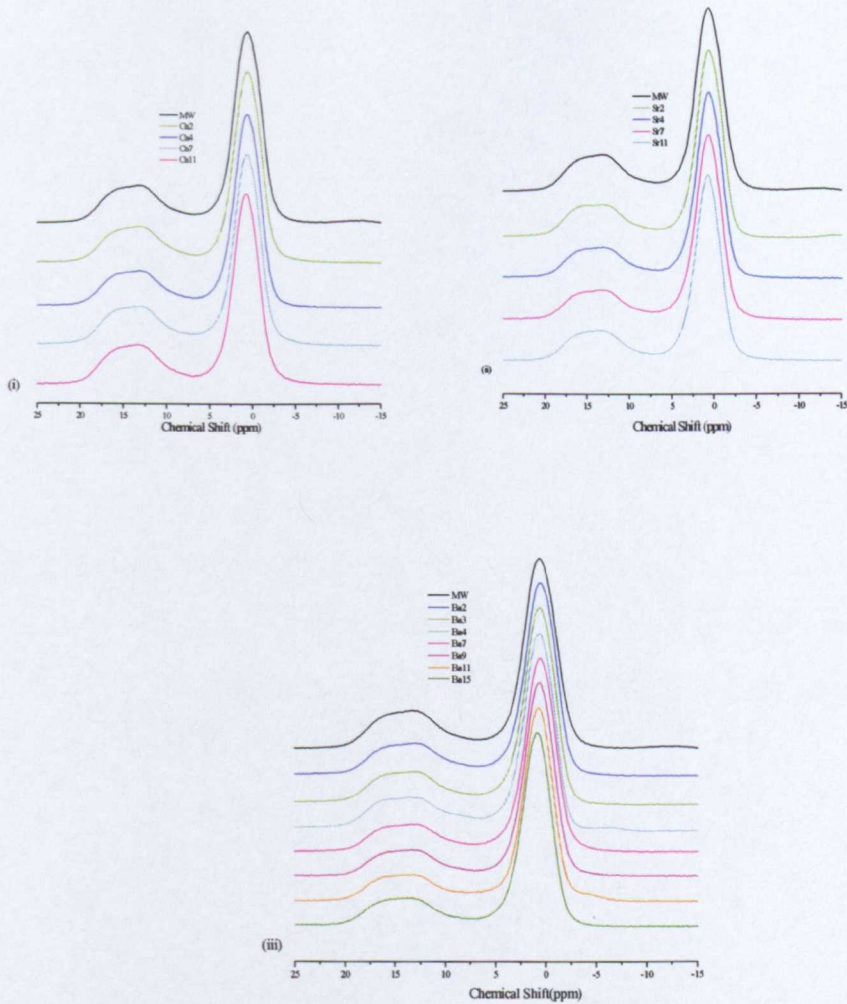
Fig. 6.01. Stack plots of the spectra obtained from ^{11}B MAS-NMR of MW glass systems containing (i) CaO (ii) SrO (iii) BaO.

On addition of BaO, CaO and SrO, to MW glass, N_4 increased with increasing alkaline earth content up to maximum values at compositions which are slightly different depending on the M^{2+} ion type. At higher content of BaO and CaO the excess oxygen in the borate network may result in formation of NBOs on asymmetric $[BO_{3AS}]$ groups rather than $[BO_4]^-$. These results are in good agreement with those found in alkaline earth borate glasses [3, 4]. It is evident from these results that alkaline earth oxides enter the structure as modifiers, so the trend of N_4 as a function of concentration is similar to that observed in alkaline earth borate glasses (Figure 3.15 Chapter 3). It is also possible that the silicate unit forms Si-O$^-$ M^{2+}O$^-$- B or Si-O$^-$ M^{2+}O$^-$-Si and, as a result, the concentration of four coordinated boron becomes saturated.

In contrast, addition of PbO and ZnO to MW causes a decrease in N_4. A decrease in N_4 can result from an increase or decrease in R, since the base glass is near maximum N_4. Figure 6.02 shows the resulting N_4 values as a function of type of additive. Adding ZnO has a greater effect on the [11]B spectrum than PbO. The decrease in N_4 most probably indicates that the alkali ions are being removed from the borate network. They may move to the silicate units. Alternatively, complexes of the type $[MO_n]^- R^+$ may form where M is Pb or Zn. It seems likely that PbO and ZnO enter as intermediate oxides so the N_4 values decrease.

If we assume that intermediate oxides are incorporated as $[MO_n]^-$ units with A^+ for charge balancing, then the remaining alkali, $[A_2O(a)]$ from equation 3.12 combines with the borate and silicate network. BaO, CaO and SrO are considered as modifier oxides and the values of $[A_2O(a)]$ are determined from equation 3.15. Using the values of $[A_2O(a)]$, and the amount of alkali associated with the borate and silicate networks $[A_2O(b)]$ and $[A_2O(Si)]$, the amount of non-bridging oxygen per silicon NBO/Si was calculated for the samples.
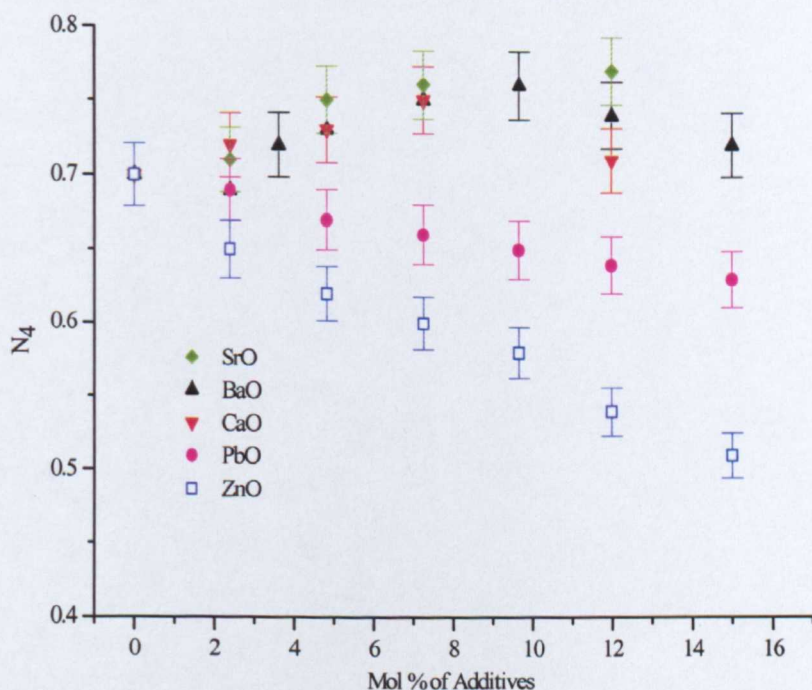
Fig. 6.02. The variation in the fraction (N_4) of tetrahedrally co-ordinated boron atoms with mol% of additives.

Sample Name	δ (ppm) ± 0.5	Sites	Q_{cc} (MHz) ± 0.05	η ± 0.05	Percent of Boron Species (±4%)
Ca2	2.8	BO_4	1.73	0.54	72.0
	19.4	BO_{3S}	2.61	0.27	10.0
	16.6	BO_{3AS}	2.31	0.05	18.0
Ca4	5.2	BO_4	1.70	0.52	73.0
	20.9	BO_{3S}	2.37	0.41	15.0
	22.6	BO_{3AS}	3.10	0.89	12.0
Ca7	4.5	BO_4	1.59	0.07	75.0
	21.0	BO_{3S}	2.54	0.32	20.0
	17.9	BO_{3AS}	2.29	0.40	5.0
Ca11	5.0	BO_4	1.60	0.54	72.0
	21.1	BO_{3S}	2.64	0.40	13.0
	20.4	BO_{3AS}	2.54	0.51	15.0

Table 6.01. [11]B simulation parameters for the MW-CaO system.

Sample Name	δ (ppm) ± 0.5	Sites	Q_{cc} (MHz) ± 0.05	η ± 0.05	Percent of Boron Species (±4%)
Sr2	4.8	BO_4	1.68	0.43	71.2
	21.6	BO_{3S}	2.65	0.40	22.2
	20.2	BO_{3AS}	2.58	0.51	6.6
Sr4	5.0	BO_4	1.66	0.52	75.3
	21.6	BO_{3S}	2.59	0.28	13.0
	18.6	BO_{3AS}	2.27	0.05	11.7
Sr7	5.0	BO_4	1.64	0.50	75.8
	21.8	BO_{3S}	2.60	0.23	6.3
	19.6	BO_{3AS}	2.35	0.04	17.9
Sr11	5.5	BO_4	1.60	0.55	77.2
	21.4	BO_{3S}	2.56	0.32	17.7
	18.4	BO_{3AS}	2.27	0.32	5.1

Table 6.02. [11]B simulation parameters for the MW-SrO system.

The behaviour of different additives can be seen from Figure 6.03, the concentration of non-bridging oxygen per silicon is increasing with the addition of CaO, BaO and SrO whereas it is decreasing with the addition of PbO and ZnO.

Sample Name	δ (ppm) ± 0.5	Sites	Q_{cc} (MHz) ± 0.05	η ± 0.05	Percent of Boron Species ($\pm 4\%$)
MW	2.7	BO_4	1.74	0.50	70.0
	18.5	BO_{3S}	2.36	0.42	15.8
	19.8	BO_{3AS}	3.00	0.84	14.2
Ba2	5.1	BO_4	1.69	0.54	69.4
	20.9	BO_{3S}	2.26	0.38	10.4
	23.3	BO_{3AS}	3.10	0.99	20.2
Ba3	2.4	BO_4	1.71	0.54	71.9
	18.3	BO_{3S}	2.33	0.41	12.9
	21.1	BO_{3AS}	3.19	0.97	15.2
Ba4	2.5	BO_4	1.70	0.52	73.3
	18.3	BO_{3S}	2.33	0.38	11.3
	19.5	BO_{3AS}	3.043	0.89	15.4
Ba7	2.6	BO_4	1.65	0.53	74.7
	18.7	BO_{3S}	2.30	0.37	12.0
	20.5	BO_{3AS}	3.07	0.99	13.3
Ba9	2.7	BO_4	1.69	0.56	76.1
	18.5	BO_{3S}	2.34	0.39	13.4
	20.4	BO_{3AS}	3.09	0.95	10.5
Ba11	2.8	BO_4	1.68	0.55	73.5
	18.6	BO_{3S}	2.32	0.40	11.7
	20.1	BO_{3AS}	3.14	0.80	14.8
Ba15	2.6	BO_4	1.69	0.57	71.6
	18.7	BO_{3S}	2.19	0.43	13.9
	20.6	BO_{3AS}	3.16	0.86	14.5

Table 6.03. ^{11}B simulation parameters for MW-BaO system.

Sample Name	δ (ppm) ± 0.5	Sites	Q_{cc} (MHz) ± 0.05	η ± 0.05	Percent of Boron Species ($\pm 4\%$)
Zn2	2.6	BO$_4$	1.7	0.49	64.7
	18.4	BO$_{3S}$	2.3	0.37	16.9
	19.6	BO$_{3AS}$	2.9	0.99	18.4
Zn4	2.5	BO$_4$	1.6	0.49	62.0
	18.5	BO$_{3S}$	2.6	0.33	35.8
	14.8	BO$_{3AS}$	1.5	0.57	2.2
Zn7	2.91	BO$_4$	1.6	0.50	60.2
	19.1	BO$_{3S}$	2.5	0.38	32.9
	13.5	BO$_{3AS}$	1.5	0.89	6.9
Zn9	1.9	BO$_4$	1.6	0.52	58.2
	17.9	BO$_{3S}$	2.5	0.38	26.9
	18.7	BO$_{3AS}$	2.9	0.68	14.9
Zn11	2.8	BO$_4$	1.6	0.55	53.8
	18.5	BO$_{3S}$	2.4	0.41	27.3
	19.9	BO$_{3AS}$	3.0	0.94	18.9
Zn15	2.1	BO$_4$	1.6	0.56	50.7
	18.3	BO$_{3S}$	2.5	0.43	34.1
	18.6	BO$_{3AS}$	2.8	0.99	15.2

Table 6.04. ^{11}B simulation parameters for MW-ZnO system.

Sample Name	δ (ppm) ± 0.5	Sites	Q_{cc} (MHz) ± 0.05	η ± 0.05	Percent of Boron Species ($\pm 4\%$)
Pb2	0.8	BO$_4$	1.7	0.44	69.2
	17.1	BO$_{3S}$	2.5	0.44	23.4
	13.5	BO$_{3AS}$	2.6	0.46	7.4
Pb4	2.6	BO$_4$	1.6	0.52	67.4
	18.7	BO$_{3S}$	2.4	0.43	17.2
	18.0	BO$_{3AS}$	2.6	1.00	15.4
Pb7	4.2	BO$_4$	1.6	0.49	66.2
	20.8	BO$_{3S}$	2.6	0.31	22.5
	17.8	BO$_{3AS}$	2.4	0.10	11.3
Pb9	2.8	BO$_4$	1.5	0.48	65.0
	19.1	BO$_{3S}$	2.6	0.35	23.0
	15.2	BO$_{3AS}$	1.5	0.49	12.0
Pb11	2.9	BO$_4$	1.6	0.54	64.2
	19.1	BO$_{3S}$	2.6	0.30	30.3
	16.2	BO$_{3AS}$	1.8	0.45	5.5
Pb15	3.2	BO$_4$	1.6	0.57	63.1
	19.1	BO$_{3S}$	2.4	0.34	24.1
	20.6	BO$_{3AS}$	2.9	0.96	12.8

Table 6.05. ^{11}B simulation parameters for MW-PbO system.

Sample	N_4	[$A_2O(a)$]	[$A_2O(b)$]	[$A_2O(Si)$]	NBO/si
MW	0.70	20.82	13.16	7.65	0.26
Ca2	0.72	22.73	12.94	9.78	0.33
Ca4	0.73	24.65	12.84	11.80	0.41
Ca7	0.75	26.54	12.91	13.62	0.49
Ca11	0.72	30.3	11.73	18.56	0.70
Sr2	0.71	22.73	13.84	8.88	0.33
Sr4	0.75	24.65	13.29	11.35	0.40
Sr7	0.76	26.54	13.03	13.50	0.48
Sr11	0.77	30.3	12.43	17.86	0.67
Ba2	0.69	22.73	12.48	10.24	0.34
Ba3	0.72	23.69	12.87	10.81	0.37
Ba4	0.73	24.65	12.88	11.76	0.41
Ba7	0.75	26.54	12.93	13.60	0.49
Ba9	0.76	28.47	12.76	15.70	0.58
Ba11	0.74	30.3	12.01	18.28	0.68
Ba15	0.72	32.69	11.26	21.42	0.83
Zn2	0.65	11.71	19.13	7.41	0.25
Zn4	0.62	10.94	17.405	6.46	0.22
Zn7	0.60	10.32	15.665	5.34	0.19
Zn9	0.58	9.76	13.98	4.21	0.16
Zn11	0.54	8.79	12.33	3.53	0.13
Zn15	0.51	7.99	10.19	2.19	0.08
Pb2	0.69	19.13	12.65	6.47	0.22
Pb4	0.67	17.40	11.82	5.57	0.19
Pb7	0.66	15.66	11.48	4.17	0.15
Pb9	0.65	13.98	11.05	2.92	0.11
Pb11	0.64	12.33	10.57	1.75	0.07
Pb15	0.63	10.19	9.94	0.24	0.01

Table 6.06. Values of the amount of alkali associated with borate and silicate networks and NBO/Si for the systems containing MW-BaO, MW-CaO, MW-SrO, MW-PbO and MW-ZnO based on ^{11}B NMR experiment.
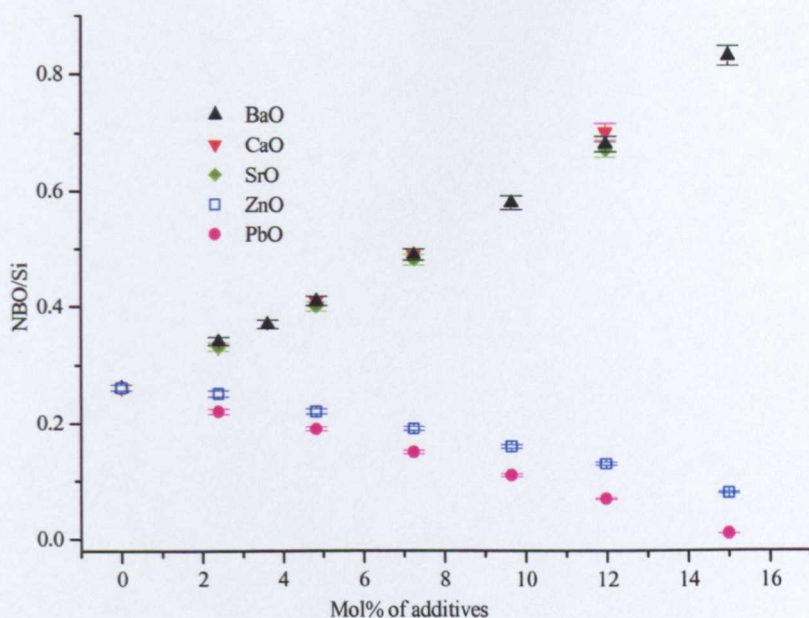
Fig. 6.03. Variation of the derived value of non-bridging oxygen per silicon based on ^{11}B NMR with the mol percent of different additive oxide.

6.3. ^{29}Si MAS-NMR

The ^{29}Si MAS-NMR spectra obtained from glasses containing BaO, CaO and SrO are shown in Figure 6.04. To determine the silicon speciation Q^n as the divalent oxide additive is introduced into the base glass, the spectra were fitted with at least two Gaussian line shapes using the peak fitting module in Microcal® Origin v.7.

The fits obtained are shown in Figures 6.05 – 6.07. A simulation was made including the intensity from spinning side bands. As can be seen from Figure 6.04 (i-iii) the addition of CaO, SrO and BaO glass produces similar effects on chemical shift, the ^{29}Si peaks move towards more positive values which means that these oxides act as modifiers in MW glass, introducing more NBO.

In the CaO system the chemical shift of ^{29}Si in Q^4 species ranges from - 93.8 to -103.4 ppm and Q^3 species from -86.6 to - 91.3 ppm. The intensity of the Q^4 units was found to decrease with the increasing concentration of CaO.

The chemical shift values of Q^4 structural units for the MW-SrO system range from -91.0 to -103.2 ppm and for Q^3 species the chemical shift values found range from -86.5 to -91.4 ppm. FWHM of the Q^4 species decreases with the increasing content of SrO.

Fig. 6.04. ^{29}Si NMR spectra obtained from several glasses based on the MW composition doped with (i) CaO (ii) SrO and (iii) BaO.
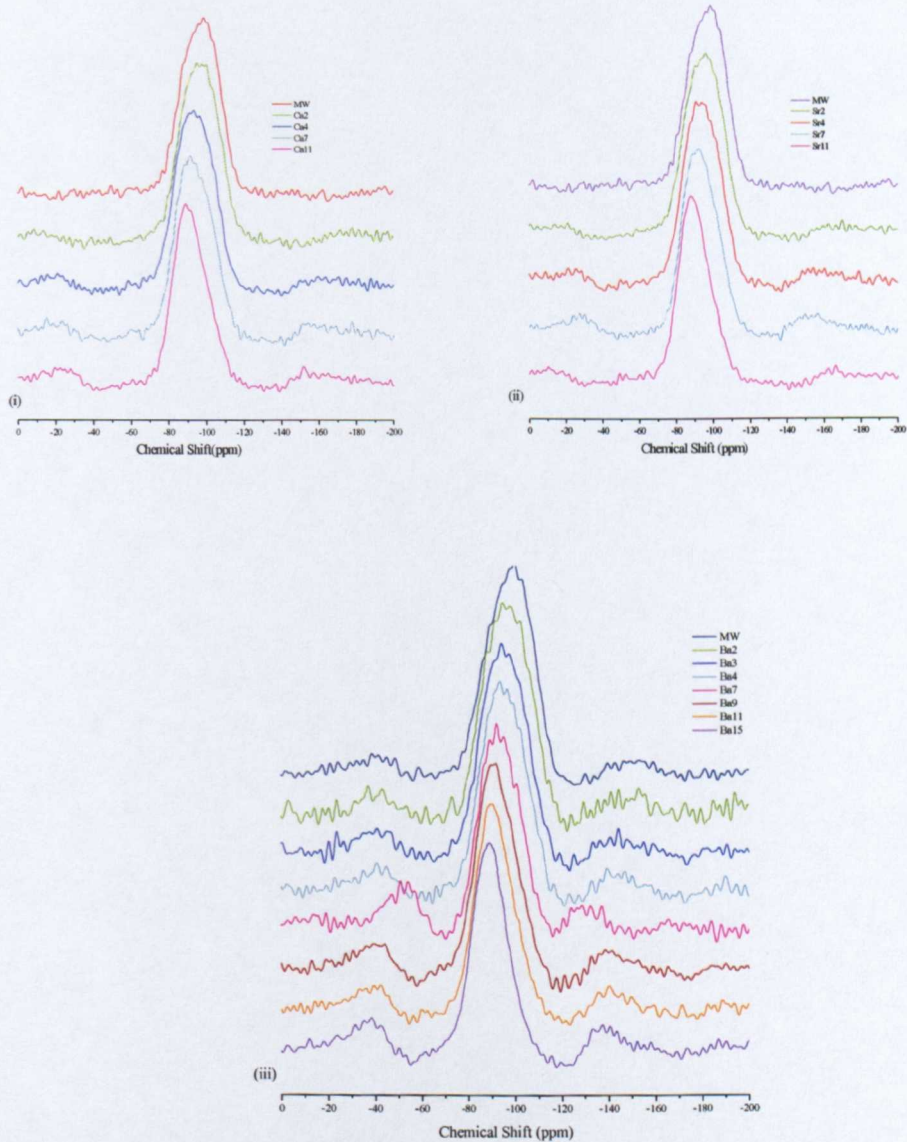
From Figure 6.07 it can be seen that, with increasing BaO, Q^3 structural units become more dominant and the spectra could be fitted with just one Q^3 peak at a BaO concentration of 15 mol percent. Deconvolution of the peak indicated that the

intensity of the Q^4 structural unit decreases with increasing concentration of BaO since the NBO are increasing in these glasses. The chemical durability study of MW-BaO glasses described in chapter 7, shows a decrease in chemical durability of these glasses which reflects the increasing concentration of non-bridging oxygen atoms [5, 6]. The complete dissolution of the glass sample at 15 mol% of BaO indicates the presence of significant concentration of non-bridging oxygen atoms in the glass matrix, adversely affecting the durability of the glass.

The chemical shift values from the overall fit are shown in Tables 6.07 - 6.09. Chemical shift values for Q^4 and Q^3 structural configurations of silicon have been found to move towards more positive values with the increase in content of CaO, SrO and BaO.

Fig. 6.05. Examples of the peaks used to fit the ^{29}Si spectra obtained from the MW-CaO glass system. Individual peaks are shown in blue Q^3 and green Q^4 and the fit is highlighted in red (a) MW (b) Ca2 (c) Ca4 (d) Ca11.

Sample Name	$\delta\,Q^4$ (±1ppm)	% of the fitted peak (±10%)	FWHM (±1ppm)	$\delta\,Q^3$ (±1ppm)	% of the fitted peak (±10%)	NBO/Si
MW	-103.8	44	15.0	-92.0	56	0.56
Ca2	-103.4	28	15.7	-91.3	72	0.72
Ca4	-102.7	25	14.1	-90.3	75	0.75
Ca7	-102.6	22	13.8	-90.0	78	0.78
Ca11	-93.8	20	13.0	-86.6	80	0.80

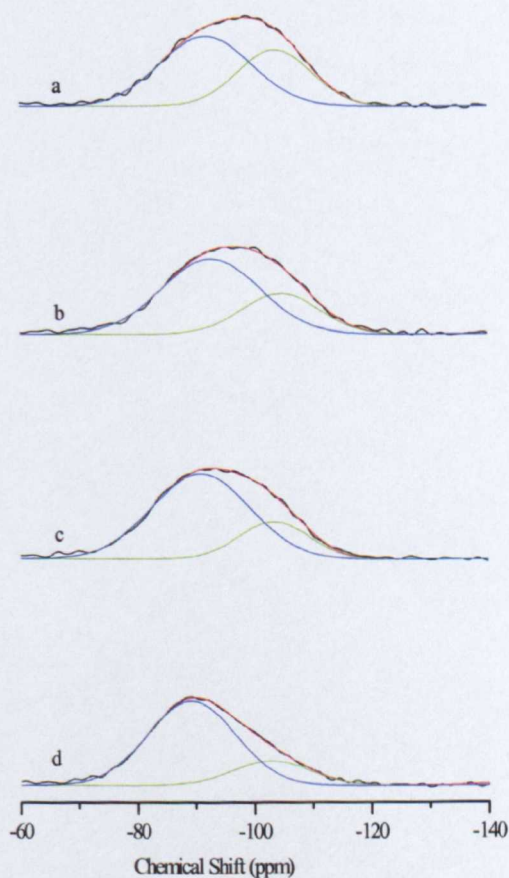*Table 6.07. Chemical Shift values obtained from ^{29}Si NMR for MW-CaO.*

Fig. 6.06. Examples of the peaks used to fit the ^{29}Si spectra obtained from the MW-SrO glass system. Individual peaks are shown in blue Q^3 and green Q^4 and fit is highlighted in red (a) MW (b) Sr2 (c) Sr4 (d) Sr11.

Sample Name	$\delta\,Q^4$ (±1ppm)	% of the fitted peak (±10%)	FWHM (±1ppm)	$\delta\,Q^3$ (±1ppm)	% of the fitted peak (±10%)	NBO/Si
MW	-103.8	44	15.0	-92.0	56	0.56
Sr2	-103.1	25	14.6	-91.3	75	0.75
Sr4	-103.3	23	14.0	-91.1	77	0.77
Sr7	-100.1	21	12.9	-89.2	79	0.79
Sr11	-91.0	12	12.4	-86.5	88	0.88

Table 6.08. Chemical Shift values obtained from ^{29}Si NMR for MW-SrO.

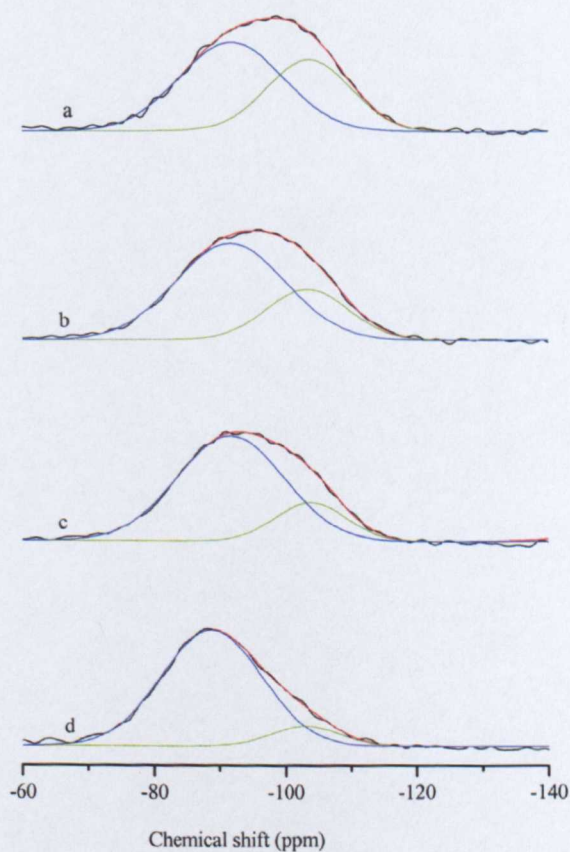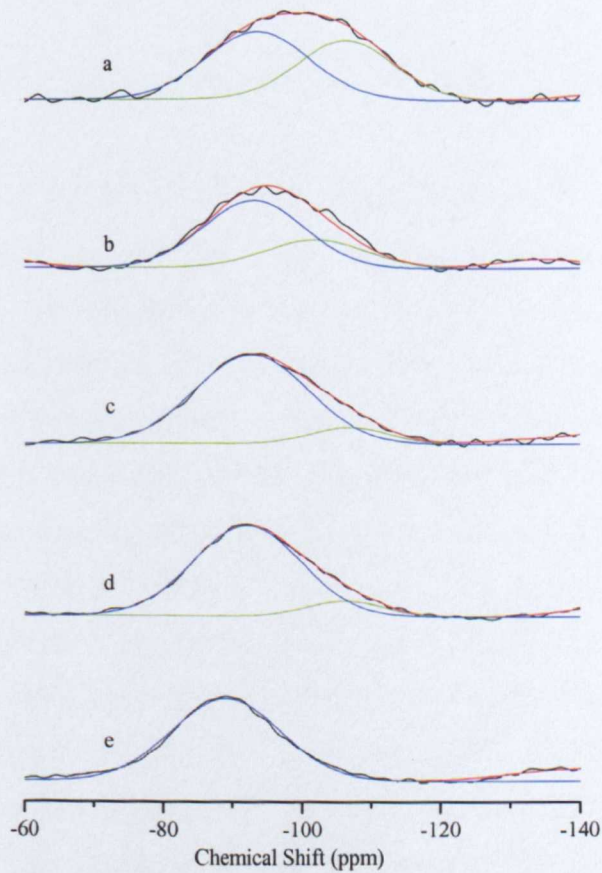*Fig. 6.07. Examples fit to the ^{29}Si spectra obtained from the MW-BaO glass system. Individual peaks are shown in blue Q^3 and green Q^4 and the fit is highlighted in red (a) Ba2 (b) Ba7 (c) Ba9 (d) Ba11 (e) Ba15.*

Sample Name	δQ^4 (±1ppm)	% of the fitted peak	FWHM (±1ppm)	δQ^3 (±1ppm)	% of the fitted peak	NBO/Si
MW	-104.6	40	14.6	-93.3	60	0.60
Ba2	-103.5	38	15.4	-92.9	62	0.62
Ba3	-103.9	37	14.5	-92.4	63	0.63
Ba4	-104.3	35	13.2	-92.8	65	0.65
Ba7	-99.4	20	12.8	91.1	80	0.80
Ba9	-92.3	12	12.6	-88.8	88	0.88
Ba11	-92.0	7	10.6	-87.8	93	0.93
Ba15	-	-	-	-88.1	100	1.0

Table 6.09. Chemical Shift values obtained from ^{29}Si NMR for MW-BaO.

The predicted values of NBO per silicon based on ^{11}B NMR are shown in Table 6.06. The percentage of Q^3 was found to increase with the amount of BaO, CaO and SrO. However, the calculation based on ^{29}Si NMR shows the number of non-bridging oxygens per silicon, for the alkaline earth additives, are higher than the predicted values. Various assumptions have been made: that there is no change in composition during melting; and that the sideband correction to N_4 is negligible. If these are true, then there is confidence in the predicted NBO/Si values and the problem must lie with the fitting of the ^{29}Si spectra. The most likely source is intensity contribution from $Q^4(B)$ being counted as Q^3 - i.e. a 3-peak fit is required. However, there is insufficient information in the spectra to allow a 3-peak fit to be performed.

Previous work from ^{29}Si NMR studies on mixed alkali borosilicate glasses with the addition of Bi_2O_3, Al_2O_3 and La_2O_3 [7] showed that the number of non-bridging oxygens per silicon atom decreases as the amount of additive oxides increases. This implies the formation of Si-O-X bonds i.e. the formation of the structural unit $Q^4(X)$, which is a Q^4 unit with one Si-O-X linkage. From the fitted spectra of ^{29}Si NMR with the alkaline earth additives indicates that there is no additional formation of Si-O-X bonds, where X = Ca, Sr and Ba.

The predicted non-bridging oxygen per silicon decreases with increasing concentration of PbO and ZnO from the calculation based on the ^{11}B MAS NMR. Due to the complexity of possible silicon speciation in the systems with ZnO and PbO, it was found difficult to obtain an appropriate fit with a view to extract any structural information from ^{29}Si NMR study. Therefore, more detailed studies are required in order to investigate the possible structural units which are Q^4, $Q^4(X)$, Q^3, $Q^3(B)$. Nevertheless, a spectral deconvolution using two peaks was attempted for these glasses and the results are presented in Table 6.10 - 6.11.
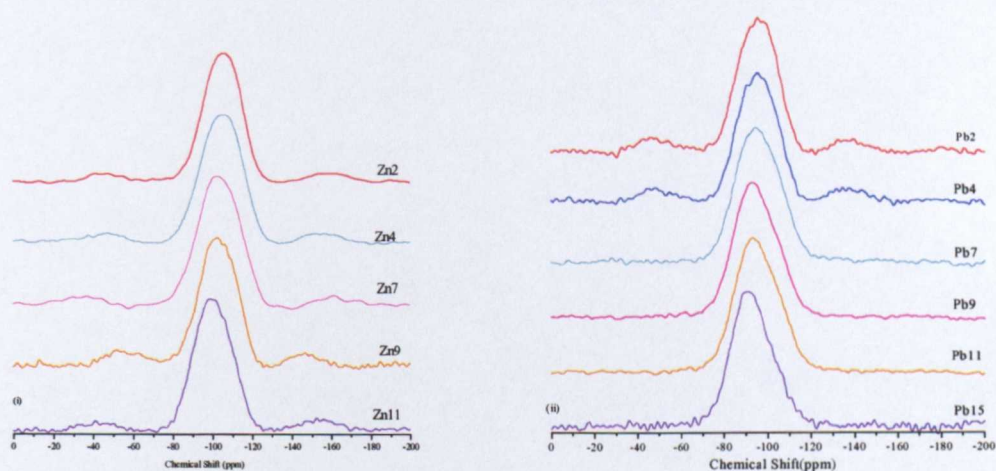
Fig. 6.08. ^{29}Si NMR spectra obtained from (i) MW-ZnO (ii) MW- PbO glasses.

Sample Name	Position of the fitted peak (± 1ppm)	% of the fitted peak
Zn2	-112.8 -103.0	17.4 82.6
Zn4	-112.5 -101.3	26.4 73.6
Zn7	-113.7 -101.6	12.1 87.9
Zn9	-112.2 -101.6	8.7 91.3
Zn11	-108.6 -97.1	26.4 73.6

Table 6.10. Chemical Shift values obtained from ^{29}Si NMR for MW-ZnO.

Sample Name	Position of the fitted peak (±1ppm)	% of the fitted peak
Pb2	-102.0 -91.5	37.4 62.6
Pb4	-102.5 -91.7	34.7 65.3
Pb7	-102.5 -90.5	44.7 55.3
Pb9	-95.2 -89.2	90.7 9.3
Pb11	-106.7 - 92.7	18.4 81.6
Pb15	-105.4 -90.7	16.2 83.8

Table 6.11. Chemical Shift values obtained from ^{29}Si NMR for MW-PbO.

6.4. UV Visible

6.4.1. UV- visible spectra MW-MnO system

The UV– visible spectra of the MW-MnO glasses are shown in Figure 6.09.
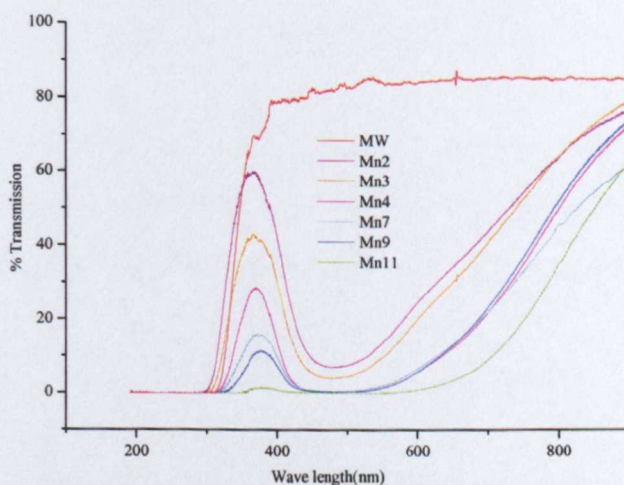

Fig. 6.09. Change in the UV-Visible transmission characteristics of the MW-MnO system with increasing concentration of MnO.

It can be seen that the transmittance decreases as the concentration of MnO increases. This is manifest as a change in colour from pale brown to purple. The transmittance was corrected to sample thickness.

With increasing concentration of MnO, the absorption edge of these glasses moves toward longer wavelengths. The increase in UV cut-off wavelength may reflect the generation of NBOs on the $[SiO_4]$ tetrahedra unit.

It is known that manganese ions have a strong bearing on optical and magnetic properties of glasses. The manganese ions can exist in different valence states in different glass matrices [8] Mn^{3+} occurs in borate glasses with octahedral coordination whereas in silicate and germanate glasses, the ions exist in the Mn^{2+} state with both octahedral and tetrahedral coordination [9]. The content of manganese in different oxidation states depends on the proportions of modifiers and glass formers, the size of the ions in the glass structure, their field strength and the mobility of the modifier cations.

In soda lime silica or sodium calcium silicate glass, manganese is present as divalent or trivalent ions. The trivalent form in this glass produced a single asymmetric absorption band centred at 490nm [10]. The optical absorption of divalent manganese reported in these glass systems is at 430 nm [10]. In sodium borate glasses, the manganese ion gives a brown colouration, the optical absorption is a single asymmetric band centred at 450nm [11]. Recent studies [8] on the role of manganese ions in the stability of the ZnF_2-P_2O_5-TeO_2 glass system have shown that manganese ions mostly exist in the Mn^{2+} state in these glasses when the concentration of MnO $\leq$ 0.4 % and above this concentration manganese ions predominantly exist in the Mn^{3+} state [8].

The absorption band in this system at ~ 490nm [10] may be due to the Mn^{3+} state, however further study is needed in order to get complete structural information on the system containing MW-MnO.

6.5. Conclusion

The addition of PbO and ZnO results in a decrease in N_4 values with increase in additives and adding ZnO has a greater effect than PbO. The decrease in N_4 indicates that the alkali ions are being removed from the borate network possibly by formation of complexes $[MO_n]^-R^+$.

On the other hand it was found that N_4 increased with alkaline earth content, and attained maximum values at compositions depending on the M^{2+} ion type. It can

be concluded from this work that, if the additive oxide enters the glass network as an intermediate or glass former the N_4 values will decrease. If the oxide enters as a modifier in the structure, the trend of N_4 as a function of additives is similar to that observed in alkaline earth borate glass.

From the calculations based on ^{11}B NMR it was predicted that, if the additive oxide acts as a network modifier, the number of non-bridging oxygens on silicon is increased with the additive oxide content. For the case of ZnO and PbO, the non-brdiging oxygen decreases with the level of oxide.

Investigation of the UV visible transmission characteristics of MnO-doped glasses has shown a gradual decrease in transmittance at ~380nm. With the increasing concentration of MnO, the UV absorption edge of these glasses moves towards longer wavelengths. The increase in UV wavelength may be caused by generation of NBOs on the $[SiO_4]$ tetrahedral units. The absorption at ~ 490 nm is due to the Mn^{3+} state.

6.6. References

[1]   D. Massiot, F. Fayon, M. Capron, I. King, S. Le Calvè, B. Alonso, J. O. Durand, B. Bujoli, Z. Gan and G. Hoatson, Magnetic Resonance in Chemistry **40** (2002) 70.

[2]   W. J. Dell, P. J. Bray and S. Z. Xiao, J. Non-Cryst. Solids **58** (1983) 1-16.

[3]   Hiroshi Yamashita, Kazuhiko Inoue and Takeshi Nakajin J. Non-Cryst. Solids **331** (2003) 128-136.

[4]   Norikazu Ohtori, Keiichi Takase, Isoa Akiyama and Yoshihiro Suzuki, J. Non-Cryst. Solids **293-295** (2001) 136-145.

[5]   J. M. Stevels, Progress in the theory of the physical properties of glass, Elsevier, New York (1948).

[6]   R. W. Geldart and C. H. Kindle, PNL - 6333, Pacific Northwest Laboratory, Richland, Washington (1988).

[7]   A. Duddridge, PhD Thesis, Department of Physics, University of Warwick, UK (2004).

[8]   D. K. Durga and N. Veeraiah, J. Phys. Chem. Solids **64** (2003) 133-146.

[9]   A. Van Die, A. C. H. Ileenares and W. F. Van Der Weg, J. Non-Cryst. Solids **99** (1988) 32.

[10]   C. R. Bamford, Colour generation and control in glass, glass science and technology, Elsevier, New York (1997).

[11]   C. R. Bamford, Phys. Chem. Glasses **3** (1962) 189.

Chapter 7

Chemical Durability and Ionic (DC) Conductivity

7.1. Introduction

Corrosion of nuclear waste glasses affects their long-term chemical durability and fracture strength [1]. Determination of the initial rate of glass dissolution can be used for safety assessments in the case of water access to the waste repository. A Soxhlet leaching (dynamic) method was conducted to determine the chemical durability of the glass. Tests were carried out in a flowing deionised water system for 14 days at a temperature of approximately 75°C at the sample along with a 'Blank' Soxhlet for the baseline analyses. Sample weight loss and leachate pH were recorded. The leachate was analysed for sodium and lithium content and barium where appropriate [2]. The phase composition of the corrosion layer was identified using high-resolution X-ray diffraction.

7.2. MW-MO (M = Ca, Sr, Ba)

7.2.1. Weight loss

The weight loss behaviour of the MW glasses containing CaO, SrO and BaO is shown in Figure 7.01. It can be seen that the amount of sample lost after fourteen days increases with increasing amount of BaO and SrO but weight loss only increases up to ~ 6 mol% for CaO and thereafter decreases.

Weight loss reaches 100 % for the glasses at 15 mol% of BaO, 40 % at 11.98 mol% of SrO and the maximum loss for MW-CaO is ~ 22% at ~ 6 mol%. Weight loss follows the trends BaO > SrO > CaO. The relative effect of different divalent oxides is expected to depend on the ionic radii Ba (1.35) > Sr (1.13) > Ca (0.99); the field strength Ba (0.27) < Sr (0.32) < Ca (0.36); and the bond strength Ba (0.74) < Sr (0.80) < Ca (0.85). At > 6 mol % concentration of CaO, the weight loss decreases. This may be due to micro phase separation or may be the result of the formation of a barrier layer at the surface.
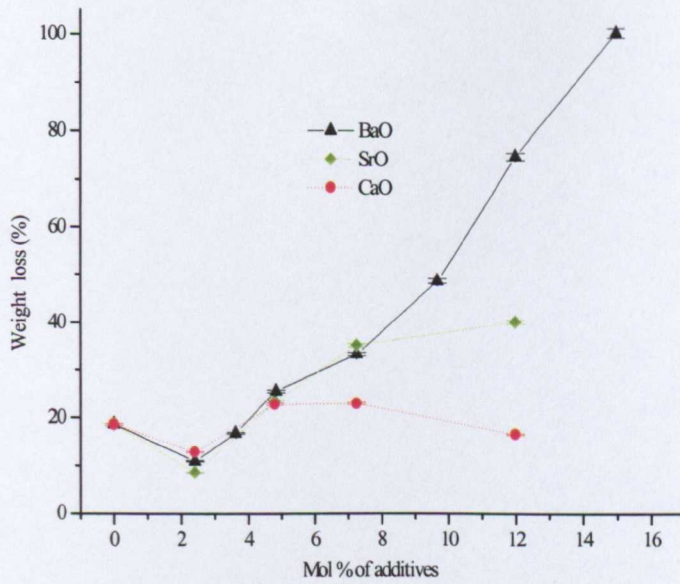
Fig. 7.01. Weight loss (%) of sample after 14 days leach testing as a function of modifier additives in MW glass.

7.2.2. Leachate Analysis

Addition of alkaline earths results in an increase in leachate pH whereas PbO and ZnO cause a decrease in pH (Figure 7.02).
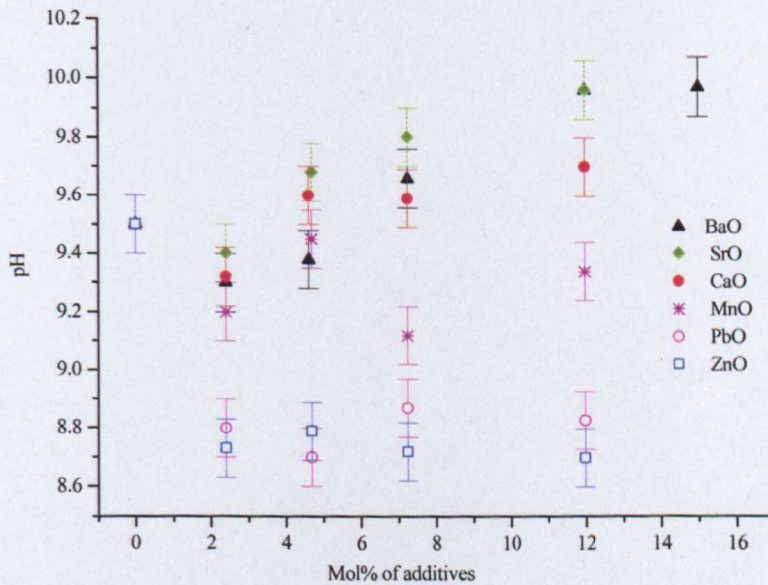

Fig. 7.02. Variation pH values of leachate with mol% of additives.

The amounts of sodium and lithium present in the leachates from systems containing SrO and BaO are shown in Figures 7.03 and 7.04 and the barium leached from the MW-BaO samples is shown in Figure 7.05. Although there is a small decrease of Na/Li content of the leachate when 2.4 mol % oxides are added to MW, beyond that

the dissolution of sodium and lithium increases. The trends of weight loss measurement were found to be consistent with the leachate analysis result i.e. BaO >SrO. The MW-CaO leachate was not analysed, however it is expected from weight loss measurement that the trend for leachate composition will be the same. The Ba content of the leachate (Figure 7.05) follows the same trend with the weight loss measurement showing the highest amount of barium leached out at 15 mol %.
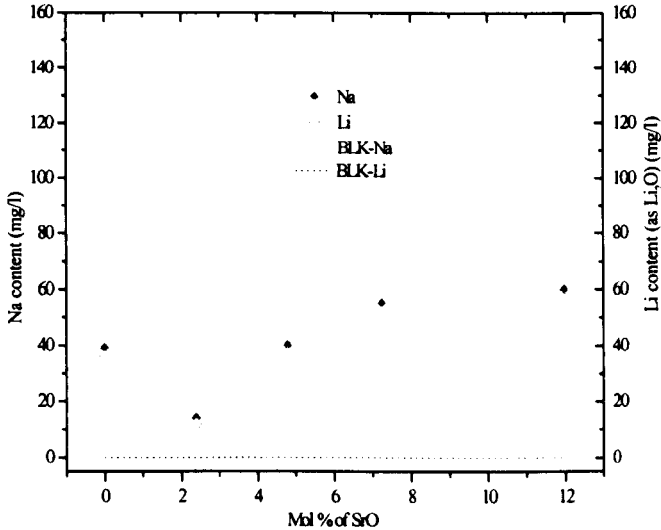

Fig. 7.03. Chemical analysis results [2], after 14 days Soxhlet leach test, of the amount of sodium and lithium (in mg/l) in leachates as a function of SrO in MW glass. Error bars are smaller than the symbols used.
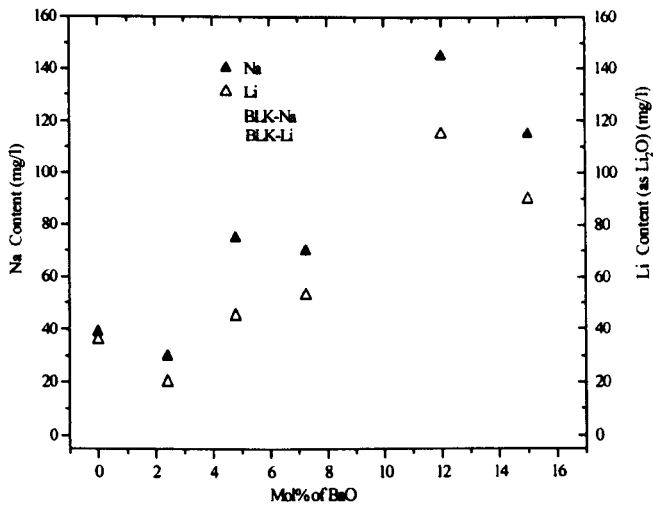

Fig. 7.04. Chemical analysis results [2], after 14 days Soxhlet leach test, of the amount of sodium and lithum (in mg/l) in the leachates as a function of BaO content. Error bars are smaller than the symbols used.

The total amount of Na in the initial Ba15 sample was ~ 39 mg and Li (as Li_2O) was ~ 25 mg. These values are close to the analysed quantities for Na and Li (as Li_2O) in 100ml of leachate (34.5 mg Na, 27 mg Li_2O).
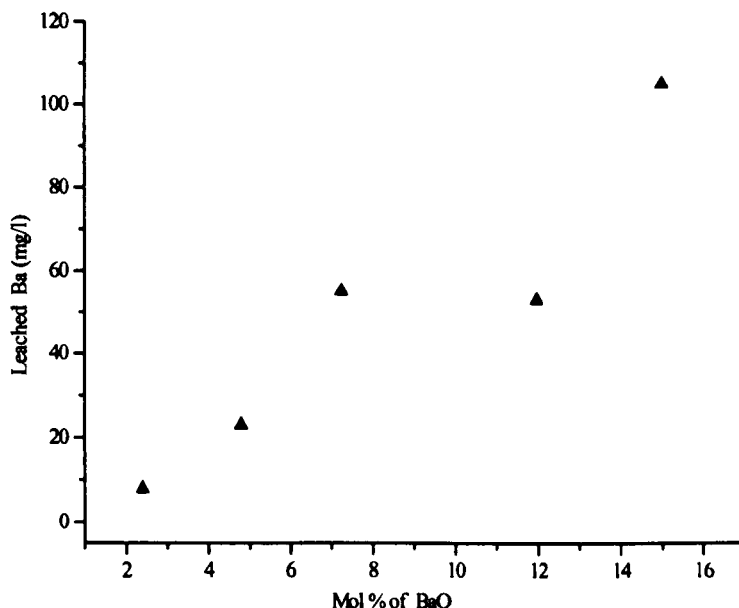

Fig. 7.05. Chemical analysis results [2], after 14 days Soxhlet leach test, of the amount of barium leached out of MW-BaO glasses.

7.2.3. Leach surface characterisation

All samples before leach testing showed no remarkable optical features, but after leach testing the surfaces showed obvious corrosion features depending on the additive used. These are briefly discussed for each series of glass.

7.2.3.1. MW-CaO

Figures 7.06 (a-d) show the corroded surfaces of the glasses containing CaO. The 2.4 mol% CaO sample shows small pits. These increase in size at higher CaO contents up to 7.25 mol% CaO but then decrease again. This mirrors the weight loss data. XRD examination of the leached surfaces of these glasses show them to be amorphous in nature (Figure 7.07). XRD of the corrosion layer is taken at glancing angle, so that only the surface of the corroded sample is measured.
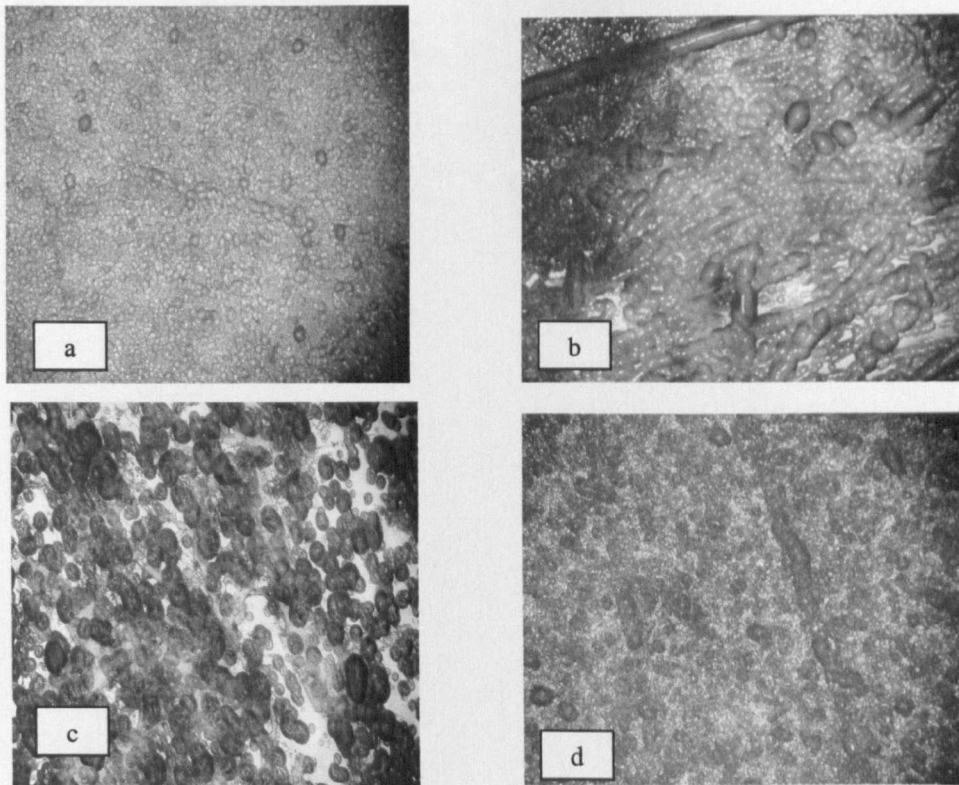
Fig. 7.06. MW-CaO Optical micrographs (magnification × 50) after leach testing (a) Ca2 (b) Ca4 (c) Ca7 (d) Ca11.
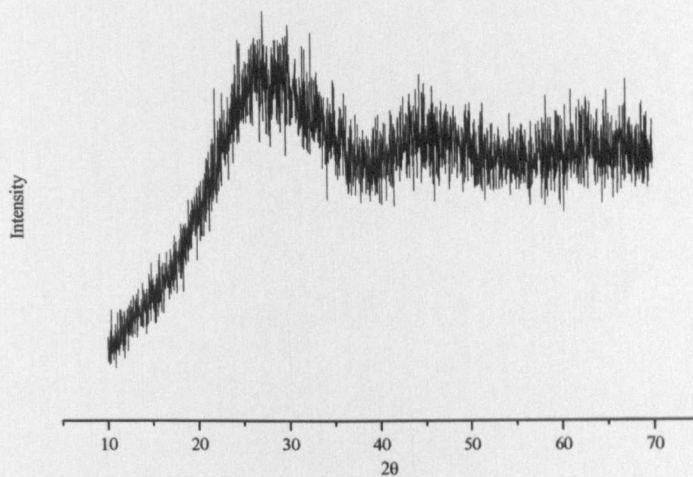

Fig. 7.07. Typical XRD analysis of corrosion layer on the sample with 7.25 mol% of CaO.

7.2.3.2. MW-SrO

The surfaces of the MW-SrO sample after leach testing are shown in Figure 7.08 (a-d). Up to 7.25 mol% SrO, the leached surfaces resemble those from MW-CaO. At 11.98 mol% of SrO there is a noticeable difference with the formation of bubbles and surface blistering. XRD of the surfaces did not show any crystalline phase (Figure 7.09).
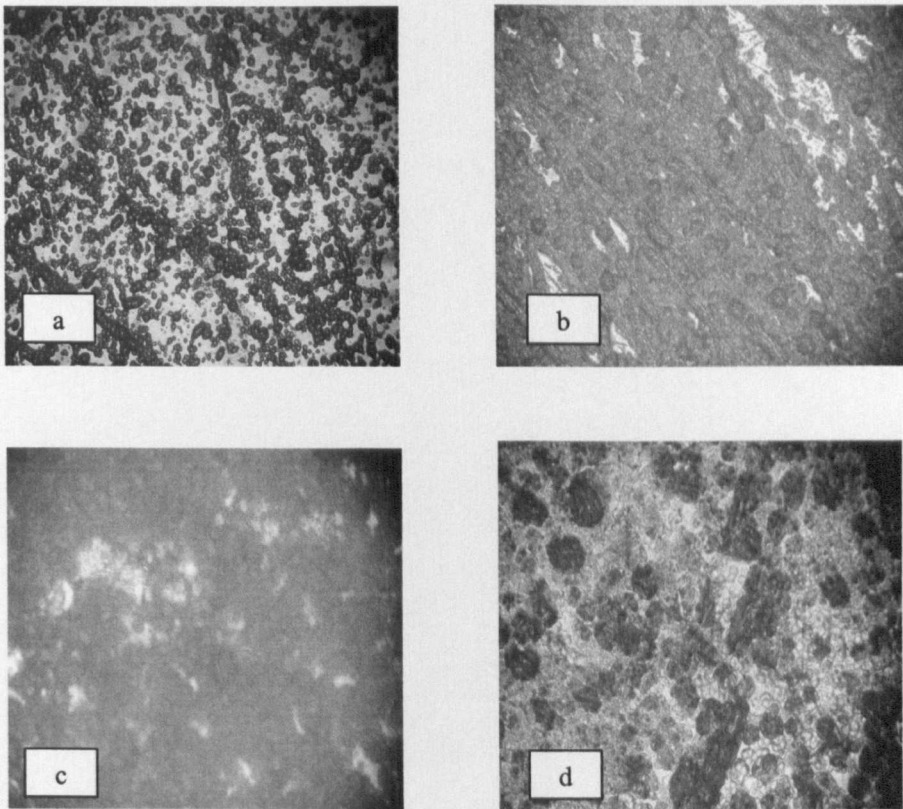

Fig. 7.08. Optical micrographs of the corroded surface (magnification× 50) of MW-SrO glass system after 14 days leach testing (a) Sr2 (b) Sr4 (c) Sr7 (d) Sr11.
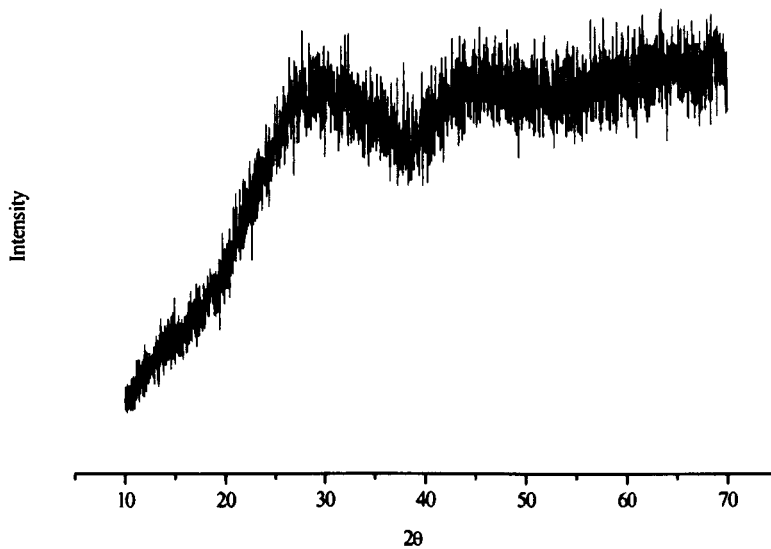
Fig. 7.09. XRD of leached surface layer on the sample with 7.25 mol % of SrO.

7.2.3.3. MW-BaO

Figures 7.10 (a-f) are scanning electron micrographs of the MW- BaO series glass surfaces. There were marked differences in the surface condition of each sample after the leaching tests.

Bubble like features can be seen in the corroded 2.4 mol% BaO sample. Figures (b) (c) (d) (e) and (f) show increased layer formation followed by exfoliation as the % of BaO increases respectively. In addition, severe surface damage was found for the 11.98 mol% of BaO as shown in Figure 7.11. Complete dissolution of the 15 mol% prevented surface examination. A high-resolution XRD trace of the leached surface layer on the 11.98 mol% sample MW-BaO shown in Figure 7.12 is completely amorphous.
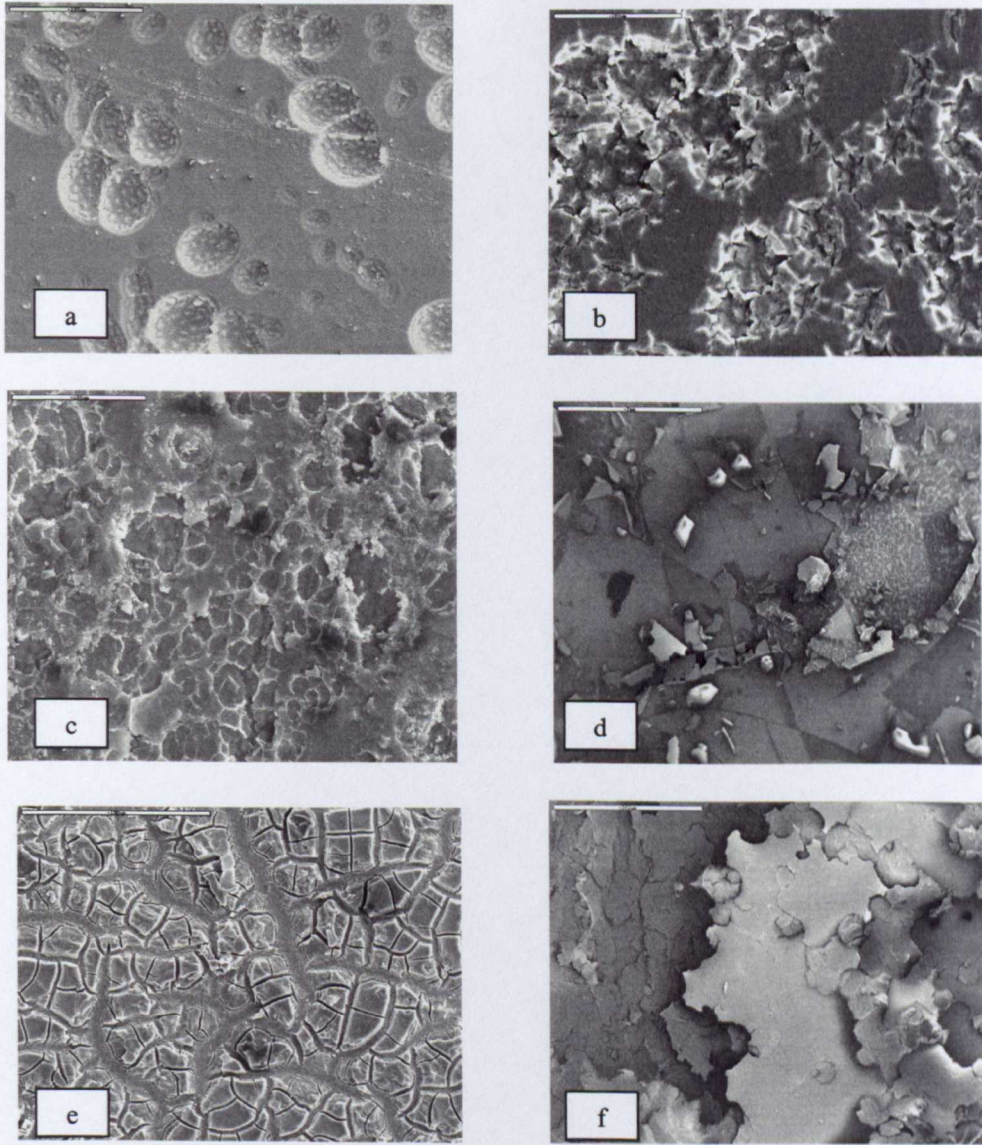
Fig. 7.10. Scanning electron micrographs (100μm) of the corroded surfaces for the MW- BaO glasses system after 14 days leach testing in deionised water (a) Ba2 (b) Ba3 (c) Ba4 (d) Ba7 (e) Ba9 (f) Ba11.

Fig. 7.11. The remains of the corroded sample containing 11.98 mol% of BaO, after 14 days leach testing.
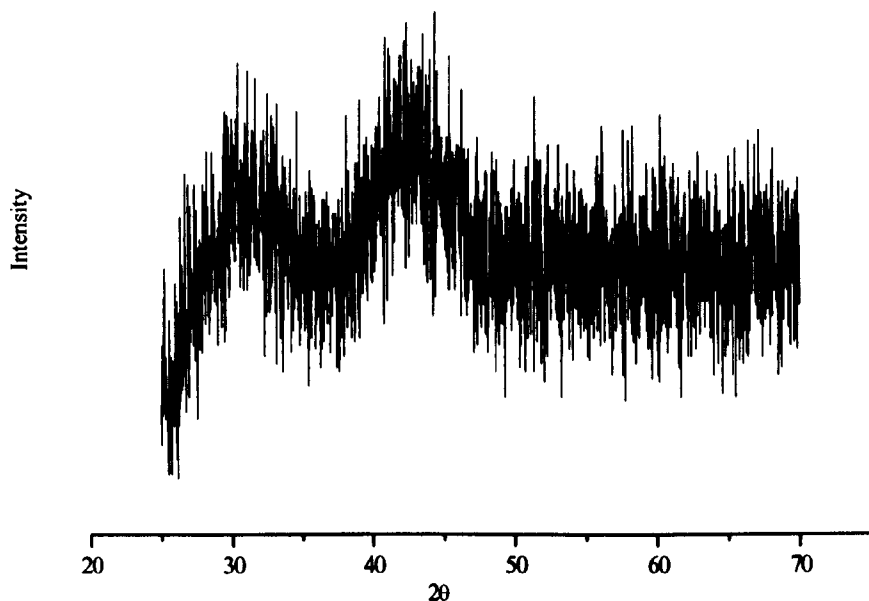
Fig. 7.12. XRD of the leached surface layer on the sample MW-BaO (11.98 mol% of BaO) shows amorphous phase.

7.3. MW-M'O (M' = Pb, Zn)

7.3.1. Weight loss

The weight loss of each sample after 14 days is shown in Figure 7.13 as a function of additive oxide content. It can be seen from Figure 7.13 that adding ZnO and PbO produce different trends from the alkaline earths e.g. BaO. The chemical durability of the glass increases with PbO and ZnO and decreases with BaO. However, there seems to be a small increase in weight loss at higher PbO concentration.

Fig. 7.13. Weight loss of sample after 14 days leach testing as a function of additives (BaO, ZnO, PbO) in MW glass.

7.3.2. Leachate Analysis

The amounts of sodium and lithium present in the leachates from the glass system containing PbO and ZnO are shown in Figures 7.14 and 7.15 respectively. Lo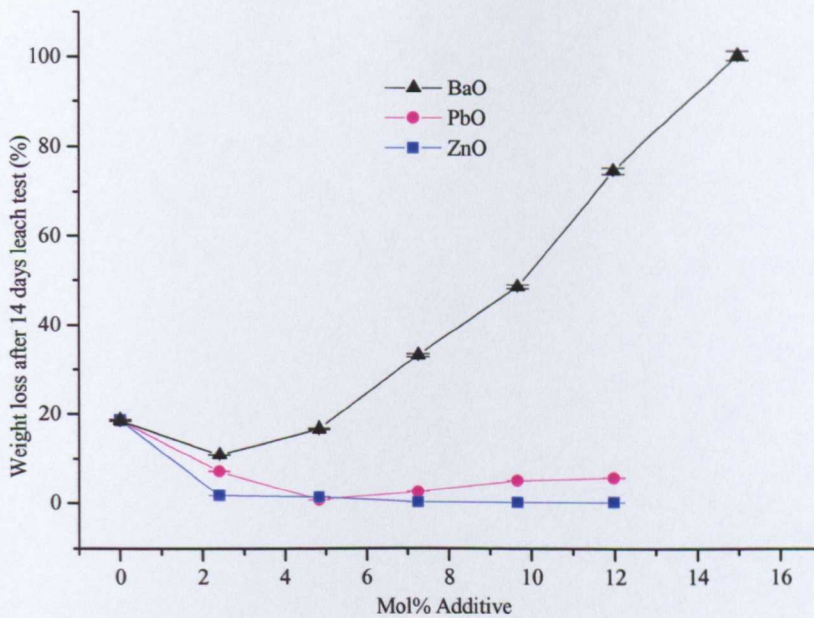w concentrations of PbO improve the chemical durability but when the concentration of the additive oxides exceeds 4.6-mol% dissolution increases again. This shows the intermediate role of PbO in these glasses. Studies by several authors [3-5] on the effect of lead addition in sodium ultra phosphate glasses also found that it improved the chemical durability. From Figure 7.15 it can be seen that, as the concentration of ZnO increases, the amount of Na and Li in the leachate decreases to the baseline, showing the better durability of MW-ZnO glasses. The leach rate is reduced by increasing ZnO in zinc borosilicate glass [6,7]. Calestani [6] also reported that the diffusion of alkali ions is strongly depressed by the presence of zinc.

It is well known that reducing alkali ion mobility in glasses would be expected to lower the rate of chemical attack. The trends in ionic conductivity described in section 7.6 show that the chemical durability of MW-ZnO glass and PbO parallels the change in alkali ion mobility reasonably well.

97
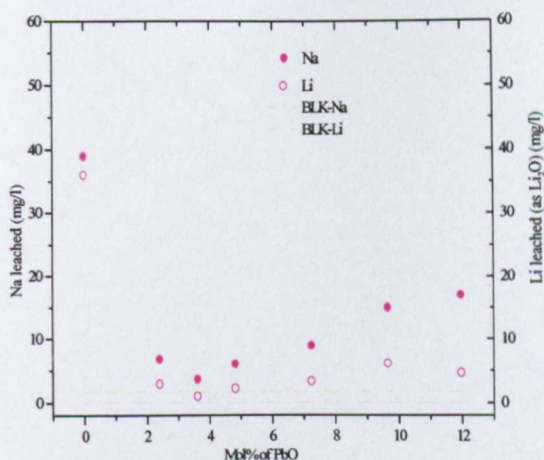
Fig. 7.14. Chemical analysis results [2], after 14 days Soxhlet leach test, of the amount of sodium and lithium (in mg/l) in leachates as a function of PbO in MW glass.
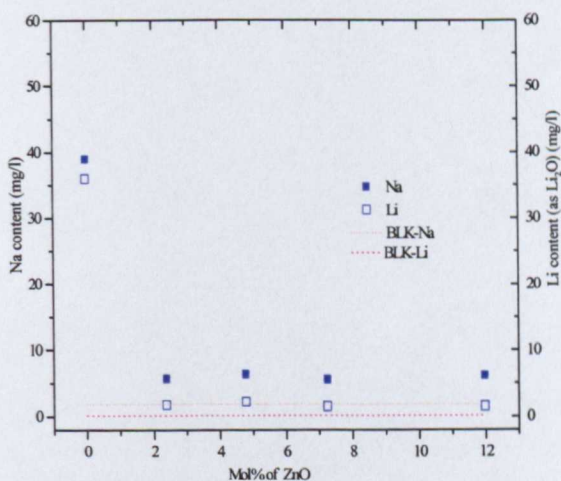
Fig. 7.15. Chemical analysis results [2], after 14 days Soxhlet leach test, of the amount of sodium and lithium (in mg/l) in leachates as a function of ZnO in MW glass.

7.3.3. Leach surface characterisation

7.3.3.1. MW-PbO

The optical micrographs of PbO containing glasses are shown in Figure 7.16 (a-d). The surfaces of the samples containing 2.4 and 3.6 mol% did not show any significant change after leach testing. Glasses with 7.25 and 9.66 mol% show slightly rougher surfaces, due to the higher dissolution of these glasses.
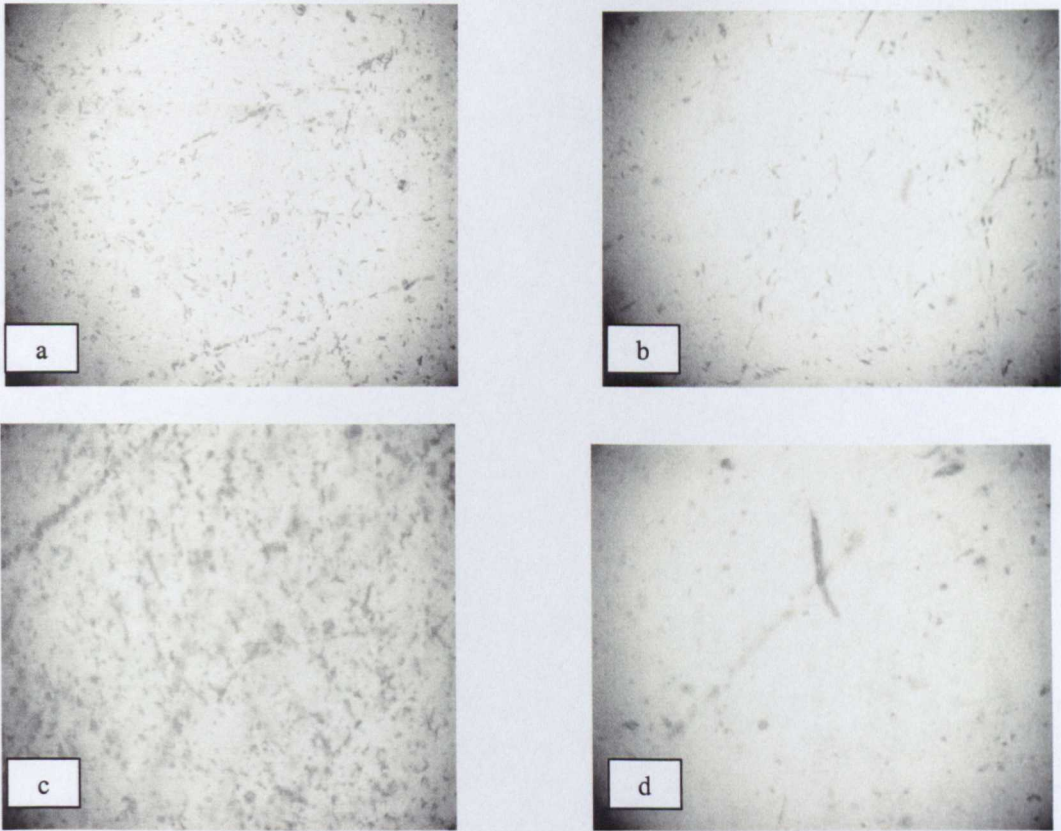
Fig. 7.16. Optical micrographs image (magnification ×50) from surfaces of the samples containing. PbO as an additive samples after 14 days leach testing (a) Pb2 (b) Pb3 (c) Pb7 (d) Pb9.

7.3.3.2. MW-ZnO

The optical microscope images of some of the ZnO containing glasses are shown in 7.17 (a-d). All the glasses in this series show few optical features, indicating the good chemical durability of these glasses. No detectable crystalline precipitates were found on the surface of these glasses.
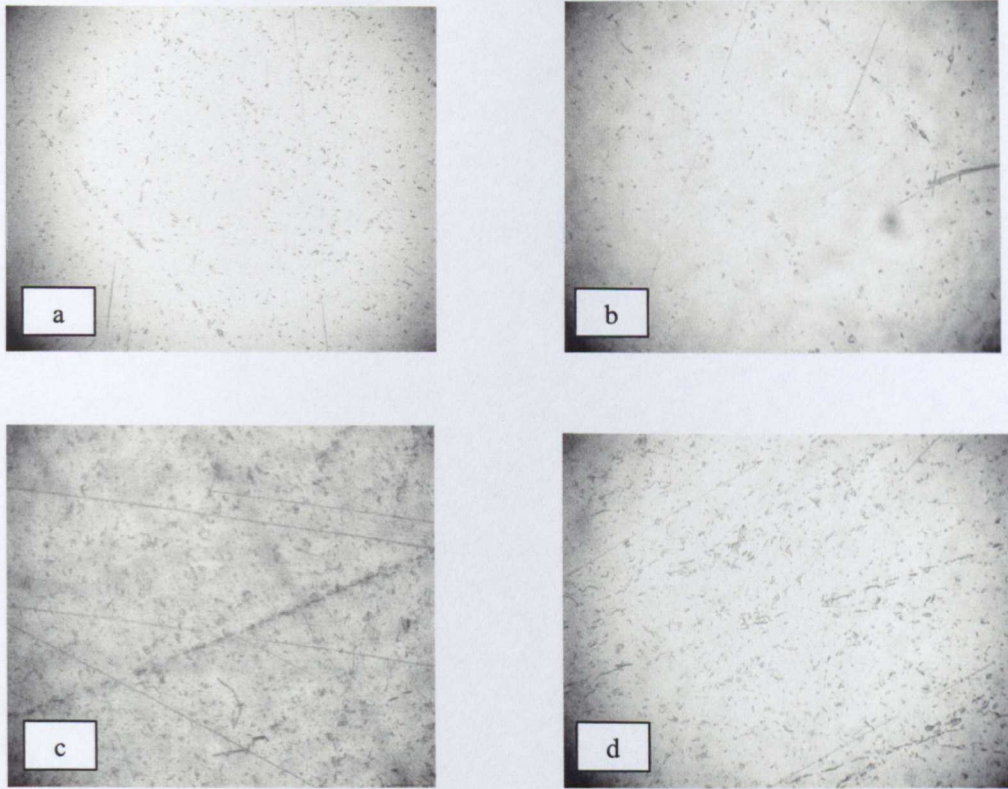
Fig. 7.17. Optical micrographs images from surfaces (magnification ×50) of the samples containing ZnO as an additive, after leach test (a) Zn2 (b) Zn4 (c) Zn7 (d) Zn11.

7.4.   MW-MnO

7.4.1. Weight loss

Figure 7.18 shows the sample weight loss as a function of the concentration of MnO. The maximum weight loss of MnO glass was ~13 %. The weight loss of these glasses may depend on the relative proportions of Mn^{2+} and Mn^{3+} present and also on the surface crystal deposition process.
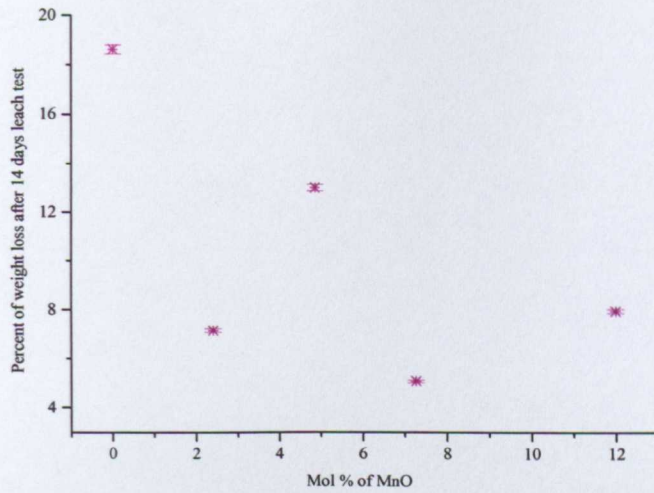
Fig. 7.18. Weight loss of samples after 14 days leach testing as a function of MnO in MW glass.

7.4.2. Leachate Analysis

From the leachate analysis of the MW-MnO system it was found that the alkali loss decreased as more MnO was added but increased again at high concentration of MnO. Deposits of crystalline phase may also affect the rate of dissolution of Na/Li in the glass and hence durability of the glass.
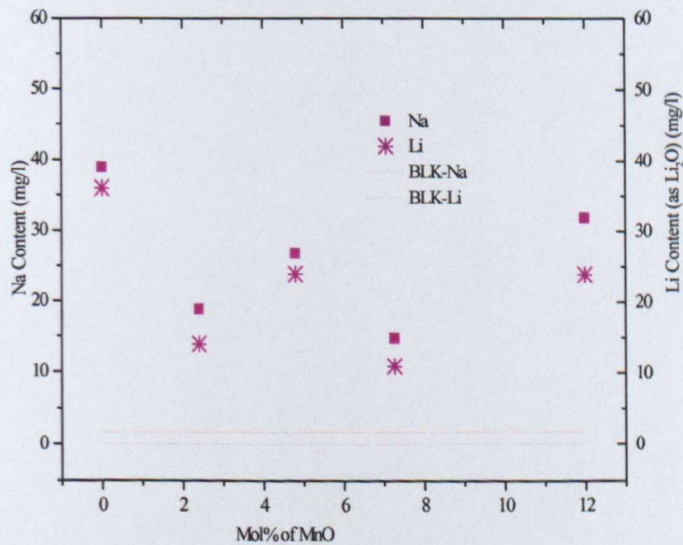
Fig. 7.19. Chemical analysis results [2], after 14 days Soxhlet leach test, of the amount of sodium and lithium (in mg/l) in leachates as a function of MnO in MW glass.

7.4.3. Leach surface characterisation of MW-MnO

Glasses containing MnO developed surface layers on the samples after 14 days. These corrosion layers were characterized using SEM and high-resolution X-ray diffraction. SEM micrographs of each sample after leach testing are shown in Figures 7.20 (a-f), where it can be seen that at lower concentration of MnO the corroded surface shows less crystalline deposit.
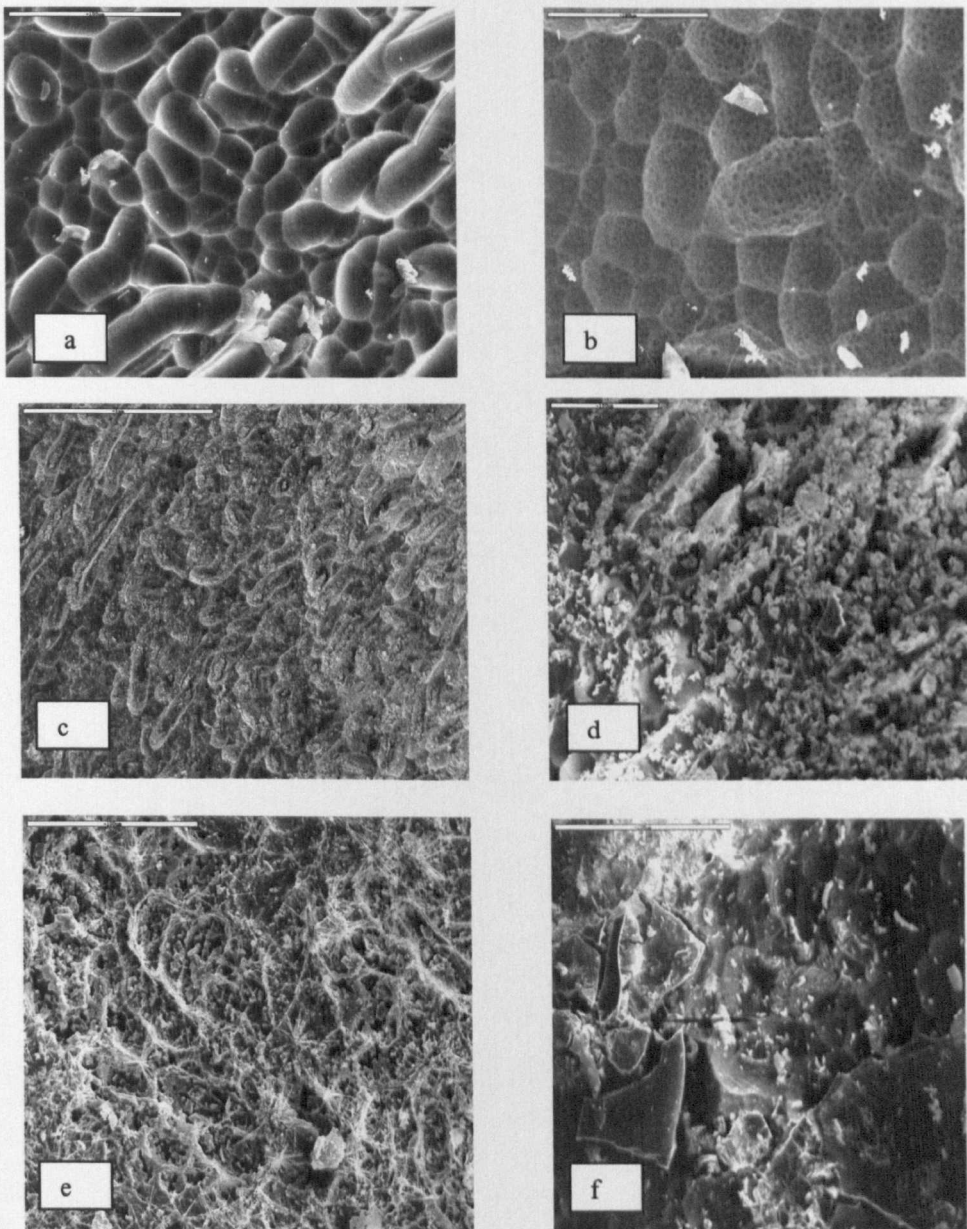
Fig. 7.20. Scanning Electron Micrographs (100μ m) of MW-MnO after 14days leach testing (a) Mn2 (b) Mn3 (c) Mn4 (d) Mn7 (e) Mn9 (f) Mn11.

The XRD patterns obtained are shown in Figure 7.21. The best fit to the peaks comes from the X-ray diffraction spectrum of manganese silicon oxide Mn_7SiO_{12} [8, 9] Figure 7.22.
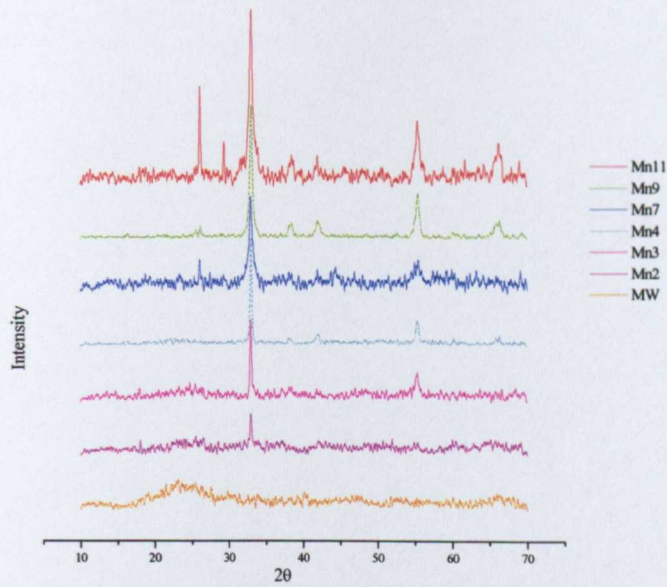
Fig. 7.21. XRD patterns of MW- MnO glass samples after corrosion, peaks are attributed to Mn_7SiO_{12}.
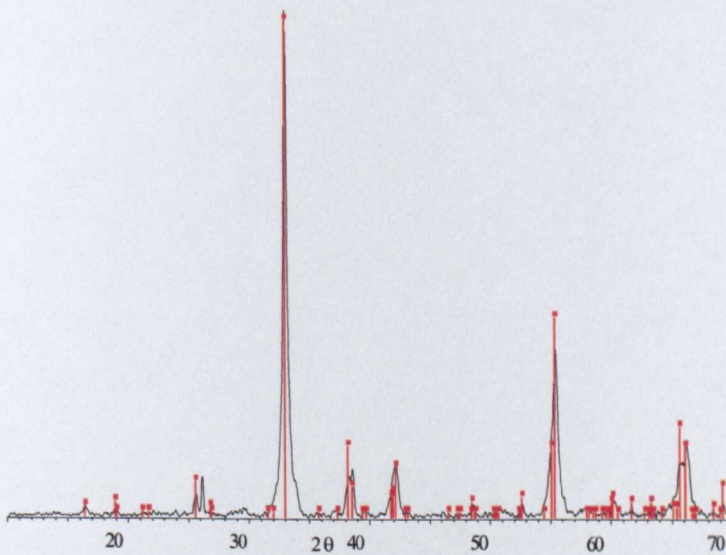
Fig. 7.22. High resolution XRD trace of samples after leaching in deionised water for 14 days at 75 °C, peaks attributed to Mn_7SiO_{12} [8, 9].

103

7.5. Conclusions

The leaching process is a diffusion controlled ion-exchange process involving the exchange of protons or hydronium ions for the alkalis present in glass. The extent of this reaction depends on the composition of the glass and the conditions under which leaching occurs. In general, there will be a selective removal of elements present in the interstices of the glass network as glass modifiers, because they are weakly attached.

Chemical durability studies have shown that the addition of alkaline earth oxides to the base glass results in an increase in corrosion in the order CaO < SrO << BaO. Clearly bond strength is a factor affecting the chemical durability. Glass formers have larger X-O bond strengths than glass modifiers [10]. Several authors have suggested that [11,12] the rate of dissolution of glass containing alkaline earth cations is correlated to the hydration free energy of the glass. This energy is assumed to equal the sum of the component hydration free energies weighted by their mole fraction in the glass. The hydration free energies toward water for BaO, SrO, CaO containing glasses are respectively -40, -34, -27 kJmol^{-1}. Moreover, the Ba glass shows a significant increase in radial crack size after immersion in water.

From the analysis of the leachate it can be concluded that chemical durability depends on the structural role of the additive oxides in the (MW) base glass. The presence of the modifiers BaO and SrO increases dissolution of Na$^+$ and Li$^+$ whereas PbO, ZnO and MnO reduce the rate of chemical attack. In addition, it can also be seen from Figures 7.20 and 7.21 that, MnO produces a crystalline surface deposit.

The alkaline earth cations break the Si-O-Si with the introduction of non-bridging oxygen sites. Intermediate oxides make the glass more durable either by decreasing the number of non-bridging oxygens or by making the ion exchange with H$_3$O$^+$ for the glass system containing PbO and ZnO more difficult [13].

The different behaviour of the calcium, strontium, barium, lead, zinc and manganese containing glasses which is shown in sample weight loss and chemical analysis (Figures 7.01, 703-7.05, 7.13-7.15, 7.18-7.21) is evidenced also by the optical images and SEM photographs of leached glasses.

A consistent qualitative picture of the composition dependence of the resistance of the glasses to water has been obtained using this approach. However the data did not allow for detailed quantitative investigation of the leaching kinetics. It was shown that

the nature of the corrosion is strongly dependent on the identity of the cation present in the glass system. Ba glass is shown to be the most reactive towards water.

The corrosion layer can give useful information on the leaching mechanism and it might be examined by means of surface techniques of photoelectron spectroscopy (XPS) or secondary ion mass spectrometry (SIMS) or by means of nuclear techniques such as Rutherford backscattering (RBS) and specific nuclear reactions (NRA).

7.6. Ionic (DC) Conductivity

7.6.1. Introduction

Alkali ion motion in glass is important because of its fundamental relation to properties such as electrical conductivity and chemical durability [14]. Electrical conductivity measurements provide an opportunity to compare alkali ion mobility in doped mixed alkali borosilicate glasses. Ionic conductivity was investigated in MW containing ZnO, PbO, MnO and also BaO to represent the alkaline earths.

It has been established that electrical current through alkali borate and silicate glasses is carried by alkali ions. The conductivity σ of a glass follows a simple exponential dependency

$$\sigma = \sigma_0 \exp(- E_a/RT) \qquad (7.1)$$

where the pre-exponential factor σ_0 is a constant, E_a is the activation energy, R is the gas constant and T is the absolute temperature.

DC ionic conductivity of the BNFL HLW borosilicate glass with different concentrations of divalent oxides was determined using the ac impedance technique for temperatures from 200–350°C and a frequency sweep of 5Hz-1MHz. Details of the experimental procedure have been described in chapter 4. Complex impedance plots were used to determine the DC ionic conductivity of the studied glass system. The samples did not show any significant conduction below approximately 200°C.

7.6.2. Ionic conductivity MW-BaO

Ionic conductivity in the system MW-BaO has been investigated in the range 2.4 $\leq$ x $\leq$ 11.98 mol % of BaO. It was found that introducing the Ba^{2+} cation in MW glass caused a gradual reduction in conductivity.

Figure 7.23 shows typical impedance spectra at different temperatures obtained from MW-BaO glass. Values of conductivity were found in the range of 9.3×10^{-7} to 5.3×10^{-8} Scm^{-1} at ~ 300°C i.e. more than an order of magnitude decrease on adding 11.98 mol% of BaO. Variation of conductivity with increasing concentration of BaO is shown in Figure 7.24. Similar results have been reported for silicate glasses [15]. The current carriers in these samples are expected to be monovalent ions i.e. alkali ions. AC conductivity as a function of frequency is shown in Figure 7.25. At high frequency, electrical resistivity decreases as the ion displacement decreases.

Values of conductivity at different temperatures were used to produce an Arrhenius plot (Figure 7.26) from which the activation energy for conduction could be calculated. As can be seen from Table 7.01 activation energy does not change greatly with composition or with the nature of the additive. So the reduction in the conductivity maybe dominated by the number of mobile ions rather than their mobility in these glass systems. AC conductivity studies [16] show that the activation energy for Li$^+$ conduction in lithium borosilicate glass, in the temperature range 170 - 440°C, is ~ 0.51eV. This is very close to the values obtained in the present study for mixed alkali borosilicate glasses ~ 0.47 eV in the temperature range 250 - 350°C.
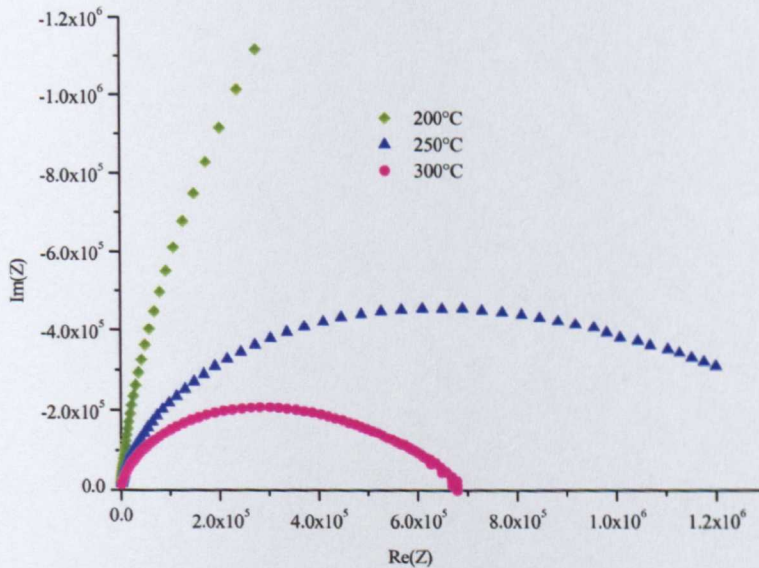

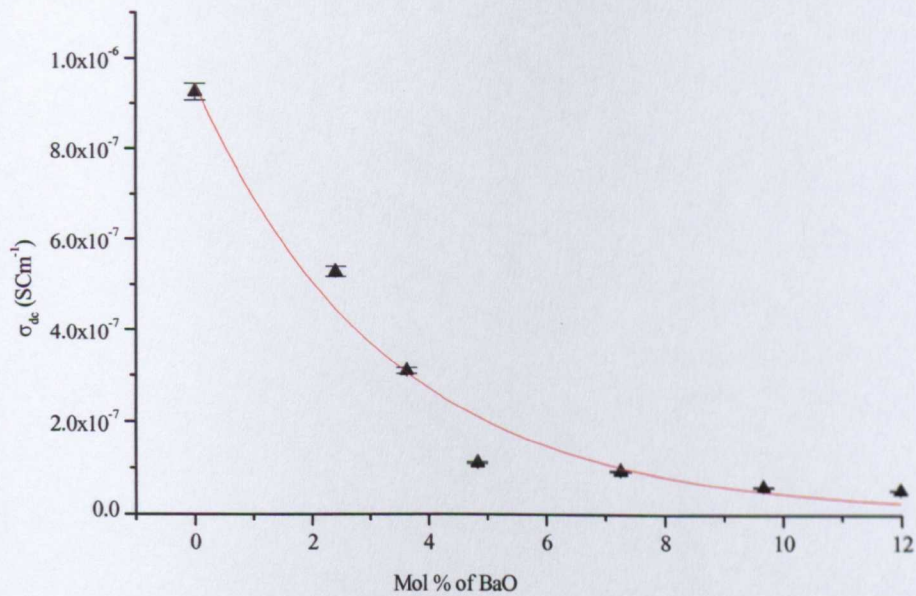Fig. 7.23. Complex impedance spectra at various temperatures obtained from MW-BaO.

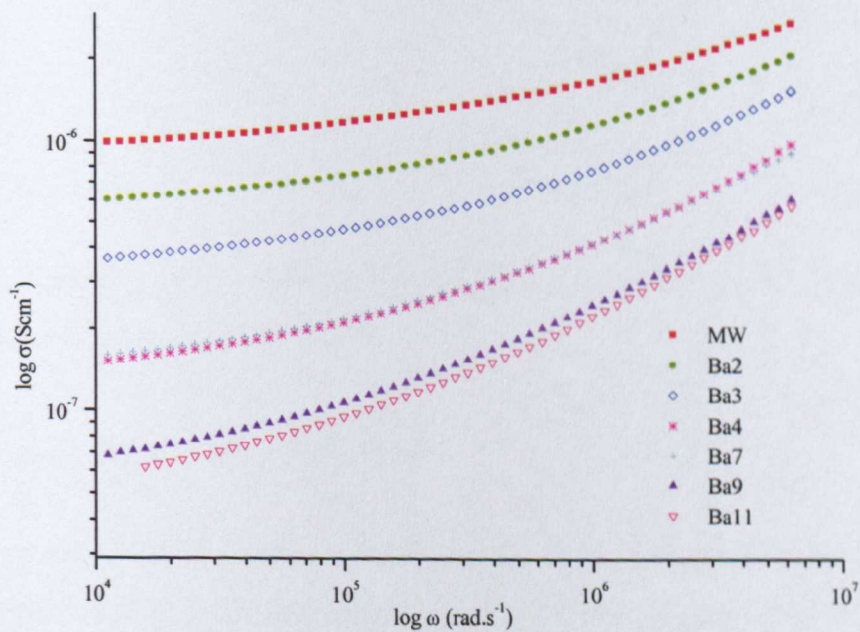Fig. 7.24. *Variation of DC ionic conductivity with BaO concentration at 300 ℃.*

Fig. 7.25. *AC conductivity spectra obtained from MW-BaO at 300 ℃.*
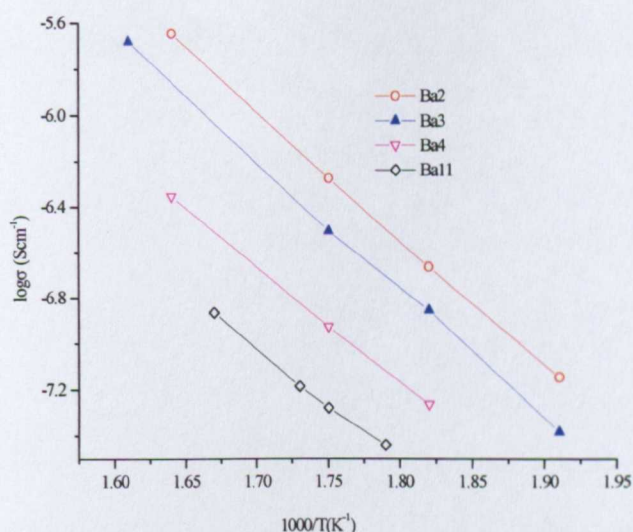
Fig. 7.26. The Arrhenius plots for MW-BaO glasses.

Sample Name	Mol percent of BaO	DC conductivity σ_{300} (Scm^{-1}) $\pm$ 0.1 $\times 10^{-7}$	Activation Energy E_a (eV) $\pm$ 0.05
MW	0	9.3×10^{-7}	0.47
Ba2	2.4	5.4×10^{-7}	0.48
Ba3	3.62	3.2×10^{-7}	0.48
Ba4	4.83	1.2×10^{-7}	0.44
Ba7	7.25	9.3×10^{-8}	0.40
Ba9	9.66	6.0×10^{-8}	-
Ba11	11.98	5.3×10^{-8}	0.41

Table 7.01. Conductivities in MW-BaO glass system at 300°C and activation energies calculated are for the range 250-350°C.

7.6.3. Ionic conductivity MW-MnO

Ionic conductivity of the system MW-MnO was determined from the complex impedance plots shown in Figure 7.27. The values of the DC ionic conductivity lie in the range 1.9×10^{-7} to 1.2×10^{-7} Scm^{-1}. The leaching of Na/Li from these glasses shows approximately the same trend as described in section 7.4.2. The activation energy calculated for PbO-As$_2$O$_3$: MnO glasses [17] containing 0.5 % MnO is ~ 0.33 eV and a similar result (0.35eV) was found for a mixed alkali borosilicate glass with 2.4 mol % of MnO. This was observed to increase with further increase of MnO. So the activation

energy 0.35 to 0.59 eV obtained in the present work can be compared to the reported results [17]. This higher value may be consequence of difference redox composition for Mn^{n+}.

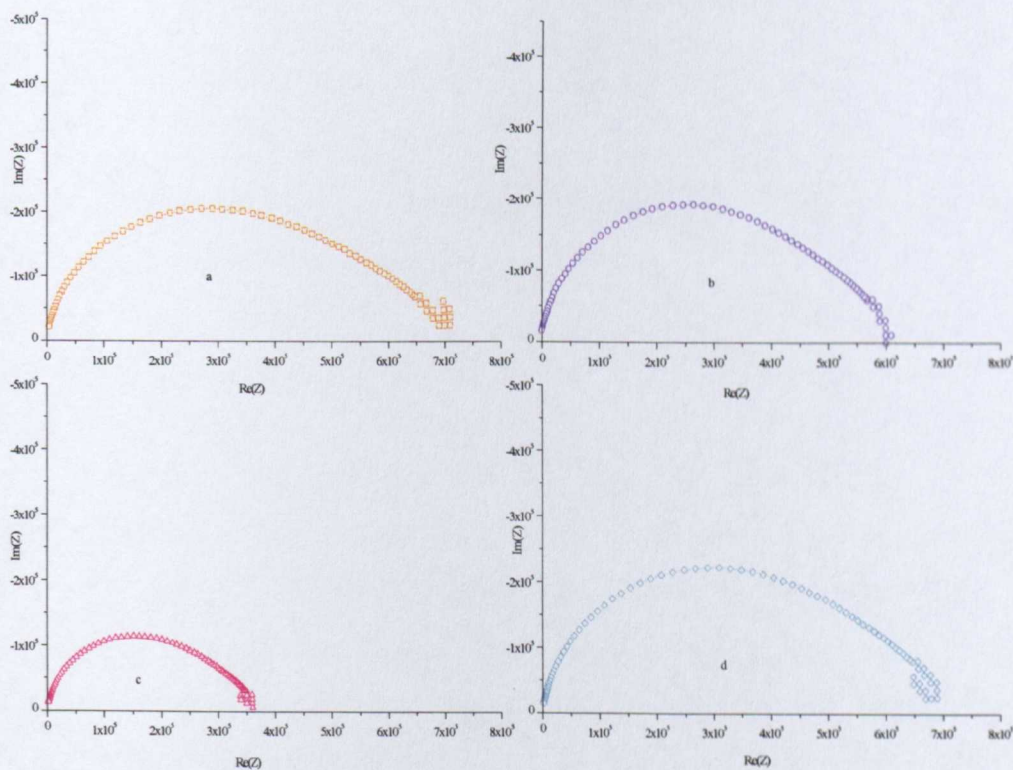Fig. 7.27. Complex impedance spectra at 300°C temperature obtained from MW-MnO system (a) Mn2 (b) Mn4 (c) Mn7 (d) Mn11.
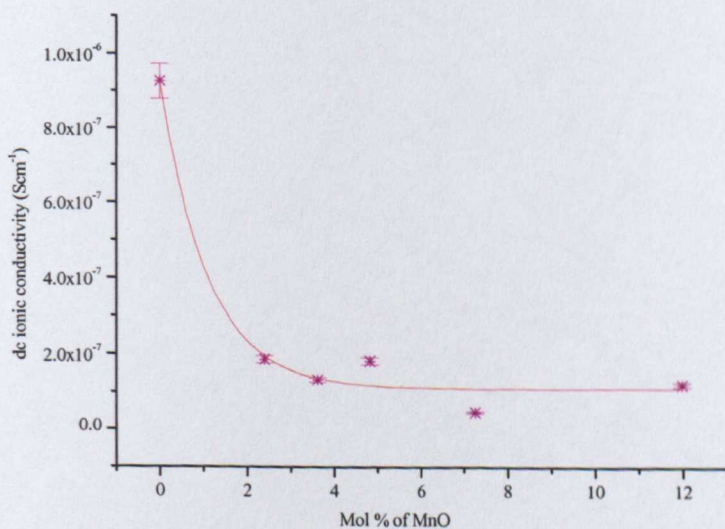
Fig. 7.28. Variation of Ionic conductivity with MnO concentration.

Sample ID	Mol. Percent of MnO	Conductivity (300° C) $(Scm^{-1}) \pm 0.1 \times 10^{-7}$	Activation energy $(250-350)°C$ $E_a (eV) \pm 0.05$
MW	0	9.3×10^{-7}	0.47
Mn2	2.4	1.9×10^{-7}	0.35
Mn3	3.62	1.3×10^{-7}	0.41
Mn4	4.83	1.8×10^{-7}	0.43
Mn7	7.25	4.7×10^{-8}	0.59
Mn11	11.98	1.2×10^{-7}	-

Table 7.02. Conductivity measurements for MW-MnO (300 °C) and activation energies calculated in the range 250-350 °C.

7.6.4. Ionic conductivity MW-ZnO

The ionic conductivity in these glasses decreases from 4.3×10^{-7} to 7.5×10^{-8} Scm^{-1} at ~ 300°C as the ZnO content is increased. A representative complex impedance plot is shown in Figure 7.29. The variation of AC conductivity with frequency is shown in Figure 7.30. It was found that the spectra show some convergence at higher frequency. The variation of DC conductivity with the mol % of ZnO is shown in Figure 7.31. Leaching of Na/Li from these glasses has shown a similar trend to the dc ionic conductivity measurement.

Fig. 7.29. Complex impedance plot for the MW-ZnO glass system at 300 °C.

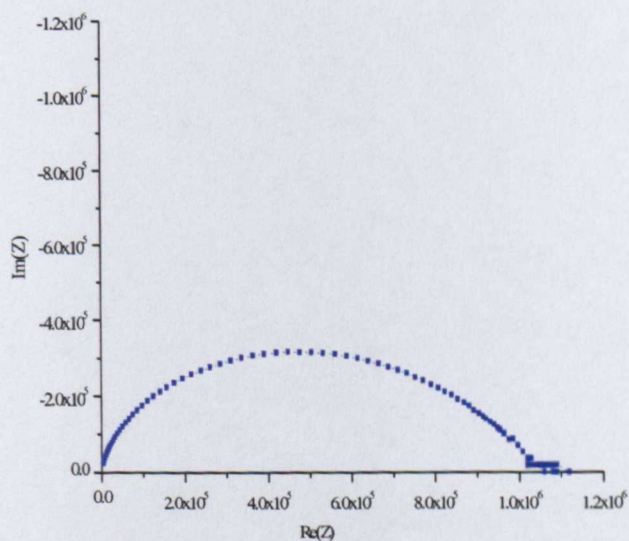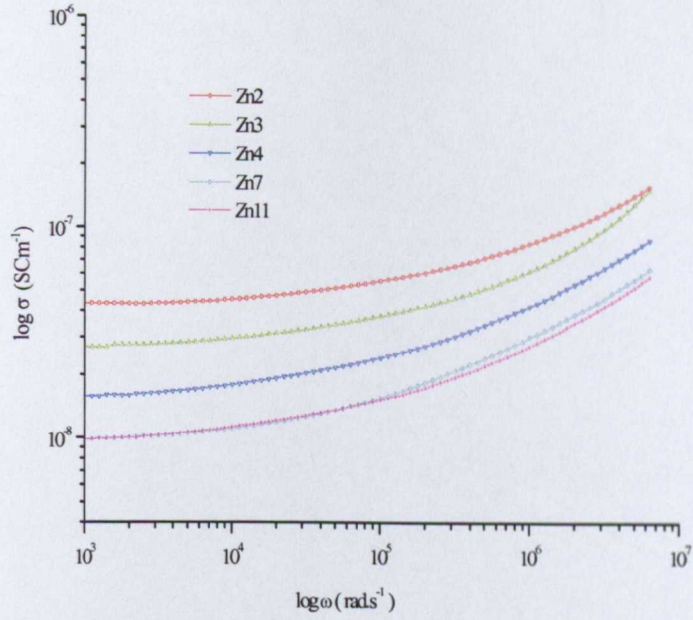*Fig. 7.30. AC conductivity spectra for MW-ZnO glasses at 300℃.*
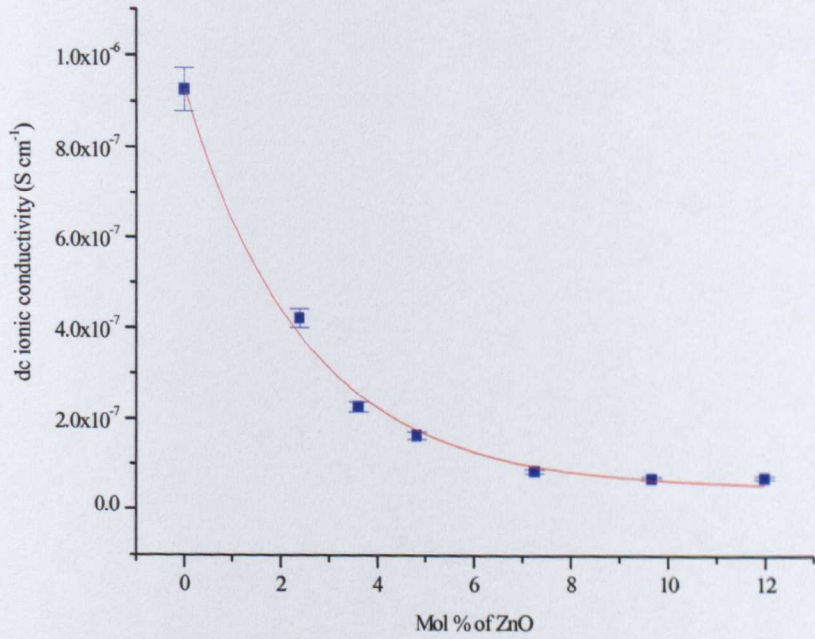
Fig. 7.31. Variation of ionic conductivity with increasing concentration of ZnO at 300℃.

Sample ID	Mol. Percent of ZnO	Conductivity (300°C) (Scm^{-1}) ± 0.1 ×10^{-7}	Activation energy (250-350)°C E$_a$(eV) ± 0.05
MW	0	9.3 ×10^{-7}	0.47
Zn2	2.4	4.3×10^{-7}	0.44
Zn3	3.62	2.3×10^{-7}	-
Zn4	4.83	1.7×10^{-7}	0.56
Zn7	7.25	8.9×10^{-8}	-
Zn9	9.66	7.3×10^{-8}	0.58
Zn11	11.98	7.4×10^{-8}	0.59

Table 7.03. Conductivities for ZnO (300°C) and activation energies calculated from the Arrhenius equation in the temperature range 250-350°C.

7.6.5. Ionic conductivity MW- PbO

At ~300°C the ionic conductivity in these glasses decreased from 2.0×10^{-7} to 3.9×10^{-8} Scm^{-1} (Figure 7.33). The complex impedance plot obtained from the glass containing 2.4 mol% of PbO glass is shown in Figure 7.32. Similar results are reported for the glass system Li_2O-PbO-B_2O_3 [18]. Measurements were not repeated at different temperatures and hence no activation energies have been calculated.
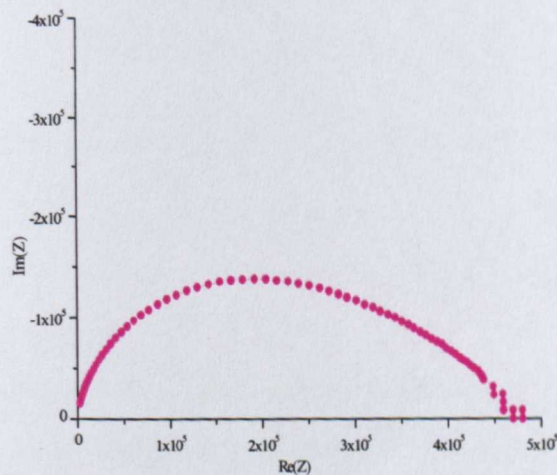
Fig. 7.32. Complex impedance spectrum obtained from MW-PbO (2.4 mol% of PbO) at 300°C.
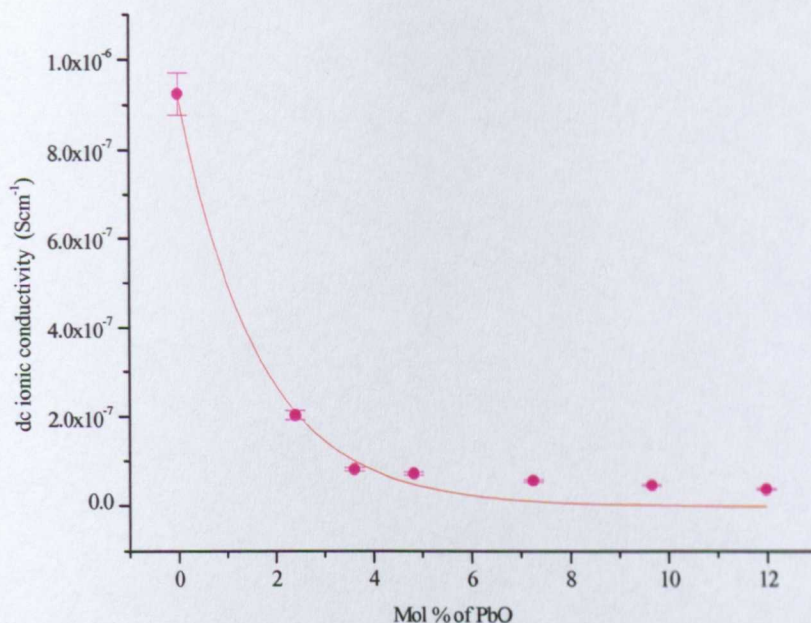
Fig. 7.33. Variation of DC conductivity with PbO concentration at 300 ℃.

Sample ID	Mol. Percent of PbO	Conductivity (300°C) $(Scm^{-1}) \pm 0.1 \times 10^{-7}$
MW	0	9.3×10^{-7}
Pb2	2.4	2.0×10^{-7}
Pb3	3.62	8.2×10^{-8}
Pb4	4.83	7.3×10^{-8}
Pb7	7.25	5.8×10^{-8}
Pb9	9.66	4.7×10^{-8}
Pb11	11.98	3.9×10^{-8}

Table 7.04. DC ionic conductivity measurements for MW-PbO at 300 ℃.

7.7. Conclusions

The present work reports the effect on ionic conductivity of different additives in the MW glass. In all cases the ionic conductivity of the base glass (MW) at the temperature 300°C was found to be $(9.3 \pm 0.1) \times 10^{-7}$ Scm^{-1}. On introduction of an additive oxide, the value of the dc ionic conductivity decreased (Figure7.34).
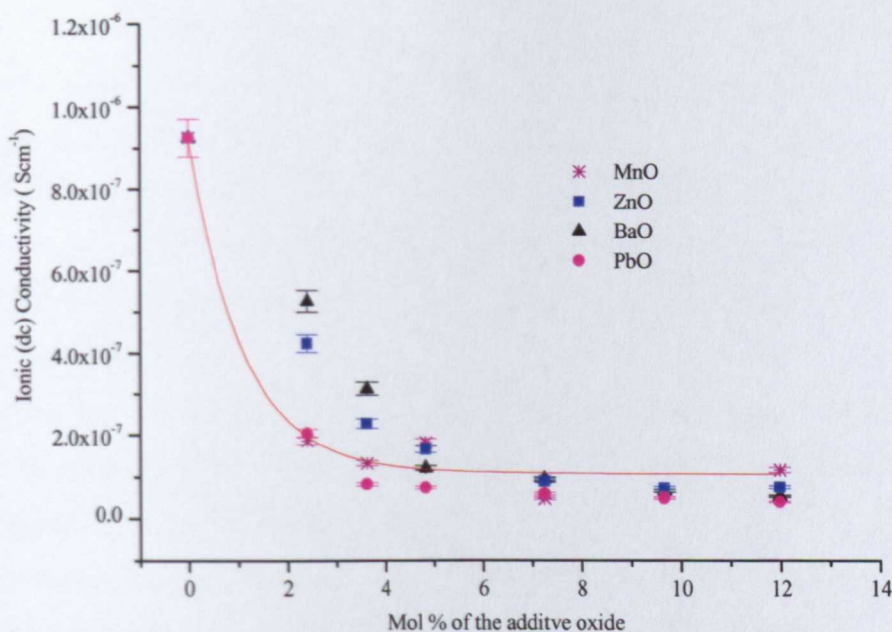
Fig. 7.34. Variation of DC ionic conductivity with increasing concentration of additive oxides in MW glass.

Conductivity in the glass system is determined by the concentration and mobility of alkali ions. Introduction of PbO, ZnO and BaO into the MW glass system reduces the conductivity because the cations with +2 charge are less mobile than alkali ions and so mobile alkali is replaced. Assuming that R^+ dominates the conduction process, in addition to the reduction of carrier number by composition change, there is also a change in mobility of R^+. The M^{2+} ions may occupy similar sites in the glass structure to alkali ions and the larger ion will produce a blocking effect and hence lower the conductivity.

The electrical conductivity of glass depends also on the type of carrier. Since the manganese ions in these glasses may exist in more than one valence state, e.g., Mn^{2+}, Mn^{3+}, conduction could also take place by the transfer of electrons from low to high valence states. However, the decrease in conductivity in MW-MnO indicates any contribution from electronic conductivity is negligible.

The change in electrical conductivity due to replacement of alkali oxides by divalent oxides is also found for similar silicate glasses. The current carriers in these samples are expected to be monovalent ions, i.e alkali ions. The Anderson and Stuart model [19] for electrical conduction in ionically conducting glasses, which is routinely

114

used to predict trends in electrical conductivity of glasses [20, 21] suggests that replacement of a monovalent alkali ion by a divalent ion should cause a decrease in conductivity due to an increase in the energy of bonding of the divalent ion to its site in the vitreous network as compared to that of an alkali ion.

The leaching of Na/Li shows a similar trend to that of ionic conductivity in glasses containing ZnO, PbO and MnO. As has been described in section 7.3 and 7.4.2 qualitatively the reduction in electrical conductivity follows the corrosion behaviour in these glass systems.

However, the effect on conductivity is less marked than the reduction in chemical durability, which occurs when an alkaline earth oxide such as BaO is added to the base glass. It is known that for glass containing heavy ions such as Ba^{2+}, surface properties may often differ appreciably from bulk properties [22]. The correlation between rate of removal of alkali by water attack and electrical conductivity does not exist for less durable glasses. Das and Douglas also showed that the values for the alkali ion diffusion coefficient from corrosion are up to 10^4 to 10^5 times greater than those obtained from conductivity measurements [23].

7.8. References

[1]   H. Darwish, Mat. Chemistry and Physics **69** (2001) 36-44.

[2]   CERAM Research Ltd. Queens Road, Penkhull, Stoke-on-Trent, ST4 71Q, England.

[3]   Y. H. Han and D. E. Day, Glass Technol. **33** (1992) 214.

[4]   M.A. Tindyala and W. R. Ott, Am. Ceram. Soc. Bull. **57** (1978) 432.

[5]   H. S. Liu, P.Y. Shih and T. S. Chin, Phys. Chem. Glasses **37** (1996) 22.

[6]   G. Calestani and A. Montenero, J. Non-Cryst Solids **84** (1986) 452-462.

[7]   G. Della Mea, A. Gasparotto and M. Bettinelli, J. Non-Cryst. Solids **84** (1986) 443.

[8]   International centre for diffraction data, XRD card No: 19073-3273, Pennsylvania, USA.

[9]   J. G. Shah, V. A. Patki and K. Raj, Waste Management **15** (5/6) (1995) 417-421.

[10]   I. L. Pegg and E. E. Sad, Scientific Basis for Nuclear Waste Management XII, **127** (1998) 215-221.

[11]   R. Pyare, M. R. C. Srivastava and P. N. Srivastava, J. Mat. Sci. **17** (1982) 2432.

[12]   G. H. Koenderink R. H. Brzesowsky and A. R. Balkenende, J. Non-Cryst. Solids **262** (2000) 80-98.

[13]   N. A. EL-Alaily and F. M. Ezz-Eldin, Radiation Physics Chemistry **44** (1994) 45-51.

[14]   Y. H. Han, N. J. Kreidl and D. E. Day, J. Non-Cryst. Solids **30** (1979) 241-252.

[15]   J. E. Shelby, J. Non-Cryst. Solids **263** (2000) 271-276.

[16]   P. Muralidharan, M. Venkateswarlu and N. Satyanarayana, Mat. Chem. and Phys. **88** (2004) 138-144.

[17]   G. Srinivasarao, N. Veeraiah, J. Alloys and Compounds **327** (2001) 52-65.

[18]   M. Ganguli, M. H. Bhat and K. J. Rao, Mat. Res. Bull. **34** (10/11) (1999) 1757-1722.

[19]   O. L Anderson and D. A. Stuart, J. Am. Ceram. Soc. **37** (1954) 573.

[20]   J. E. Shelby, Introduction to glass science and technology, RSC, Cambridge (1997).

[21]   A. K. Varshneya, Fundamentals of inorganic glasses, Academic Press, San Diego (1994).

[22]   G. O. Jones, Glass, 2nd edition, Chapman and Hall (1971) 112.

[23]   H. Rawson, Properties and application of glass, Elsevier (1980).

Chapter 8

Conclusions and further work

8.1. Introduction

The conclusions of the results chapters 5, 6 and 7 are summarized. The information acquired from the analysis of mixed-alkali borosilicate glasses containing different divalent oxide additives is shown to be useful in the selection process of radioactive waste immobilisation.

8.2. Summary

The mixed alkali modified borosilicate base glass used for BNFL high-level waste vitrification has been doped with different additives. The characteristics of the waste glass are determined by the amount and type of the oxides added to it. Therefore a selection of different additives possessing the property of network intermediate or modifier have been added to the base glass. A number of physical and structural techniques such as ^{11}B NMR, ^{29}Si NMR, UV-Visible spectroscopy, ac impedance spectroscopy and leach testing have been performed.

8.3. Structural Characterisation

The addition of BaO, CaO and SrO to the base (MW) BNFL vitrification glass caused N_4 to increase with alkaline earth content, and maximum values were attained at compositions depending on the M^{2+} ion type. In contrast, the addition of divalent oxides such as ZnO and PbO to MW reduced the N_4 values with the rate of decrease being greater for ZnO than PbO. The decrease in N_4 in these glasses indicates that the alkali ions are being removed from the borate network possibly by formation of complexes $[MO_n]^-R^+$.

From ^{29}Si NMR studies it was found that the addition of CaO, SrO and BaO glass produced similar effects on chemical shift. The ^{29}Si peaks move towards more positive values which means that these oxides act as modifiers. From the fitted spectra the percentage of Q^3 was found to increase with the amount of CaO, SrO and BaO. This increase in Q^3 is reflected in increased corrosion in an aqueous environment.

Due to the complexity of possible silicon speciation in the systems with ZnO and PbO i.e. existence of Si-O-M bonds, it was found difficult to obtain a unique fit, hence precluding a meaningful analysis from the ^{29}Si NMR study.

Investigation of the UV visible transmission characteristics of MnO-doped glasses has shown a gradual decrease in transmittance at ~ 380 nm with increasing concentration of MnO. The UV absorption edge of these glasses moves towards longer wavelengths, maybe caused by generation of NBOs on the [SiO$_4$] tetrahedral unit. The absorption band centred at ~ 490nm is due to the Mn^{3+} state.

8.4. Thermal and physical properties

From DTA, it was found that glass transition temperatures in MW with PbO, ZnO and MnO addition decreased with mol percent of additives. On the other hand, an increase in T$_g$ was observed in the case of BaO, CaO and SrO containing glasses. The effect on the glass transition temperature was also found to correlate with the heat of formation of the additive oxides, the effect becomes more evident as the concentration of the additive oxide increases. In addition, MW-MnO glass shows non-linear behaviour because of the variable valence states of manganese.

There is a linear increase in CTE of the MW-CaO and MW-SrO systems up to 11.98 mol%. In the glass system-containing BaO the CTE increased up to 9.66 mol% and then decreased due to the large size of the Ba^{2+} ion. In the MW-PbO and MW-ZnO glasses, thermal expansion increased showing the structure to be less rigid. Introduction of MnO produces an increase in CTE up to 4.83 mol percent, followed by a rapid decrease. The change in the relative amount of Mn^{2+} and Mn^{3+} with concentration causes the anomaly in CTE.

The increase in density in glasses is due to the large masses of the added cations, which exceed those of the other glass components. The density of the glass increases linearly in the order Ba > Sr > Ca. Similarly the density increases with relative molecular mass of PbO > ZnO ~ MnO. However, it was found that the molar volume of the glass system containing BaO, CaO, SrO, MnO and ZnO decreased approximately linearly with increased addition. The change in molar volume with composition is significantly non-linear for the glass system containing PbO, while the density varies quite linearly. The reduction in molar volume arises from the replacement of some network formers and also the relaxation of network oxygen

about the M^{2+} sites. However, the large size of Ba^{2+} ultimately causes an expansion of these sites. Mn^{2+} and Mn^{3+} similarly fill voids.

8.5. Chemical durability and ionic conductivity

Chemical durability studies have shown that the addition of alkaline earth oxides to the base glass results in an increase in corrosion in the order CaO < SrO << BaO. The chemical durability of barium glasses deteriorates at about at 11.98 mol% and 100% weight loss of the glass sample was found at 15 mol percent. The presence of the modifiers BaO and SrO increases dissolution of Na^+ and Li^+ whereas PbO, ZnO and MnO reduce the rate of chemical attack. The crystalline phase Mn_7SiO_{12} was detected on the surface of the leached MW-MnO glasses. The durability of glasses was found to be strongly dependent on the identity of the cation present in the glass systems and seems to be linked to Q^3 formation.

At 300°C, the value of the DC ionic conductivity reduces with increasing amount of additives. The number and/or mobility of the alkali ions are affected. Divalent cations are less mobile than alkali ions and are also an obstacle to the jumps of small ions like Na^+/Li^+.

The leaching of Na/Li shows a similar trend to that of ionic conductivity in glasses containing ZnO, PbO and MnO. Qualitatively the reduction in electrical conductivity follows the corrosion behaviour in these glass systems. However, the correlation between rate of removal of alkali by water attack and electrical conductivity does not exist for less durable glasses.

8.6. Further work

The predicted non-bridging oxygen per silicon ratio increased with the additive oxide content, if the additive oxides act as network modifiers. For the case of ZnO and PbO the predicted non-bridging oxygen per silicon decreased with the level of oxide in MW glasses. However, calculated values of non-bridging oxygen per silicon based on ^{29}Si NMR studies were higher than the values predicted from measured N_4. Due to the complexity of the systems with ZnO and PbO, it was found difficult to obtain any meaningful structural information. Therefore, further studies are required for more accurate quantification of non-bridging oxygen in the glasses containing PbO and ZnO using 2D - ^{29}Si NMR and ^{17}O NMR.

No sensible trends were found in the $[BO_{3S}]$ and $[BO_{3AS}]$ values obtained from ^{11}B NMR simulation. Using ^{11}B triple quantum magic angle spinning (3QMAS) would allow more accurate quantification of $[BO_4]$ and $[BO_3]$ groups. Higher field NMR may also improve resolution. ^{17}O magic angle spinning (MAS) and triple quantum magic angle spinning (3QMAS) nuclear magnetic resonance may show the distribution of NBO connected to either silicon or boron.

The structural analysis of manganese containing glasses can be done by X-ray absorption near edge structure (XANES). Electron Paramagnetic Resonance (EPR) could be employed as a powerful tool for study of short-range order in MW-MnO glass but only at low MnO concentration.

Finally, the combination of surface techniques and ionic transport measurements could well make a powerful partnership by virtue of its ability to differentiate the chemistry from the physics of processes occurring at the glass surface.